UNIVERSITY OF CALIFORNIA, IRVINE

Neural Mechanisms of Spatial Stream Segregation Along the Ascending Auditory Pathway

DISSERTATION

submitted in partial satisfaction of the requirements for the degree of

DOCTOR OF PHILOSOPHY

in Biological Sciences

by

Justin Daniel Yao

Dissertation Committee:
Professor John C. Middlebrooks, Chair
Professor Karina S. Cramer
Professor Raju Metherate
Professor Virginia M. Richards
Professor Georg F. Striedter

2015

DEDICATION

To

My Mother and Father
for their constant love and support

TABLE OF CONTENTS

Page

LIST OF FIGURES **v**

ACKNOWLEDGMENTS **vii**

CURRICULUM VITAE **viii**

ABSTRACT OF THE DISSERTATION **xii**

CHAPTER 1 **1**
General Introduction
- 1.1 Spatial Hearing: Cues and Neural Representation
- 1.2 Auditory Scene Analysis
- 1.3 Auditory Stream Segregation
- 1.4 Potential Mechanisms involved in Generating Spatial Stream Segregation

CHAPTER 2 **11**
Rat Primary Auditory Cortex is Tuned Exclusively to the Contralateral Hemifield
- 2.1 Summary
- 2.2 Introduction
- 2.3 Materials and Methods
  - 2.3.1 *Animal Preparation*
  - 2.3.2 *Experimental Setup and Stimulus Generation*
  - 2.3.3 *Experimental Procedure*
  - 2.3.4 *Data Analysis*
- 2.4 Results
  - 2.4.1 *Characteristics of Spatial Tuning*
  - 2.4.2 *Discrimination Between Azimuth Locations by Spike Count*
  - 2.4.3 *Spatial Sensitivity of First-Spike Latencies*
  - 2.4.4 *Frequency Independence of Spatial Tuning Properties*
- 2.5 Discussion
  - 2.5.1 *Spatial Representation in Rat Primary Auditory Cortex*
  - 2.5.2 *Species Differences in Cortical Representation of Acoustic Space*
  - 2.5.3 *Species Differences in Spatial Representation Correlate with Spatial Acuity*
  - 2.5.4 *Concluding Remarks*
- 2.6 Acknowledgements

CHAPTER 3 **35**
Transformation of Spatial Sensitivity Along the Ascending Auditory Pathway
- 3.1 Summary
- 3.2 Introduction
- 3.3 Materials and Methods
  - 3.3.1 *Animal Surgery*

3.3.2 *Experimental Setup, Stimulus Generation*
3.3.3 *Experimental Procedure*
3.3.4 *Assignment of Units to IC and MGB Subdivisions*
3.3.5 *Data Analysis*
3.4 Results
3.4.1 *Frequency Tuning*
3.4.2 *First-Spike Latencies*
3.4.3 *Spiking Patterns*
3.4.4 *Offset Responses*
3.4.5 *Examples of Spatial Sensitivity*
3.4.6 *Two Physiologically Distinct Subpopulations in the MGBv*
3.4.7 *Transformation of Spatial Sensitivity in the Ascending Pathway*
3.4.8 *Discrimination of Sound-Source Locations*
3.5 Discussion
3.5.1 *Two Parallel Pathways for Auditory Space Processing*
3.5.2 *Two Populations of Neurons Within the MGBv*
3.5.3 *Potential Behavioral Relevance for Parallel Pathways for Auditory Space Processing*
3.6 Acknowledgements

CHAPTER 4 **69**
Emergence of Spatial Stream Segregation in the Ascending Auditory Pathway
4.1 Summary
4.2 Introduction
4.3 Materials and Methods
4.3.1 *Animal Preparation*
4.3.2 *Experimental apparatus, Stimulus Generation, and Data Acquisition*
4.3.3 *Experimental Procedure*
4.3.4 *Pharmacological Procedures*
4.4.4 Data *Analysis*
4.4 Results
4.4.1 *Neural Responses to Competing Sound Sequences*
4.4.2 *Quantification of Spatial Stream Segregation*
4.4.3 *Contribution of Forward Suppression to SSS*
4.4.4 *Forward Suppression in A1 is not due to Synaptic Inhibition*
4.5 Discussion
4.5.1 *Stream Segregation Along the Ascending Auditory System*
4.5.2 *Segregating Streams Through Spatial Hearing and Forward Suppression*
4.5.3 *Potential Mechanisms of Forward Suppression*
4.6 Acknowledgements

CHAPTER 5 **101**
Summary and Conclusion

REFERENCES **107**

LIST OF FIGURES

Page

Chapter 1

Figure 1.1 Schematic of ascending auditory system and respective functions at each station 3
Figure 1.2 Schematic of spatial stream segregation stimuli and speaker arrays 6
Figure 1.3 Schematic of potential mechanisms of cortical forward suppression 9

Chapter 2

Figure 2.1 Examples of neural responses in rat A1 19
Figure 2.2 Distributions of azimuth centroids and slope locations for noise burst stimuli presented at the stated sound levels 21
Figure 2.3 Distributions of equivalent rectangular receptive field (ERRF) width, modulation depth, and maximum discrimination index 22
Figure 2.4 Pairwise *d'* matrices for corresponding pairs of stimulus locations for 1 example unit 23
Figure 2.5 Distribution of minimum separation thresholds as a function of a reference azimuth in the frontal field across suprathreshold levels 24
Figure 2.6 Grand mean first-spike latencies as a function of azimuth sound location across suprathreshold levels 25
Figure 2.7 Comparison of MDAs based on spike count vs. those based on first-spike latency for each unit at various levels above threshold 26
Figure 2.8 Spatial tuning metrics as a function of unit CF 27

Chapter 3

Figure 3.1 Histological reconstruction of recording sites in 4 animals 48
Figure 3.2 Examples of neural responses from well-isolated single units in rat ICc, BIN, and MGBv 49
Figure 3.3 Examples of neural responses of well-isolated single units in rat MGBd, MGBm, MGBs 51
Figure 3.4 Classifying distinct classes of spatial sensitivity in MGBv 55
Figure 3.5 Distribution of equivalent rectangular bandwidth values (ERB) and first-spike latencies 57
Figure 3.6 Breadth of spatial sensitivity and level dependence 59
Figure 3.7 Pairwise *d'* matrices for corresponding pairs of stimulus locations at 40 dB above threshold from the single units shown in Figs. 3.2 and 3.3 61
Figure 3.8 Distributions of percentages of discriminated location pairs for all sampled populations as a function of level above threshold 62
Figure 3.9 Grand mean RAFs across 10, 20, 30, and 40 dB above threshold from all units within each subdivision sampled 65

Chapter 4

Figure 4.1 PSTH of a well isolated single unit from cortical area A1 81
Figure 4.2 Responses to single-source and competing-source conditions 82

Figure 4.3 Distribution of the spatial release index (SRI) values across each unit population for each base rate tested 85
Figure 4.4 Discriminating competing sources 87
Figure 4.5 Cumulative distributions of best thresholds 88
Figure 4.6 Distribution of *d'* for discrimination of A and B sources 89
Figure 4.7 Cumulative distribution of forward suppression across each unit population for each tested base rate 91
Figure 4.8 Median vector strength and the proportion of synchronized units for each unit population (color coded) at varying repetition rates 92
Figure 4.9 Breadth of spatial sensitivity for the single-source versus the competing-source condition 93
Figure 4.10 Effects of $GABA_A$ or $GABA_B$ antagonists on A1 responses 95

ACKNOWLEDGMENTS

These past few years were filled with wonderful experiences. This dissertation is a product of support and assistance from a number of individuals who deserve acknowledgement and credit.

First and foremost, I would like to thank Dr. John Middlebrooks. John, thank you for being a wonderful mentor, advisor, and role model. Thank you for entrusting me with taking on the rat spatial stream segregation project and for being patient and open to taking on new aims and challenges along the way. You have taught me so much and kept me focused. I could not have asked for a better mentor.

I would like to thank all members of the Middlebrooks Lab. In particular, my fellow "rat guy", Peter. You have accelerated my training and knowledge in the field and most importantly, helped me "conquer" MATLAB. Without you, my training would have taken much longer than it should have and those late night rat experiments would not have been as fun. We shared a few hobbies and interests and I already miss our movie outings and lively discussions about The Last of Us and other video games. I thank you for being a great, colleague, co-author, and friend. A big thank you to my "lab sibling", Lauren, lab manager, Zekiye, and lab technician, Beth. Thank you all for your assistance on administrative, technical, and personal matters. It has been an honor to work alongside all of you.

I also would like to thank the members of my dissertation committee, Drs. Karina Cramer, Raju Metherate, Virginia Richards, and Georg Striedter. Thank you for your time and helpful advice in shaping my dissertation to what it is today.

Grant support of research and training was provided by the National Institute on Deafness and Other Communication Disorders Grants R01-DC000420, F31-DC013013, and T32-DC010775.

On a more personal note, I would like to thank my family who have supported me throughout these years. Their unconditional love has allowed me to strive to be my best self. Pia, you have been the calmness and my rock on this journey. Thank you for your constant love, patience, and support. Stomper, thank you for being you.

CURRICULUM VITAE

Justin D. Yao
December, 2015

Personal Information

Birth Date: February 29, 1988
Place of Birth: Manila, Philippines
Citizenship: United States of America

Education

Degree Programs

2010–2015: University of California at Irvine, Irvine, CA
Dept. of Neurobiology and Behavior Ph.D.
Dissertation: *Neural Mechanisms of Spatial Stream Segregation Along the Ascending Auditory Pathway*

2008–2010: University of California at Berkeley, Berkeley, CA
Dept. of Psychology BA
Undergraduate Honors Thesis: *Sleep-Dependent Amelioration of Emotional Reactivity*

2006–2008: Pasadena City College, Pasadena, CA
Psychology AA

Fellowships, Honors, and Recognition

- 2014: UCI School of Biological Sciences, Travel Award
- 2014: Most Outstanding Graduate Student Award, *Center for Hearing Research,* University of California, Irvine
- 2013 – Current: **NIH-NIDCD,** NRSA (F31-Diversity) Individual Research Fellowship
- 2012 – 2013: **NIH-NIDCD**, (T32-Predoctoral) Interdisciplinary Training Program in Hearing Research
- 2010: Honors in Psychology, *Dept. of Psychology*, University of California, Berkeley
- 2010: Warner Brown Memorial Prize, *Dept. of Psychology*, University of California, Berkeley (given to a graduating senior "who has shown the most promise in scientific research")
- 2008: Alpha Gamma Sigma Scholar, *Pasadena City College*, Pasadena, CA
- 2008: Extraordinary in Social Sciences Award, *Pasadena City College*, Pasadena, CA
- 2008: Completion in Scholars Program, *Pasadena City College*, Pasadena, CA
- 2006–2008: Dean's Honor List, *Pasadena City College*, Pasadena, CA

Research Experience

March 2011 – Current
Graduate Student Researcher at the University of California, Irvine, Department of Neurobiology and Behavior
Supervisor: Dr. John C. Middlebrooks

- Exploring the mechanisms of spatial hearing that facilitate segregation of multiple competing sounds
- Performed *in vivo* extracellular electrophysiology experiments in the rat auditory cortex, medial geniculate body, and inferior colliculus
- Tissue histology via vibratome sectioning and fluorescent microscopy
- Conducted pharmacological manipulations in the rat auditory cortex while simultaneously performing *in vivo* extracellular recordings
- Data analysis in MATLAB
- Presentation of research at departmental seminars and conferences

December 2009 – June 2010
Undergraduate Research Assistant at the University of California, Berkeley, Department of Psychology
Supervisor: Dr. Matthew P. Walker
- Subject recruitment and behavioral studies
- Conducted overnight Polysomnographic (PSG) sleep recordings
- Supervised and trained new research assistants
- fMRI technical assistant

Teaching Experience

2014 Fall Quarter
- **Teaching Assistant:** Upper division undergraduate course “Hearing and the Brain”

2013 Spring Quarter
- **TA Trainer:** Laboratory course “Neurobiology and Behavior Laboratory”

2013 Winter Quarter
- **Teaching Assistant:** Laboratory course “Neurobiology and Behavior Laboratory”

2012 Spring Quarter
- **Teaching Assistant:** Laboratory course “Neurobiology and Behavior Laboratory”

Other Professional Activities

Professional Memberships
- Association for Research in Otolaryngology
- Society for Neuroscience

Conferences Attended
- 38th Annual Association for Research in Otolaryngology MidWinter Meeting; Baltimore, MD, 2015
- Gordon Research Seminar & Conference “Auditory System”; Lewiston, ME, 13th July 2014
- 37th Annual Association for Research in Otolaryngology MidWinter Meeting; San Diego, CA, 2014
- 36th Annual Association for Research in Otolaryngology MidWinter Meeting; Baltimore, MD, 2013
- 35th Annual Association for Research in Otolaryngology MidWinter Meeting; San Diego, CA, 2012

Computer Proficiency

Operating systems, Programming Languages, & Statistical Software

MAC OS X, Microsoft Windows, MATLAB, Prism

Publications and Presentations

Publications

- **Yao JD**, Bremen P, Middlebrooks JC. Emergence of Spatial Stream Segregation in the Ascending Auditory System. *manuscript In Press at J Neurosci (2015)*
- **Yao JD**, Bremen P, Middlebrooks JC. Transformation of Spatial Sensitivity along the Ascending Auditory Pathway. *J Neurophysiol. 2015; March 4;113(9):3098–111*.
- **Yao JD**, Bremen P, Middlebrooks JC. Rat Primary Auditory Cortex is Exclusively Tuned to the Contralateral Hemifield. *J Neurophysiol. 2013; Aug 14;110(9):2140–51.*
- van der Helm E, **Yao J,** Dutt S, Rao V, Saletin JM & Walker MP. REM Sleep Depotentiates Amygdala Activity to Previous Emotional Experiences. *Current Biology, 2011;* 21(23):1–4.

Published Abstracts/Conference Presentations

- **Yao JD**, Bremen P, Middlebrooks JC. (2015) Emergence of Spatial Stream Segregation Along the Ascending Auditory System. *SoCal Hearing Conference, UC San Diego, San Diego, CA*
- **Yao JD**, Bremen P, Middlebrooks JC. (2015) Spatial Stream Segregation by Neurons Along the Ascending Auditory System. *38th Annual Association for Research in Otolaryngology MidWinter Meeting, Baltimore, MD.*
- **Yao JD**, Bremen P, Middlebrooks JC. (2014) Sharpening of Spatial Tuning Along the Ascending Auditory System. *SoCal Hearing Conference, Irvine, CA*
- **Yao JD**, Bremen P, Middlebrooks JC. (2014) Sharpening of Spatial Tuning Along the Ascending Auditory System. *Gordon Research Seminar & Conference "Auditory System"; Lewiston, ME.*
- **Yao JD**, Bremen P, Middlebrooks JC. (2014) Spatial and frequency sensitivity in the subdivisions of the medial geniculate body. *37th Annual Association for Research in Otolaryngology MidWinter Meeting, San Diego, CA.*
- **Yao JD**, Bremen P, Middlebrooks JC. (2013) Characterization of Spatial Sensitivity within Subdivisions of the Medial Geniculate Body: Implications for Spatial Stream Segregation in Auditory Cortex. *SoCal Hearing Conference, Los Angeles, CA*
- **Yao JD**, Bremen P, Middlebrooks JC. (2013) Rat cortical units display sharp hemifield tuning. *36th Annual Association for Research in Otolaryngology MidWinter Meeting, Baltimore, MD.*
- van der Helm E, **Yao J,** Rao V, Dutt S, Walker MP. (2011) "Overnight therapy? Sleep de-potentiates emotional brain reactivity." *Cognitive Neuroscience Society, San Francisco, CA*

Invited Presentations

- Emergence of Spatial Stream Segregation Along the Ascending Auditory System. *Talk given at the SoCal Hearing Conference; UC San Diego, San Diego, CA, 29th August 2015*

- Sharpening of Spatial Tuning Along the Ascending Auditory System. *Talk given at the Gordon Research Seminar & Conference “Auditory System”; Lewiston, ME, 13th July 2014*

ABSTRACT OF THE DISSERTATION

Neural Mechanisms of Spatial Stream Segregation

Along the Ascending Auditory Pathway

by

Justin Daniel Yao

Doctor of Philosophy in Biological Sciences

University of California, Irvine, 2015

Professor John C. Middlebrooks, Chair

In a complex auditory scene, listeners are capable of disentangling multiple competing sequences of sounds that originate from distinct sources. This process is referred to as “stream segregation”, where each “stream" represents the perception of a sound sequence from a particular source. Spatial separation of sound sources facilitates the recognition of multiple sequences of sounds (i.e., multiple “streams”) as belonging to distinct sources. Several neurophysiological studies in laboratory animals have shown that perceptual streams are represented by distinct mutually-synchronized neural populations in the auditory cortex. However, the mechanisms leading to those cortical responses are unknown. This dissertation explores the neural substrates and mechanisms of spatial stream segregation (“SSS”) at several stages in the ascending auditory pathway.

We recorded *in vivo* extracellular spike activity from neurons along different stations of the ascending auditory system of the anesthetized rat, from the midbrain, thalamus, and cortex. Several novel observations were made: (1) The rat primary auditory cortex (area A1) was exclusively tuned to the contralateral hemifield and and was level-tolerant across a 30-dB range of sound levels. (2) Level-tolerant contralateral hemifield spatial sensitivity arises independently along the tectal and lemniscal pathways, highlighting two parallel brainstem pathways for spatial hearing. (3) A linear discriminator analysis of cortical spike counts exhibited high spatial acuity for near-midline sounds and poor discrimination for off-midline locations, which is consistent with previous findings describing the rat’s sound localization behavior. (4) Under stimulus conditions at which human listeners report SSS, neural SSS is weak in the central

nucleus of the IC (ICC), it appears in the nucleus of the brachium of the IC (BIN) and in about two thirds of neurons in the ventral MGB (MGBv), and is prominent in A1. Cortical SSS reflects the spatial sensitivity of neurons enhanced by forward suppression. (5) GABA receptor blockers showed no change on cortical forward suppression, suggesting that it does not result from GABAergic inhibition but might reflect synaptic depression at the thalamocortical synapse. Overall, these findings provide substantial evidence that auditory streams are increasingly segregated along the ascending auditory pathways that culminate in distinct mutually-synchronized neural populations in the auditory cortex.

CHAPTER 1: General Introduction

1.1. Spatial Hearing: Cues and Neural Representation

Determining the location of a sound is critical for finding potential mates, prey, or avoid and escape approaching predators. In contrast to the visual system in which spatial location of an object is directly mapped on the surface of the retina the spatial location of a sound source is not directly represented on the cochlea but constructed by converging inputs from the two ears that are translated through neural computations performed along the central auditory system (reviewed by Grothe et al., 2010). In mammals, these computations are based on the neural reconstruction of acoustic space mediated by spatial cues arising at the torso, head, and pinna (Middlebrooks and Green, 1991; Wightman and Kistler, 1993; Blauert, 1997). Interaural time (or phase) differences (ITDs) and interaural level (or intensity) differences (ILDs) are utilized to localize sound sources along the horizontal dimension, i.e., azimuth. Due to the limited speed of sound (~340 m/s) and the fact that the wavelength for low frequency sounds (in humans < ~1.5 kHz) is longer than the diameter of the head, the sound wave will arrive earlier at one ear than the other, creating an ITD. For high frequency sounds where the wavelength is roughly equal to, or shorter than, the diameter of a listener's head, ITDs are ambiguous. Instead a shadowing effect is produced at the ear further from the sound source, leading to attenuation and creating an ILD. Sound localization in the vertical plane, i.e., elevation, is based on monaural spectral shape cues that can be measured as head-related transfer functions (HRTFs). This dissertation focuses on spatial hearing in azimuth.

ITDs and ILDs are initially processed by brainstem nuclei in the superior olivary complex (SOC), with ITDs extracted in the medial superior olive (MSO) (Goldberg and Brown, 1969; Yin and Chan, 1990; Spitzer and Semple, 1995; Day and Semple, 2011; Bremen and Joris, 2013) and ILDs extracted from the lateral superior olive (LSO) (Boudreau and Tsuchitani, 1968; Tollin and Yin, 2002; Tollin and Yin, 2005). ITD sensitivity is first created in the MSO when its neurons receive binaural excitatory inputs from spherical bushy cells (SBCs) in the ipsilateral and contralateral anteroventral cochlear nucleus (AVCN) as well as binaural inhibitory inputs from the lateral and medial nucleus of the trapezoid body (LNTB and MNTB, respectively) (reviewed by

Grothe et al., 2010; Ashida and Carr, 2011). ILD sensitivity is first created in the LSO by neurons that receive excitatory inputs from the ipsilateral ear through the SBCs of the ipsilateral AVCN and inhibitory inputs from the contralateral ear via neurons in the ipsilateral MNTB, which in turn receive excitatory input from the globular bushy cells (GBCs) of the contralateral AVCN (reviewed by Tollin, 2008). Monaural spectral shape cues for localization in elevation are analyzed in the dorsal cochlear nucleus (reviewed by Young and Davis, 2002). Space-related information from these nuclei converge at the level of the midbrain in the inferior colliculus (Fujita and Konishi, 1991; Kelly et al., 1991; Irvine et al., 1995; McAlpine et al., 1998; Fitzpatrick et al., 2002; Park et al., 2004; Zwiers et al., 2004; McLaughlin et al., 2014) and are further processed in the medial geniculate body of the thalamus (Calford, 1983; Ivarsson et al., 1988; Stanford et al., 1992; Clarey et al., 1995; Stanford et al., 1992; Fitzpatrick et al., 1997; Proctor and Konishi, 1997; Pérez and Peña, 2006; Perez et al., 2009) before reaching the auditory cortex (Middlebrooks et al., 1980; Middlebrooks and Zook, 1983; Rajan et al., 1990; Semple and Kitzes, 1993; Kelly and Judge, 1994). Cortical sensitivity to these cues has been characterized (Brugge et al., 1969; Brugge and Merzenich, 1973; Kitzes et al., 1980; Kelly and Sally, 1988; Reale and Brugge, 1990; Irvine et al., 1996; Ftizpatrick et al., 2000; Malone et al., 2002; Scott et al., 2007; Scott et al., 2009; Higgins et al., 2010) with further discussion on their relationship to free-field spatial sensitivity (for review, see King and Middlebrooks, 2011). Figure 1.1 displays a schematic summary of some of the major stations of the ascending auditory system and their respective functions.

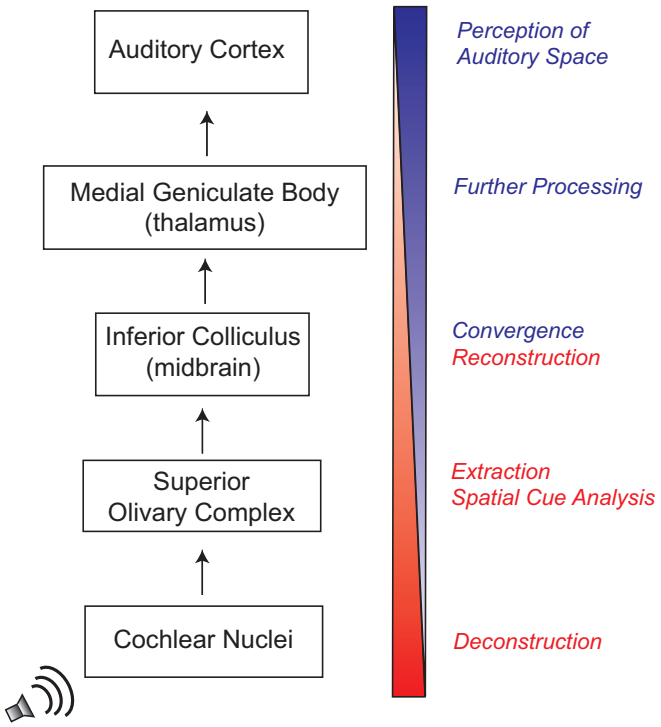

Figure 1.1. Schematic of ascending auditory system and respective functions at each station. As sound enters the auditory system, its properties are deconstructed at low levels, with cues regarding its spatial location extracted within brainstem nuclei. Information of the acoustic stimuli is then reconstructed and converges at the midbrain. Further processing occurs within the thalamus and projects to the auditory cortex to support sound perception.

Despite the substantial body of work on binaural information processing we lack a deeper understanding of how the representation of acoustic spatial information transforms along the ascending and descending auditory pathways that might lead to perceptual phenomena such as level-invariance of sound localization (Sabin, Macpherson, and Middlebrooks, 2005; Miller and Recanzone, 2009; Gai et al., 2013) and spatial stream segregation (Middlebrooks and Onsan, 2012; Middlebrooks and Bremen, 2013). In addition, whereas the differences in the locations of competing signal and masker sound sources have been thought to aid in effective hearing in a complex auditory scene (Cherry, 1953), less is known about the neural mechanisms that are involved. In the sections that follow, I will describe a phenomenon known as “Auditory Scene Analysis” and potentially how the auditory system succeeds in managing complex sound mixtures in order for listeners to effectively listen to sounds of interest in complex acoustic environments. The benefits of spatial hearing for effective listening in complex acoustic environments will also be described, specifically in the form of

"Auditory Stream Segregation". Forward suppression, a precursor or product of stream segregation, is also introduced.

1.2. Auditory Scene Analysis

The acoustic environment is complex and contains a number of sound sources impinging at the ear drums. This complex mixture of acoustic stimuli that surround us form the auditory scene. To extract and pick out a particular sound source from the acoustic environment containing an *a priori* unknown number of sources is a daunting neuro-computational problem; one that is mathematically ill-posed. Nevertheless, the auditory system succeeds in parsing out and recognizing complex sound mixtures. For example, a listener can follow a conversation at a crowded cocktail party, where one is able to correctly parse and follow strings of syllables and words from different talkers. Furthermore, the listener can switch one's attention to the music playing, or even eavesdrop on other conversations. This process of parsing the acoustic environment has been termed auditory scene analysis (ASA) (Bregman, 1990). ASA is thought to rely on the specific properties and characteristics of sound sources, such as their spectral and temporal contents, internal heuristics, spatial location, etc. (reviewed by Moore & Gockel, 2002). When acoustic signals share similar properties, they tend to be grouped and perceived as one "auditory object", or "stream" (i.e., integration). On the other hand, when auditory signals differ along certain property dimensions they will be segregated and consequently be perceived as distinct auditory objects or streams (i.e., segregation). Auditory objects and streams are a computational result of the auditory system's ability to extract, group, and segregate acoustic regularities or irregularities from the acoustic environment. More formally, an auditory object is the perceptual construct of an acoustic sound source (e.g., bird song) and an auditory stream is a sequence of acoustic events (e.g., syllables) that belong to one source. Hearing-impaired listeners have substantial problems with ASA, as current hearing aids and cochlear implants are still not able to adequately disentangle complex auditory mixtures.

1.3. Auditory Stream Segregation

In complex auditory scenes, such as a cocktail party, listeners can disentangle competing sound sequences from multiple sources, a phenomenon known as "stream segregation" (Bregman, 1990). The segregation of streams has been extensively

demonstrated by behavioral (van Noorden, 1979) and electrophysiological (Fishman et al., 2001, 2004; Bee and Klump, 2004; Micheyl et al., 2005) studies of tone-based stream segregation lacking a spatial component. Such studies utilize a sequence of repeating and alternating high and low frequency tones ("...ABAB...", where A and B represent tones with different frequencies) emitted by the same loudspeaker to examine possible perceptual and neural correlates of stream segregation. The overall findings from these tone-based stream segregation studies are largely consistent with each other. Specifically, two factors largely determine stream segregation: 1) frequency separation, where a larger difference between the frequencies of the alternating and competing tones makes it more likely that two discrete streams will be formed, one for each tone sequence; 2) stimulus presentation speed, where a listener is more likely to perceive two discrete streams when the presentation rate of the tone stimuli is increased. These observations are also reflected by responses from cortical neurons (e.g., differences in cortical spikes elicited by each competing sound sequences).

Spatial cues also contribute strongly to stream segregation, particularly for segregating sequences of sounds interleaved in time (Shinn-Cunningham, 2005). A recent study in our lab utilized objective measures to show a robust spatial component in stream segregation (Middlebrooks and Onsan, 2012). In that particular study, listeners were required to discriminate between two rhythmic patterns (target) in the presence of an interleaved competing masker that varied in spatial location. Listeners were unsuccessful at distinguishing the patterns when both target and masker patterns were colocated (i.e., presented from the same free-field speaker). However, when the target and masker were separated by as little as 8° listeners could successfully segregate the patterns and perceptually form two discrete streams, which permitted reliable rhythm discriminations.

Whereas the processing of spatial cues is relatively well understood up to the level of the auditory cortex, considerably less is known about the neuronal processes underlying the role of spatial hearing for stream segregation. As a follow up to the human psychophysics study that demonstrated SSS (Middlebrooks and Onsan, 2012), another study in our laboratory (Middlebrooks and Bremen, 2013) examined a potential cortical correlate of SSS by recording single- and multiple-neuron responses from the

primary auditory cortex (area A1) of anesthetized cats while presenting interleaved broadband noise burst sequences that human listeners would experience as segregated streams. The competing sound sequences alternated between pairs of speaker locations along the frontal horizontal plane (Fig. 1.2). Middlebrooks and Bremen (2013) tested the hypothesis that individual neurons in A1 could segregate sound sequences from sources that are separated in the horizontal plane. They found that when the competing sources were presented across different spatial configurations, responses from cortical neurons preferentially synchronized to one source over the other. Thus, responses from a cortical neuron were captured by one source over the other, thereby displaying a cortical correlate of spatial stream segregation. It is important to note that when competing sources were co-located, their corresponding responses from cortical neurons were roughly equal and about half of that seen compared to responses elicited by a single source from the same location. This reduction in response demonstrates forward suppression, in which responses of the cortical neuron declined with increasing stimulus presentation rate. Furthermore, a cortical neuron's spatial sensitivity sharpened in the competing source condition versus the single source condition. Therefore, forward suppression, and possibly its interaction with a neuron's spatial sensitivity, are possible precursors or products of SSS displayed in the cortex.

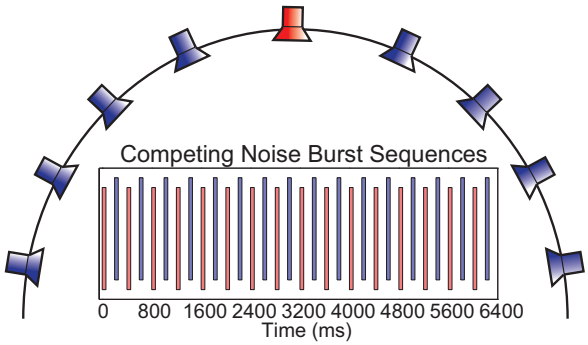

Figure 1.2. Schematic of spatial stream segregation stimuli and speaker arrays. Competing 5-ms broadband noise burst sequences (red and blue vertical bars) alternated between pairs of speakers located along the horizontal plane. In this case, the red sequence ("A source") is presented at the midline speaker, while the blue sequence ("B source") could be presented from any one of the speakers. Note that the competing sequences are interleaved in time and alternate between speaker locations.

The amplification of SSS by forward suppression accords with the differential suppression effects of varying tone frequencies and presentation rates from tone-based

streaming studies (Fishman et al., 2001, 2004; Bee and Klump, 2004). Such studies posit that perceptually segregated streams correspond to partially nonoverlapping populations of neurons that are segregated by tonotopy and enhanced by forward suppression (Bidet-Caulet & Bertrand, 2009). With regards to acoustic space in SSS, location sensitivity derived from binaural computations within the brainstem would substitute tonotopic channels in such a model. Thus, a cortical neuron receives a spatial bias, via brainstem computations, favoring one of the two competing sound sources, that is amplified by forward suppression, which enhances the segregation of streams.

1.4. Potential Mechanisms involved in Generating Spatial Stream Segregation

Forward suppression and the low-pass modulation filter between the auditory cortex and it's subcortical input are possible precursors to SSS and are potentially manifested by intracortical inhibition or synaptic depression/fatigue at the thalamocortical synapse. Cortical neurons are limited in the rate at which they can synchronize to modulated sound waveforms. Specifically, most reports of phase locking to click trains or to amplitude modulated sounds have indicated that driven spike rates peak at "best modulation frequencies" (i.e., stimulus repetition rate that evokes the strongest synchrony of responses) around 8–10 Hz and that little phase locking to modulated sounds is observed for modulation frequencies around 18 Hz or greater among cortical neurons (Gaese and Ostwald, 1995; Kilgard and Merzenich, 1999), whereas the phase-locking limit in subcortical structures is much higher (Joris et al., 2004). For example, the maximum frequencies at which neurons synchronize to stimulus envelopes reaches up to ~100 Hz in the MGB (guinea pig: Creutzfeldt et al., 1980; marmoset: Bartlett and Wang, 2007) and up to 340 Hz in the IC (rat: Rees and Møller, 1987). Thus, subcortical neurons synchronize to much faster repetition rates compared to A1 neurons. These comparisons demonstrate a low-pass modulation filter between the MGB and A1, perhaps due to inhibition occurring within the cortex or at the thalamocortical synapse.

There are a number of hypotheses involving the specific mechanisms of forward suppression. Several lines of evidence suggest that cortical and subcortical circuits contribute to forward suppression in the auditory cortex. For example, forward suppression may involve intracortical GABAergic circuits (Fig. 1.3*A*) or thalamocortical

synaptic depression (Fig. 1.3*B*). Previous studies provide evidence towards an intracortical contribution to forward suppression (Calford & Semple, 1995; Brosch & Schreiner, 1997), potentially involving GABAergic mechanisms. For example, cortical responses are often completely suppressed immediately after a stimulus and that suppression typically lasts ~50 ms (Brosch & Schreiner, 1997). This can be interpreted as evidence that forward suppression of cortical neurons is potentially generated by intracortical mechanisms. Other studies argue that forward suppression in the cortex involves synaptic depression or fatigue along the thalamocortical synapse. A study of forward suppression in the rat auditory cortex that utilized a forward masking paradigm found that inhibitory post-synaptic potentials elicited by maskers did not last longer than 50-100 ms whereas spike responses and synaptic inputs remained suppressed for up to ~100 ms (Wehr and Zador, 2005). Thus, forward suppression on a longer time scale could not be a result of synaptic inhibition from those cortical neurons but involve inhibition from other populations of cells pre-synaptic to those recorded, or synaptic depression. Bayazitov and colleagues (2013) conducted a series of experiments in the mouse auditory cortex that revealed $Ca_v3.1$-dependent synaptic depression at thalamocortical projections contributes to forward suppression in the cortex. Specifically, they found that the paired-pulse synaptic depression at thalamocortical projections lasts for hundreds of milliseconds and is attributable to a switch from burst- to single-firing modes from thalamic neurons. The switch from burst- to single-firing modes directly depends on specific calcium channels that are enriched in thalamic relay neurons. Thus, pharmacologically inhibiting $Ca_v3.1$ T-type calcium channels in the auditory thalamus substantially reduced synaptic depression at the thalamocortical projections and subsequently diminished forward suppression in auditory cortex.

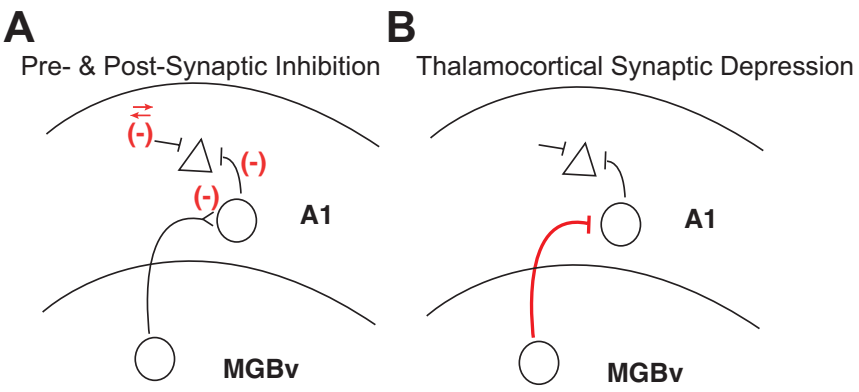

Figure 1.3. Schematic of potential mechanisms of cortical forward suppression. Cortical forward suppression could be due to pre- and/or post-synaptic GABAergic inhibition (*A*) or synaptic depression/ fatigue along the thalamocortical synapse (*B*).

Topics addressed in this dissertation. A central question in auditory neuroscience is how auditory streams are formed in the brain. The goal of this dissertation is to further explore the neural correlates of spatial stream segregation, as well as uncover its cellular mechanism. Whereas cats have been favored as experimental models for spatial hearing research, they are impractical for *in vivo* intracellular and pharmacological experiments. Small rodents like the rat are well-suited for these kind of experimental methods because not only is it amenable to modern intracellular and pharmacological manipulations, the rat also shows good spatial acuity in psychophysical tests, at least across the frontal midline (Heffner and Heffner, 1985; Kavanagh and Kelly, 1986; Ito et al., 1996), its neurons in cortical area A1 show homogeneous patterns of spatial sensitivity (Yao et al., 2013), and its midbrain, thalamic, and cortical structures are readily accessible for study (Yao et al., 2015). Thus, we utilized the rat as a model to compliment the ongoing auditory scene analysis research in humans and cats in our laboratory. In the following three chapters I provide data to further support the overarching hypothesis that spatial stream segregation is enhanced along the ascending auditory pathway and can be attributed to an increase in spatial sensitivity and a decrease in a low-pass envelope filter cutoff between area A1 and its subcortical input. I first present data demonstrating rat A1 neurons display contralateral-hemifield spatial tuning that is largely level-tolerant (Chapter 2). In addition, the characteristics of the rat's sound localization psychophysics are evident in the characteristics of the spatial sensitivity of its cortical neurons. The study in Chapter 3

surveyed the ascending auditory pathways in anesthetized rats to identify the brain level(s) at which level-tolerant contralateral-hemifield spatial sensitivity arises and describes two parallel brainstem pathways for spatial hearing (Chapter 3). The tectal pathway, in which sharp, level-tolerant spatial sensitivity arises between the central nucleus of the inferior colliculus (ICC) and the brachium of the inferior colliculus (BIN), projects to the superior colliculus (SC) and could support reflexive orientation to sounds. The lemniscal pathway, in which sharp, level-tolerant spatial sensitivity arises between the ICC and the ventral division of the medial geniculate body (MGBv), projects to the auditory cortex to support perception of sound location. Finally, I provide evidence that at temporal scales at which SSS is seen behaviorally, neurons in the ICC showed little evidence of SSS, but SSS emerges in the BIN and in about two-thirds of neurons in the MGBv, and spatial stream segregation is ubiquitous in A1 (Chapter 4). Neural SSS seen within the responses of neurons along the ascending auditory pathway reflect increased spatial sensitivity and increased forward suppression. A pharmacological procedure was utilized to examine the potential mechanisms of cortical forward suppression, which demonstrated that cortical forward suppression is not due to synaptic inhibition, but may reflect synaptic depression at the thalamocortical synapse. Taken together, our findings indicate that auditory streams are increasingly segregated along the ascending auditory system as distinct mutually-synchronized neural populations.

CHAPTER 2: Rat Primary Auditory Cortex is Tune Exclusively to the Contralateral Hemifield

This work has been published in J Neurophysiol 110: 2140–2151, August 14, 2013.

2.1 Summary

The rat is a widely used species for study of the auditory system. Psychophysical results from rats have shown an inability to discriminate sound source locations within a lateral hemifield, despite showing fairly sharp near-midline acuity. We tested the hypothesis that those characteristics of the rat's sound localization psychophysics are evident in the characteristics of spatial sensitivity of its cortical neurons. In addition, we sought quantitative descriptions of *in vivo* spatial sensitivity of cortical neurons that would support development of an *in vitro* experimental model to study cortical mechanisms of spatial hearing. We assessed the spatial sensitivity of single- and multiple-neuron responses in the primary auditory cortex (A1) of urethane-anesthetized rats. Free-field noise bursts were varied throughout 360° of azimuth in the horizontal plane at sound levels from 10 to 40 dB above neural thresholds. All neurons encountered in A1 displayed contralateral-hemifield spatial tuning in that they responded strongly to contralateral sound source locations, their responses cut off sharply for locations near the frontal midline, and they showed weak or no responses to ipsilateral sources. Spatial tuning was quite stable across a 30-dB range of sound levels. Consistent with rat psychophysical results, a linear discriminator analysis of spike counts exhibited high spatial acuity for near-midline sounds and poor discrimination for off-midline locations. Hemifield spatial tuning is the most common pattern across all mammals tested previously. The homogeneous population of neurons in rat area A1 will make an excellent system for study of the mechanisms underlying that pattern.

2.2 Introduction

Previous psychophysical studies have evaluated the ability of carnivores, humans, and other primates to identify or discriminate the locations of sounds (e.g., Heffner and Masterton, 1975; Jenkins and Masterton, 1982; Makous and Middlebrooks, 1990; May and Huang, 1996; Nodal et al., 2008; Populin, 2006; Tollin et al., 2005). Generally, these species show highest spatial acuity for locations straddling the frontal

midline, but they also can discriminate locations within a lateral hemifield (Brown et al., 1982; Heffner and Heffner 1988a, 1990; Kavanagh and Kelly, 1987; Middlebrooks and Onsan, 2012; Recanzone et al., 1998; Recanzone and Beckerman, 2004). In rats, spatial acuity around the frontal midline is high like that of other tested animals, but unlike carnivores and primates rats fail to discriminate among lateral locations (Kavanagh and Kelly, 1986).

Results from carnivores and primates indicate that firing patterns of cortical neurons can signal sound source locations throughout most of auditory space (e.g., Middlebrooks et al., 1994, 1998; Miller and Recanzone, 2009). Here we have examined the spatial sensitivity of neurons in cortical area A1 of the rat. We wished to test the hypothesis that the failure of rats to distinguish lateral source locations is mirrored by an absence of off-midline spatial discrimination by responses of cortical neurons. A second motivation was to obtain descriptive data characterizing cortical spatial sensitivity that would support future study of the cortical mechanisms of spatial hearing in a preparation amenable to modern intracellular, optical imaging, and optogenetic methodologies.

Results demonstrated that every sampled neuron displayed a spatial receptive field favoring the contralateral hemifield, that most showed steepest cutoffs within ~20° of the midline, and that all showed weak or no responses throughout most of the ipsilateral hemifield. Contralateral-hemifield spatial tuning is the most common pattern seen in the mammals that have been studied thus far. The presence of a largely homogeneous population of neurons showing such spatial tuning in rat A1 will facilitate future study of the mechanisms that underlie that pattern of spatial tuning.

2.3 Materials and Methods

2.3.1 *Animal Preparation*

Data presented here are from 15 adult male Sprague-Dawley rats (median age: 18.5 wk) (Charles River Laboratories, Hollister, CA) weighing 245–430 g (median weight: 360 g). All procedures were performed with the approval of the University of California at Irvine Institutional Animal Care and Use Committee according to National Institutes of Health guidelines. Surgical anesthesia was induced with urethane (1.5 g/kg ip) and xylazine (10 mg/kg ip) and supplemented at ~1-h intervals as needed to maintain an areflexive state. Atropine sulfate (0.1 mg/kg ip) and dexamethasone (0.25

mg/kg ip) were administered at the beginning of the surgery and every 12 h thereafter to reduce the viscosity of bronchial secretions and to prevent brain edema, respectively. Core body temperature was monitored with a rectal thermometer and maintained at ~37°C with a warm-water heating pad. Respiratory rate, heart rate, and front paw withdrawal reflexes were monitored to ensure that a moderately deep anesthetic state was maintained as uniformly as possible throughout recordings.

A midline incision was made, and the skull was cleared. A flat-head machine screw was fastened to the skull, screw head down, with skull screws and dental acrylic cement. The machine screw was used to support the rat's head. The temporal bone was exposed by partially removing the temporalis muscle. A craniotomy was performed, and the exposed brain was kept moist. Experiments lasted ~6–18 h.

2.3.2 *Experimental Setup and Stimulus Generation*

The experimental setup and stimulus generation techniques used here were similar to those described in earlier reports from this lab (Harrington et al., 2008; Middlebrooks et al., 1998; Middlebrooks and Bremen, 2013; Stecker et al., 2003, 2005a). Stimulus presentation and data acquisition used System 3 equipment from Tucker-Davis Technologies (TDT, Alachua, FL) controlled by a personal computer running custom MATLAB scripts (The MathWorks, Natick, MA). The animal was positioned in the center of a double-wall sound- attenuating chamber, which was lined with 60-mm-thick absorbent foam (SONEXone, Seattle, WA). The rat's head was supported from behind with a 10-mm-diameter rod that was attached to the screw that was mounted to the head. The area around the head and ears was unobstructed. Sounds were presented one at a time from 8.4-cm two-way coaxial loudspeakers (Pioneer Electronics, Long Beach, CA) that were located 1.2 m from the rat's head and spaced 20° apart on the ear-level horizontal plane. Loudspeaker locations are expressed in degrees of azimuth relative to the loudspeaker directly located in front of the rat's head (0°). Negative azimuths were on the left, contralateral to the right-sided recording sites. The loudspeakers were calibrated to flatten and equalize their frequency responses (Zhou et al., 1992). All stimuli were generated with 24-bit precision at a 97.7-kHz sampling rate. Stimuli were 80-ms Gaussian noise bursts with abrupt onsets and offsets or 80-ms pure tones with 5-ms raised-cosine onset/offset ramps.

Noise and tone bursts ranged from –10 to 70 dB SPL and varied in 10-dB steps. Tone frequencies ranged from 1 to 40 kHz.

2.3.3 *Experimental Procedure*

Extracellular spike activity was recorded with single-shank silicon-substrate probes having sixteen 413-μm^2 recording sites spaced at 100-μm intervals (NeuroNexus, Ann Arbor, MI). Neural waveforms were digitized and stored for off-line analysis. The 16-channel probes were positioned with cortical surface landmarks, verified by functional properties described below. The probe was aligned visually to be as orthogonal as possible to the cortical surface prior to advancement into the cortex and subsequently was adjusted in depth to maximize the number of recording sites in active cortical layers. Typically, neural spike activity was limited to 12–14 sites, with the most superficial and the deepest 1 or 2 sites lying outside of the cortical gray matter. Neural spikes were detected online for monitoring purposes, although all reported results are based on spikes that were identified off-line, as described in *Data Analysis*. At each recording probe location, the characteristic frequencies (CFs) of neurons were estimated with pure tones. Cortical area A1 was distinguished from neighboring auditory areas by brisk short- latency responses to noise bursts (latencies ~10–15 ms), V-shaped frequency tuning curves, and a caudal-to-rostral increase in CFs (see, e.g., Polley et al. 2007; Sally and Kelly 1988). The borders of A1 were defined by reversals in tonotopy and increases in latencies (Doron et al., 2002; Rutkowski et al., 2003). After a probe was positioned in A1 at a desired position in the tonotopic map, the cortex was covered with warmed 2% agarose in Ringer solution. The agarose cooled to form a gel that reduced brain pulsations and kept the cortical surface moist. Frequency response areas (FRAs) were measured with pure tones presented at a rate of 1/s from the loudspeaker at –40°. The tones varied in frequency in 1/6-octave steps from 1 to 40 kHz and in level in 10-dB steps, typically from 0 to 60 or 70 dB SPL, 10 repetitions at each combination of frequency and level. Off-line, the CF of each unit was defined by the frequency that evoked a reliable response that was significantly greater than spontaneous activity at the lowest sound level.

The spatial sensitivity of each unit was measured with a stimulus set that consisted of 80-ms noise bursts presented at a 1/s repetition rate from 18 locations in the horizontal plane (–180° to 160°, in 20° increments), varying in 10-dB level steps, typically from 0 to 60 or 70 dB SPL, with 15–40 repetitions per level. A silent condition also was included for the purpose of measuring spontaneous activity. Sounds at every combination of location and level were presented once in a random order during each repetition. Collection of the data reported here was accomplished in ~2.5 h at each recording probe placement. Experiments yielded data from one to five probe placements per animal.

2.3.4 *Data Analysis*

Spike sorting. Neural action potentials were discriminated on the basis of waveform shapes with off-line spike-sorting procedures (Kirby and Middlebrooks, 2010; Middlebrooks, 2008). Of the 168 units studied, 18 (11%) were classified as well-isolated single units and 150 (89%) consisted of unresolved spikes from two or more neurons. We did not observe differences between tuning properties calculated from the single units or multiunits across any measure of spatial sensitivity at any suprathreshold level (K = 0.14–0.33, P = 0.11–0.95, 2-sample Kolmogorov-Smirnov test) and therefore use the term “unit” to refer to both. The unit count did not include the small number of units that were excluded from the analysis because they responded with less than an average of one spike per trial to their most effective stimulus or with a maximum spike rate less than 2 standard deviations above their spontaneous rates. Spike times were stored as latencies relative to the estimated time of arrival of sound at the animal’s head, i.e., stimulus onset was taken as the time of onset of sound at the loudspeaker plus the 3.5-ms acoustic travel time from each loudspeaker to the location of the center of the rat’s head. Most responses to noise bursts consisted of bursts of spikes restricted to a range of >10 to ~40 ms after stimulus onset. Spikes were counted in the 10- to 80-ms interval after the onset of each stimulus.

Discrimination of sound source locations with a linear discriminator model. We used procedures based on signal detection theory (Green and Swets, 1966; Macmillan and Creelman, 2005) to estimate excitation thresholds and thresholds for discrimination between pairs of stimulus locations. In both cases, we accumulated spike counts for all

repetitions of each of two stimuli. An empirical receiver operating characteristic (ROC) curve was formed from those two distributions. The area under the ROC curve gave the proportion of trials in which a particular stimulus elicited more spikes than the other stimulus. That proportion was expressed as a *z* score, and the *z* score was multiplied by $\sqrt{2}$ to yield the discrimination index, *d′* (Green and Swets, 1966; Macmillan and Creelman, 2005; Middlebrooks and Snyder, 2007). When the area under the ROC curve was 1.0 (and the corresponding *z* score was undefined), *d'* was written as 2.77, corresponding to 97.5% correct discrimination. Magnitudes of *d'*, therefore, could range between 0 (chance-level discrimination) and 2.77. A *d'* value of 1 indicates a one-standard deviation separation of the means of the two distributions and is conventionally taken as the criterion for significant discrimination of two stimuli.

Excitation thresholds were estimated by computing *d'* for successive increasing pairs of noise burst levels, plotting *d′* versus sound level, and taking as threshold the interpolated sound level at which $d' = 1$. Spatial discrimination thresholds were estimated by specifying a reference sound source location, computing *d′* for successively increasing sound source separations, and interpolating with 1° resolution to find the separation at which $d' = 1$. The minimum discriminable angle (MDA) was the minimum discrimination threshold for each unit observed across all reference locations. We also report the maximum *d′* for each unit across all pairs of locations. The maximum *d′* provides an indicator of the overall spatial sensitivity of a unit and has the advantage of incorporating both the stimulus-dependent mean and the trial-by-trial variance in maximum and minimum spike counts. A closely related measure is "modulation depth," which is $100 \times (\mathrm{Spk}_{\mathrm{max}} - \mathrm{Spk}_{\mathrm{min}})/\mathrm{Spk}_{\mathrm{max}}$ for maximum and minimum spike counts $\mathrm{Spk}_{\mathrm{max}}$ and $\mathrm{Spk}_{\mathrm{min}}$. We report modulation depth in addition to maximum *d′* because modulation depth can be compared with a similar metric used in previous reports and because modulation depth provides a somewhat more intuitive measure of spatial sensitivity than maximum *d′*.

Locations of centroids and steepest slopes. The preferred stimulus location of each unit was characterized by its spatial centroid (Middlebrooks et al., 1998), which was computed as follows. First, the peak of the rate-azimuth function (RAF) was

identified by finding the range of one or more contiguous locations at which responses exceeded a criterion spike rate of 0.75 times the maximum spike rate. Then, the spike rate-weighted vector sum was computed from these peak locations plus the two flanking below-criterion locations (i.e., from a total of 3 or more locations). The angle of the resultant vector gave the spatial centroid. Units showing no more than 50% modulation of their spike rates throughout all tested locations were classified as having no centroid (NC).

The location of the steepest slope for each unit was determined by smoothing its RAF (circular convolution with a 40° boxcar). Slopes were given by the first spatial derivative of the smoothed RAF. We identified the location at which the slope magnitude was maximal.

Equivalent rectangular receptive field. The spatial tuning of each unit was represented by the width of its equivalent rectangular receptive field (ERRF). The ERRF was computed by integrating the area under the RAF and reshaping it to form a rectangle of equivalent peak rate and area (see Supplementary Fig. 1 in Lee and Middlebrooks, 2011). The ERRF width was favored over more conventional measures of tuning width because it reflects both the breadth of tuning and the depth of location-dependent spike rate modulation. Also, ERRF widths are computed from responses to all stimulus locations. For that reason, they are less sensitive to trial-by-trial response variability than metrics that are based on particular criteria on RAFs (e.g., tuning width at half-maximal response).

Tests of statistical hypotheses. Data analysis employed custom MATLAB scripts (The MathWorks), incorporating the MATLAB Statistics Toolbox when appropriate. Multiple comparisons used the Bonferroni correction. Data sets for most measures were not normally distributed across units. For those measures, median and interquartile values were reported and nonparametric statistical tests were used for comparison across/between conditions. Distributions of ERRF widths were normally distributed, however, permitting characterization by means ± SE and parametric statistical tests. To test for statistically significant correlations between the spatial sensitivity measures with CF, we performed a Spearman rank correlation analysis on the data set with 10,000 bootstrapped replications. For each replication we randomly drew with

replacement 10 units per 1-oct CF bin from the sampled population. From these distributions of Spearman rank correlation coefficients (ρ) empirical two-tailed 98.75% confidence intervals (CIs) were calculated. A statistically significant relationship between CF and the tested metric at $P < 0.05$ (Bonferroni corrected for tests at 4 sound levels) was determined if zero fell outside the 98.75% CI.

2.4 Results

Data were obtained from 168 units recorded from 22 probe placement sites in 15 animals. Across the sample, CFs ranged from 1 to >40 kHz (median = 14.3 kHz, interquartile range = 8.5–32 kHz); 10th and 90th percentiles were 4 and >40 kHz. The 15% of units that showed minimum thresholds at 40 kHz, the highest frequency that was tested, were designated as having CFs ">40 kHz" because we assume that a higher CF would have been seen had we tested at a higher frequency. The FRA of one unit with a CF of 14.3 kHz is shown in Fig. 2.1*A*. The response pattern of this unit to noise bursts presented at 40 dB above threshold and varying in azimuth is represented by a dot raster plot in Fig. 2.1*B*. This unit was representative of the entire sample in that it responded phasically to the onset of a noise burst and most strongly and with shortest latencies to sounds in the contralateral hemifield. Across the population of units, first-spike latencies for the most effective stimuli ranged from 10 to 15 ms (median = 12.5 ms).

2.4.1 *Characteristics of Spatial Tuning*

Spatial tuning is summarized in Fig. 2.1, *C* and *D*, for the unit represented in Fig. 2.1, *A* and *B*. At the highest sound level that was tested (40 dB above threshold), this unit had a centroid of –74°, steepest slope at –1°, an ERRF width of 200°, a modulation depth of 75%, and a maximum d' of 2.66. Those values were comparable with the median or mean values across the population at 40 dB above threshold (centroid median: –69.8°, steepest slope location median: –1°, ERRF width mean: 195.9°, modulation depth median: 83%, maximum d' median: 1.57).

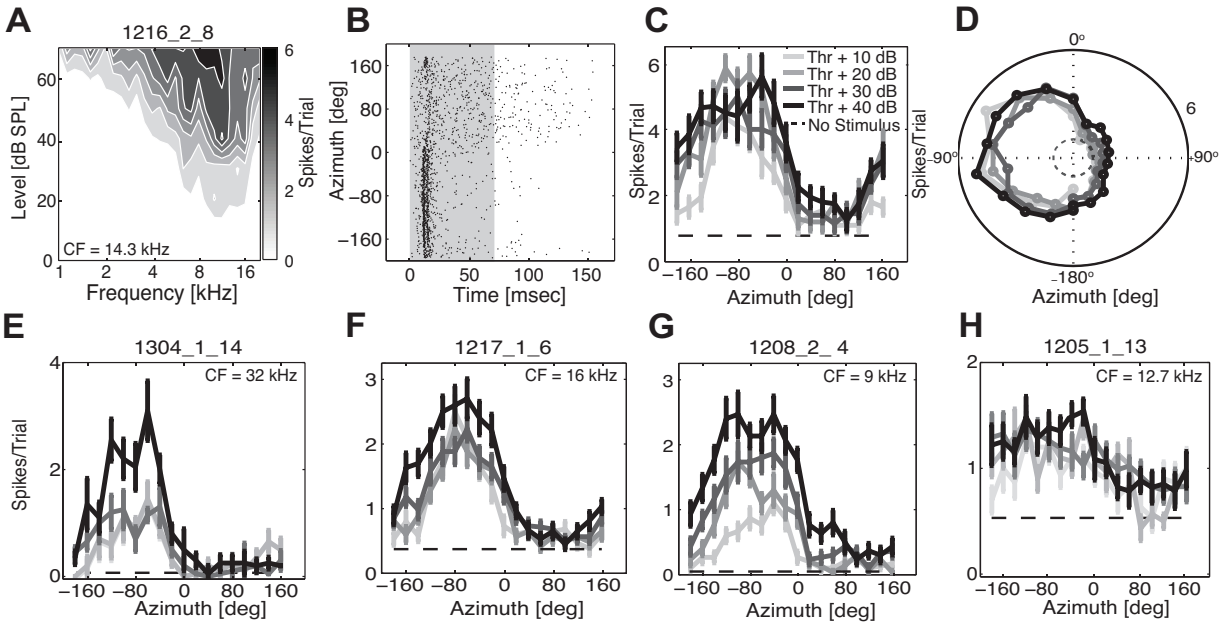

Figure 2.1. Examples of neural responses in rat A1. *A–D:* One example unit. *A:* Contour plot of the frequency response area (FRA) plotted as the average spike count per trial in response to pure-tone stimulation varying in frequency (x-axis) and sound level (y-axis). Dark colors indicate high spike rate. *B:* Dot rasters of spike times (x-axis) elicited by noise stimuli at 40 dB above the unit's threshold, varying in azimuth (y-axis). Each dot in the plot represents one spike. Gray shading represents the stimulus duration. *C:* Rate-azimuth-functions (RAFs) of mean spike count per trial plotted against stimulus azimuth locations at levels 10, 20, 30 and 40 dB above threshold. *D:* The same responses from *C,* re-plotted in polar coordinates. *E–H:* RAFs from 4 additional units that represent the range of spatial tuning among cortical units with sharp spatial tuning (*E*) to slightly broad spatial tuning (*H*). Darker shades of grey represent higher stimulus levels above threshold. Dashed black lines represent spontaneous rate. Error bars indicate standard error of the mean. CFs are indicated for each example unit.

The overall range of sharpness of spatial tuning is well represented by the RAFs of four units shown in Fig. 2.1, *E–H*. These examples are ranked from the unit showing the narrowest ERRF width (102°; Fig. 2.1*E*) to the unit having the broadest ERRF width (289.5°; Fig. 2.1*H*). The three units shown in Fig. 2.1, *E–G*, all possessed steepest slopes located around the frontal midline, and all showed maximum d' values > 2. The most broadly tuned unit of the sample (Fig. 2.1*H*), in contrast, had maximum d' values < 1 at all tested sound levels and a modulation depth < 50% at the highest tested sound level (40 dB above threshold). Although this unit did not possess a spatial centroid at this level, it showed the same general RAF shape as those of the other units. The other example units had centroids located in the contralateral field, toward the lateral pole. The similarity among the five example units in Fig. 2.1 and the entire population of sampled units indicates that the distribution of spatial tuning among units in rat area A1 was remarkably homogeneous, with RAFs consistently centered near the contralateral

pole of the sound field, encompassing the contralateral hemifield, and steepest slope locations near the midline. Consistent with previous reports (e.g., Middlebrooks and Pettigrew, 1981), we refer to this as “contralateral-hemifield” tuning.

The distributions of preferred azimuth locations (“centroids”) and steepest slope locations are depicted in Fig. 2.2. Large majorities of units (100%, 99%, 97%, and 94% at 10, 20, 30, and 40 dB above threshold, respectively) had modulation depths ≥ 50%, and therefore had measurable centroids. The < 6% of units that had modulation depths < 50% responded with more than half of their maximum spike rates to sound sources throughout 360° of azimuth—those units are indicated as “NC” (for “no centroid”) in Fig. 2.2. Every unit preferred contralateral locations, toward the contralateral pole, regardless of stimulus level (Fig. 2.2, *A–D*: centroid medians: –75.4°, –75.1°, –76.3°, and –69.8°; interquartile ranges: –91.2° to –56.5°, –96.6° to –57.4°, –100.5° to –58.3°, and –95.2° to –55.9° at 10, 20, 30, and 40 dB above threshold, respectively), whereas the borders of the receptive fields, represented by steepest slope locations, were clustered around the frontal midline (Fig. 2.2, *E–H*: steepest slope medians: –1°, –1°, –1°, and –1°; interquartile ranges: –41° to 1°, –21° to 14°, –21° to 13°, and –21° to 9° at 10, 20, 30, and 40 dB above threshold, respectively). The distributions of centroids and steepest slope locations showed no significant differences across sound levels of 10, 20, 30, and 40 dB above threshold (centroids: $X^2_{(3,651)} = 2.01$, $P = 0.57$, Kruskal-Wallis; steepest slope locations: $X^2_{(3,668)} = 4.97$, $P = 0.17$, Kruskal-Wallis), indicating that the sampled population of units maintained their basic tuning properties across a 30-dB range of levels.

The breadth of spatial tuning of each unit was represented by the width of its ERRF (see MATERIALS AND METHODS). The distributions of ERRF widths from the sampled population of units and across suprathreshold levels are shown in Fig. 2.3*A*. ERRF width means (±SE) at 10, 20, 30, and 40 dB above thresholds were 161.3° (±3.7°), 178.5° (±3.3°), 194.3° (±3.3°), and 195.9° (±3.2°), respectively. The spatial tuning broadened slightly with increasing sound level ($F_{(3,668)} = 22.73$, $P < 10^{-6}$, ANOVA), with Bonferroni-corrected pair-wise comparisons indicating significant broadening from 10 to 20, 30, and 40 dB above threshold as well as 20 to 30 and 40 dB

above threshold ($P < 0.05$), as indicated in Fig. 2.3*A*. The only nonsignificant difference in ERRF width was between 30 and 40 dB above threshold.

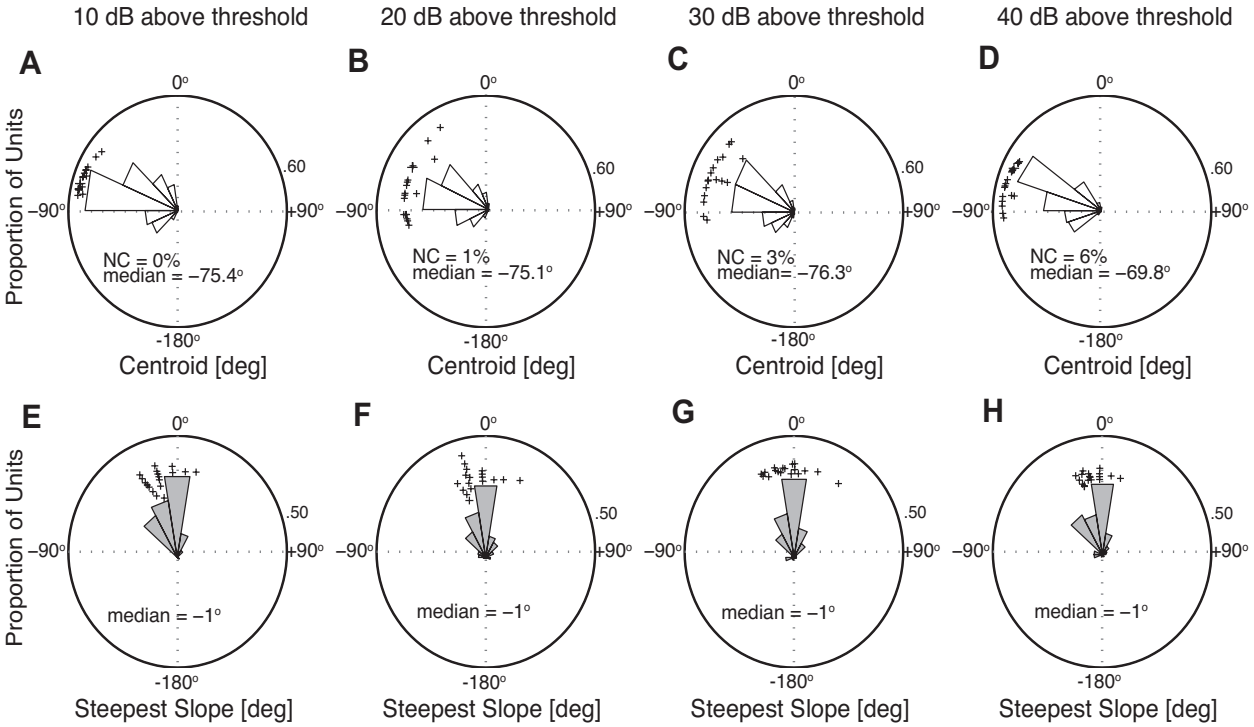

Figure 2.2. Distributions of azimuth centroids (*A–D*) and steepest slope locations (*E–H*) for noise burst stimuli presented at the stated sound levels. The area of each sector gives the proportion of units per 20° bin for centroids and steepest slope locations. Crosses represent data from well-isolated single-units; radial distances of crosses are varied to improve readability. Plots are shown from an overhead perspective with 0° directly in front of the animal (frontal midline), –180° directly behind the animal, and –90° (+90°) on the left (right) of the animal. The percentage of units with no centroid ("NC") and median values are given in the appropriate panels.

The magnitude of spatial sensitivity was represented by the depth of modulation of spike rate by azimuth (see MATERIALS AND METHODS) and by the maximum *d′* across all location pairs for each unit. Figure 2.3*B* displays the distribution of modulation depths at 10, 20, 30, and 40 dB above threshold, with medians of 93%, 90%, 86%, and 83% (interquartile ranges: 81–99%, 78–96%, 72–94%, and 71–90%), respectively. Modulation depth showed a small, but significant, decrease with increasing stimulus level ($X^2_{(3,668)} = 29.88$, $P < 10^{-6}$, Kruskal-Wallis). Bonferroni-corrected pairwise comparisons indicated significant differences between 10 and 30 dB above threshold, 10 and 40 dB above threshold, and 20 and 40 dB above threshold ($P < 0.05$), as indicated in Fig. 2.3*B*. Maximum *d′* values were level invariant ($X^2_{(3,668)} = 0.40$, $P = 0.94$,

Kruskal-Wallis), with medians of 1.55, 1.62, 1.57, and 1.62 (interquartile ranges: 1.03–2.34, 1.12–2.33, 1.05–2.10, and 1.17–2.17) at 10, 20, 30, and 40 dB above threshold, respectively (Fig. 2.3*C*). Maximum *d′* was ≥ 1 for 75%, 80%, 75%, and 82% of units at 10, 20, 30, and 40 dB above threshold, respectively. Overall, the great majority of units in the sample showed robust, level-invariant, contralateral-hemifield spatial tuning.

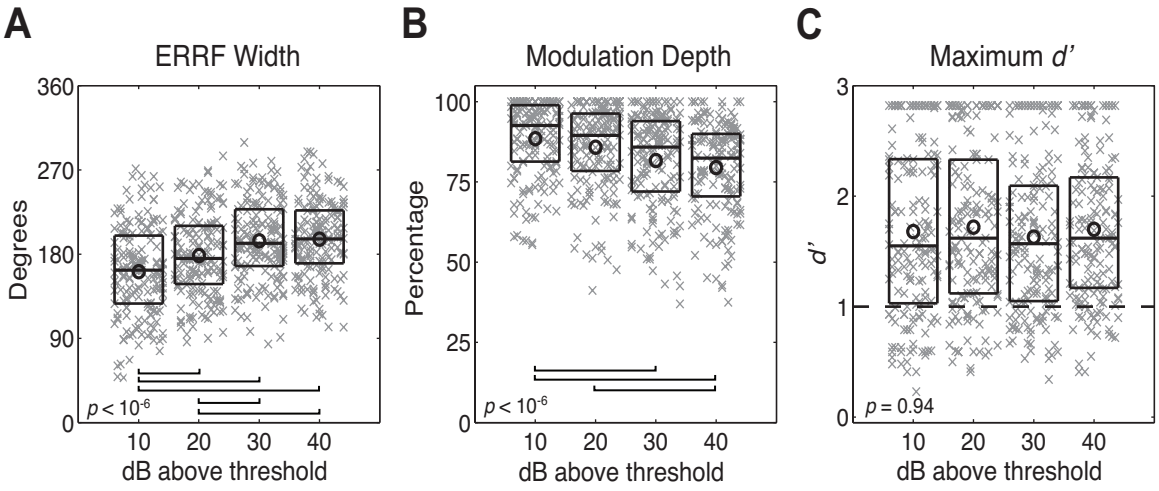

Figure 2.3. Distributions of ERRF width (*A*), modulation depth (*B*), and maximum *d′* (*C*). For each box plot, horizontal lines forming the boxes indicate the 25th, 50th, and 75th percentiles. Symbols ("x") indicate data from individual units, and circles represent the means. A random horizontal offset was added to each symbol to minimize overlap. The *p*-values shown in each panel indicate results of analysis of variance (A) or Kruskal-Wallis (B–C) tests. Horizontal bars in the bottoms of panels A and B indicate pairs of levels showing significant differences at the Bonferroni-corrected $p < 0.05$ level. In panel C, the horizontal dashed line indicates discrimination threshold of $d' = 1$.

2.4.2 *Discrimination Between Azimuth Locations by Spike Count*

We tested the accuracy with which a linear discriminator could distinguish between azimuth locations on the basis of trial-by-trial distributions of spike counts (as described in MATERIALS AND METHODS). The matrices in Fig. 2.4, *A* and *B*, show, for one unit, *d′* for discrimination of every pair of locations at levels of 20 dB (Fig. 2.4*A*) and 40 dB (Fig. 2.4*B*) above threshold. Values of $d' \geq 1$ indicate significant discrimination between the compared spatial locations. Significant discriminations generally were high for comparisons between lateral hemifields (i.e., upper left and lower right quadrants in Fig. 2.4, *A* and *B*). In contrast, discriminations were relatively poor, as reflected by low *d′* values, for comparisons within a hemifield (i.e, upper right and lower left quadrants in Fig. 2.4, *A* and B). The differences among within- and between-hemifield location

discriminations are summarized in Fig. 2.4*C* across all units by the white and gray boxes, respectively. For all suprathreshold levels, pairwise comparisons between left and right hemifields yielded significantly higher *d′* values than for comparisons within hemifields ($Z = 39.3$, 45.2, 51.7, and 51.8, $P < 10^{-6}$, Wilcoxon rank sum at all suprathreshold levels). Note that while population median and mean values for between-hemifield comparisons were below $d' = 1$, many location pairs for individual units exhibited values well above 1.

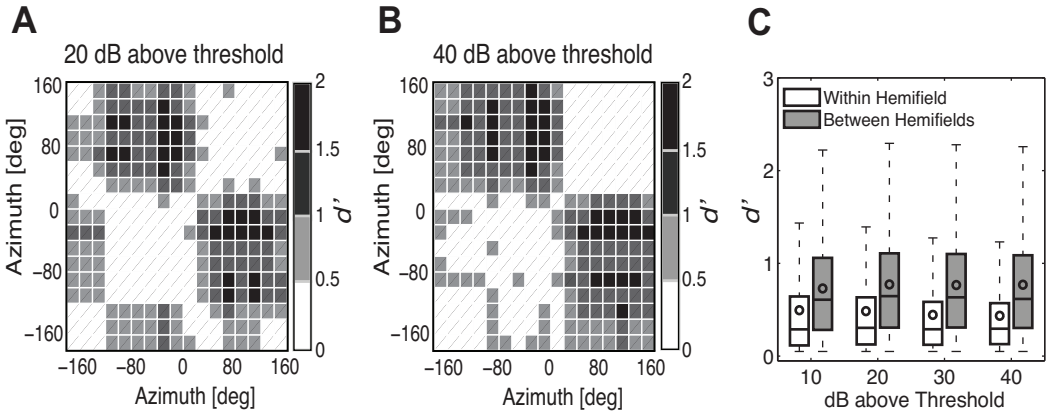

Figure 2.4. Pairwise *d′* matrices for corresponding pairs of stimulus locations for one example unit at 20 dB (*A*) and 40 dB (*B*) above threshold. Stimulus locations were separated by 20°. Darker colors signify higher *d′* values. Pair-wise location comparisons with *d′* values ≥ 1 indicate successful discrimination. *C*: Distribution of all pair-wise location comparison *d′* values from all sampled units. Each box plot displays the distribution of *d′* values for *within* (white) and *between* (gray) hemifield location comparisons across suprathreshold levels, as indicated. Horizontal lines indicate the 25th, 50th, and 75th percentile. Whiskers represent 1.5 times the interquartile range. Circles within the boxes indicate the means.

We estimated the spatial acuity of all units by finding the threshold sound source separation at which *d′* was ≥ 1. Figure 2.5, *A–D*, display the distribution of threshold separations as a function of each reference location in the frontal field. In this plot, each data point represents the smaller of the threshold spatial separations to the left and right of the reference location. For each suprathreshold level, separation thresholds varied significantly across reference locations ($X^2_{(8,857)} = 199.5$, $X^2_{(8,911)} = 201.7$, $X^2_{(8,857)} = 164.9$, $X^2_{(8,895)} = 178.7$, $P < 10^{-6}$, Kruskal-Wallis), with near-midline locations (0° and ±20°) showing significantly lower separation thresholds than locations within either lateral field (±40°, ±60°, and ±80°) (post hoc multiple comparison, Bonferroni corrected:

$P < 0.05$). For each unit, the MDA was given by the narrowest threshold separation observed across all reference source locations. Distributions of MDA, across all units, are shown in Fig. 2.5, *E–H*, at each indicated suprathreshold level. Median MDAs at all suprathreshold levels were within the range of 35–40° (interquartile range: 20–67°), with no significant difference across sound levels ($X^2_{(3,511)} = 1.72$, $P = 0.63$, Kruskal-Wallis). As an indication of the acuity of the most sensitive units, the 10th and 25th percentiles of MDAs ranged from 15° to 16° and from 20° to 25°, respectively, across all levels and CFs sampled.

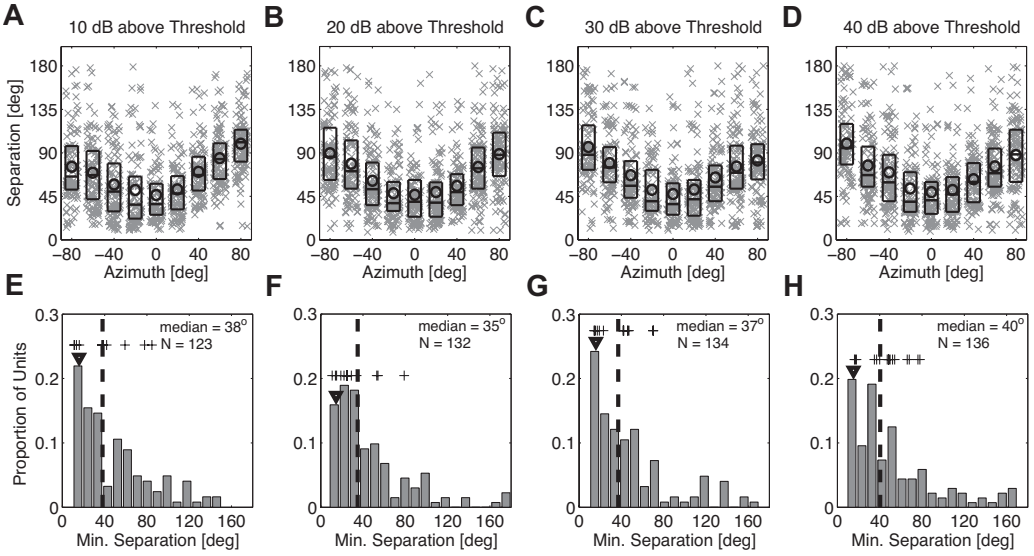

Figure 2.5. *A–D:* Distribution of minimum separation thresholds (y-axis) as a function of a reference azimuth location in the frontal field (x-axis) across suprathreshold levels. Each symbol ("x") represents a data point from one unit. Details regarding plot format are as described for Fig. 3. *E–H:* Distribution of MDA values across all units. Values on the y-axis give the total proportion of units per 10° bin. Vertical dashed lines indicate the medians. Downwards arrowheads indicate the 10th percentiles. Crosses represent data from well isolated single-units. Median values and total number of units ("N") are indicated in the appropriate panels. Each column represents a specific level above threshold, as indicated.

2.4.3 *Spatial Sensitivity of First-Spike Latencies*

Rat area A1 units exhibited spatial sensitivity of their first-spike latencies. Figure 2.6, *A–D*, plot the grand means of first- spike latency corresponding to all sound source locations for all sampled units at the indicated suprathreshold level. Generally, first-spike latencies were shorter for sound source locations in the contralateral field, with the steepest location- dependent increases in latency occurring across the frontal midline. This is inversely related to the higher spike rate responses to contralateral sounds

(normalized grand means, Fig. 2.6, *E–H*). This inverse relationship was quantified by computing the Spearman ρ between normalized spike rate and first-spike latencies for each unit across all tested sound locations. The distributions of those coefficients are shown in Fig. 2.6, *I–L*. At each suprathreshold level, units demonstrated a strong negative correlation of first-spike latency and spike count (median ρ = –0.62, –0.63, –0.67, and –0.67; inter- quartile ranges: –0.79 to –0.38, –0.81 to –0.22, –0.82 to –0.44, and –0.83 to –0.47 for 10, 20, 30, and 40 dB above threshold, respectively).

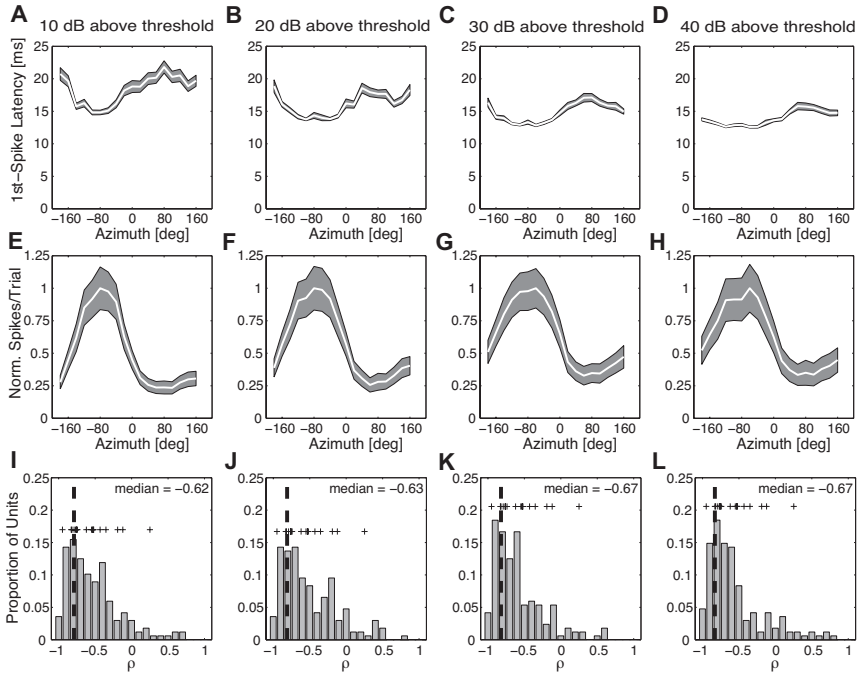

Figure 2.6. *A–D*: Grand mean first-spike latencies as a function of azimuth sound location across suprathreshold levels, as indicated. *E–H*: Grand mean spike rates (normalized spikes per trial) as a function of azimuth sound location across suprathreshold levels. White curves and shading in panels A–H indicate means and standard errors of the mean, respectively. *I–L*: Distributions of Spearman rank correlation coefficients (ρ) between first-spike latency and spike count from all sampled units across suprathreshold levels. Values on the y-axis give the total number of units per bin of 0.10 on the x-axis. Vertical dashed-line indicates the median. Crosses represent data from well isolated single-units.

The strong correlations between first-spike latency and spike count suggest that the information conveyed by response latency is redundant with, or supportive of, the information conveyed by the modulation and distribution of spike counts. We further tested this notion by comparing the accuracy with which units could discriminate between azimuth locations on the basis of first-spike latency to spike count-based discriminations. Direct comparisons of MDAs for each unit on the basis of spike count

versus first-spike latency are shown in Fig. 2.7, *A–D*, at 10, 20, 30, and 40 dB above threshold. Depending on the sound level, MDAs based on spike counts were 11.5–20.5° (medians) narrower than those based on latency; the difference was significant at all sound levels after Bonferroni correction ($Z = -5.98$, -6.60, -5.12, and -4.89, $P < 10^{-6}$, Wilcoxon rank sum), as indicated in Fig. 2.7. Although this indicates that azimuth discrimination based on first-spike latencies was not as acute as that seen on the basis of spike count (Fig. 2.4), we note that spike counts and first-spike latencies shared the property that discrimination acuity was finer between hemifields than within a hemifield.

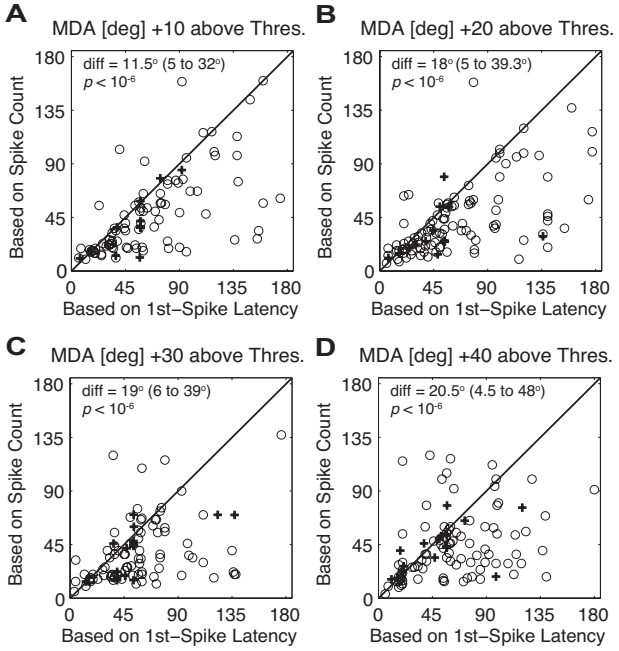

Figure 2.7. *A–D*: Comparison of MDAs based on spike count (y-axis) versus that based on first-spike latency (x-axis) for each unit at various levels above threshold, as indicated. The solid diagonal line indicates equal MDA derived from both measures. Median and interquartile range of the differences and *p*-values for pairwise comparisons are indicated within each panels. Crosses and circles represent data points from well isolated single- and multi-units, respectively.

2.4.4 *Frequency Independence of Spatial Tuning Properties*

Our sample of unit CFs ranged from 1 to >40 kHz (>5 octaves), with half of the sample between 8.5 and 32 kHz; the upper boundary of the sample was determined by the calibrated frequency range of our speakers. For reference, the rat's behavioral audiogram shows greatest sensitivity from 8 to 40 kHz, thresholds within a ~25-dB range from 1 to 40 kHz, and thresholds increasing sharply at frequencies <1 kHz and

>40 kHz (Heffner et al., 1994; Heffner and Heffner, 2007; Kelly and Masterton, 1977). Scatterplots of spatial tuning metrics at 40 dB above threshold as a function of corresponding unit CF are shown in Fig. 2.8. As described in MATERIALS AND METHODS, we performed a Spearman rank correlation analysis with 10,000 bootstrapped replications in order to test for statistically significant correlations between spatial tuning metrics and CF. Across all tested levels, only the data at 40 dB above threshold showed slight but significant correlations of more contralateral steepest slope location and narrower ERRF width with increasing CF (steepest slope locations: CI = [–0.79 –0.09], $P < 0.05$; ERRF widths: CI = [–0.72 –0.03], $P < 0.05$; Spearman rank correlation; Bonferroni-corrected for tests at 4 sound levels). No significant correlation existed for steepest slope location and ERRF width at 10-, 20-, or 30-dB levels or for any other spatial tuning metric at any tested level ($P > 0.05$; Spearman rank correlation; Bonferroni-corrected for tests at 4 sound levels). This indicates that the spatial tuning properties of neurons in rat area A1 are largely frequency independent across the rat's audible range.

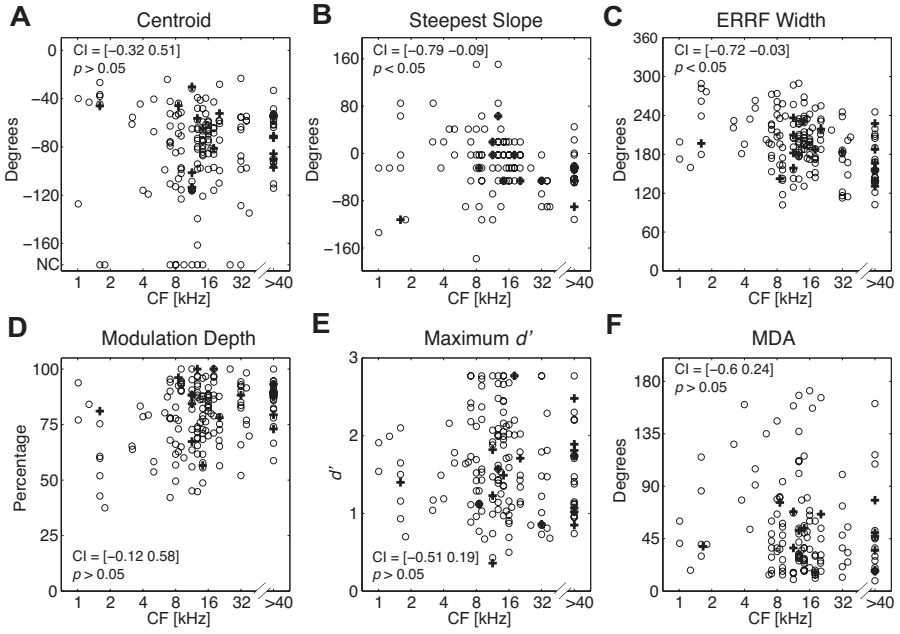

Figure 2.8. Spatial tuning metrics as a function of units' characteristic frequencies (CF; kHz). Each panel displays a scatter plot of a spatial tuning metric (*A*: Centroid. *B*: Steepest Slope. *C*: ERRF width. *D*: Modulation Depth. *E*: Maximum *d'. F*: MDA) at 40 dB above threshold on the y-axis as a function of corresponding unit CF on the x-axis. Crosses and circles represent data points from single- and multi-units, respectively. Empirical two-tailed 98.75% confidence intervals (CIs) from the bootstrapped

distribution of Spearman rank correlation coefficients and corresponding *p*-values are indicated within each panel.

2.5 Discussion

2.5.1 *Spatial Representation in Rat Primary Auditory Cortex*

The present results demonstrate that neurons in rat area A1 display contralateral-hemifield tuning across a 30-dB range of suprathreshold sound levels. The distribution of spatial tuning is homogeneous, showing little systematic variation across the sample of units within area A1. A linear discriminator based on either spike count or first-spike latency demonstrated that cortical units discriminate best between pairs of locations from opposing hemifields and show little or no discrimination among pairs of locations that were both within a lateral hemifield. Spatial acuity is greatest for pairs of locations that straddled the frontal midline.

The present study of the spatial sensitivity of neural spikes complements a recent study by Chadderton and colleagues (2009) that focused on the spatial sensitivity of excitatory postsynaptic potentials (EPSPs) in urethane-anesthetized rats. In that study, neural EPSPs tended to respond to sounds presented throughout the range of ±78.75° of azimuth that was tested. The majority of units showed maximum EPSP amplitudes in response to contralateral sound sources, but a minority of units showed maximum EPSP amplitudes in response to central or ipsilateral locations. The EPSPs of all studied units, however, showed fastest EPSP rise times for contralateral sounds. In a small subset of neurons for which spatial tuning was measured for both EPSPs and spiking, spike latencies and variability of latencies tended to decrease with increasing EPSP rise times, meaning that, for those neurons, contralateral sound sources elicited the most reliable responses.

We are aware of no other detailed studies of spatial sensitivity of spiking activity of cortical neurons in the rat. There have been, however, studies of cortical representation of interaural differences in sound pressure level (ILD), which probably are the principal acoustic cue for horizontal sound location in the rat; we note that rats apparently cannot distinguish the locations of low-frequency tones, for which interaural time differences would be the principal cue (Wesolek et al., 2010). Kelly and Sally (1988) mapped the topographic distribution in rat area A1 of units showing various

patterns of sensitivity to ILD. Some 42.2% of units showed suppression of responses by ipsilateral stimulation at all contralateral levels, and 18.5% showed “mixed” responses that included ipsilateral suppression at moderate levels. Both of those unit classes, totaling 60.7%, responded best to ranges of ILD that would be produced by contralateral free-field sound sources. It is more difficult to predict the spatial preference of the 35.3% of units that showed summation of contra- and ipsilateral inputs. Higgins and colleagues (2010) studied the ILD sensitivity of multiple-unit clusters in rat area A1 and reported that all recordings showed preference for ILDs favoring the contralateral side. The finding that the majority (or all) of units in the rat prefer contralateral-favoring ILDs contrasts with results of similar studies in the cat (Imig and Adrian, 1977; Middlebrooks et al., 1980), in which only about one-third of the samples of area A1 showed suppressive responses. The lower incidence of ipsilateral suppression in the cat is reflected in a lower incidence of neurons showing contralateral spatial receptive fields. In one study in the cat, for instance (Middlebrooks and Pettigrew, 1981), only 48% of units showed contralateral (“hemi-field” and “axial”) spatial tuning, and 52% showed “omnidirectional” tuning, which likely would have been scored as “no centroid” in the present study.

Koka and colleagues (2008) measured the horizontal location dependence of ILD in the rat. Consistent with the small size of the rat’s head, ILDs were small at frequencies < 5 kHz. Maximum ILDs, and the rate of change of ILD with sound source distance from the midline, increased systematically with frequency up to ~20 kHz, beyond which the patterns became more complicated. On the basis of those results, one might have expected the sharpness of spatial sensitivity of rat cortical units to increase with CF increasing between at least 5 and 20 kHz. The present results do not support that expectation. Although we found statistically significant negative correlations between steepest slope location and ERRF width with CF for stimuli 40 dB above threshold, we found no such correlation for any other spatial sensitivity metric or for steepest slope location or ERRF width at lower levels. We note that the analysis by Koka and colleagues (2008) computed ILDs within 0.12-oct bandwidths, which were substantially narrower than the FRAs of rat A1 units (e.g., Fig. 2.1*A*). The broader physiological bandwidths might have blunted the frequency dependence seen in the

acoustical measurements. Also, it might be the case that the ILD cues that are available to the rat around 5 kHz are sufficient to support the contralateral-hemifield spatial tuning that we have observed. Any additional sharpening of spatial tuning resulting from sharper spatial ILD dependence might have been obscured by the overall between-neuron variance in spatial tuning. The present auditory cortex data suggest that the rat should be able to use a broad range of frequencies equally well for localization and discrimination across the midline.

2.5.2 *Species Differences in Cortical Representation of Acoustic Space*

The homogeneity and level invariance of spatial tuning seen in rat area A1 contrast with the diversity of spatial tuning that has been described in area A1 of carnivores and primates, in both anesthetized conditions (cat: Brugge et al., 1996; Harrington et al., 2008; Imig et al., 1990; Middlebrooks and Bremen, 2013; Middlebrooks and Pettigrew, 1981; Rajan et al., 1990; Stecker et al., 2003, 2005a; ferret: Mrsic-Flogel et al., 2003, 2005; Nelken et al., 2005) and unanesthetized conditions (cat: Lee and Middlebrooks, 2011, 2013; Mickey and Middlebrooks, 2003; non-human primate: Recanzone et al., 2000, 2011; Werner-Reiss and Groh, 2008; Woods et al., 2006; Zhou and Wang, 2012). Generally, the primary auditory areas in primates and carnivores show large populations of “omnidirectional” neurons that respond with at least half of their maximum firing rates to stimuli from all tested locations. Among the remainder of units showing greater spatial sensitivity, the majority favor contralateral locations, but sizable populations of neurons display a preference for ipsilateral or midline locations. In contrast, nearly all units encountered in the present study of rat area A1 displayed sharp hemifield tuning comparable to the most common class of spatially selective neurons seen in carnivores and primates (i.e., the contralateral-hemifield units).

Although carnivores and primates exhibit greater diversity of spatial tuning than the rat, those species share with the rat the property that neural spatial acuity is greatest for near-midline locations. In cat area A1, for instance (Stecker et al., 2005b), spatial acuity is sharpest around 0° azimuth, and the distribution of discrimination thresholds (i.e., MDAs) has a median of 40°, which is close to the medians of 35–40°, depending on sound level, that we observed in the rat.

Many neurons studied in anesthetized carnivores display a broadening of spatial tuning associated with increased sound level. Neurons in awake carnivore and primate preparations, in contrast, tend to be more level tolerant (Mickey and Middlebrooks, 2003; Miller and Recanzone, 2009; Zhou and Wang, 2012). Spatial sensitivity in the present urethane-anesthetized rat preparation was largely level invariant, more like that in awake animals than in previous anesthetized preparations. The difference in level sensitivity might reflect a true species difference. Alternatively, it might be the case that the urethane anesthesia that was used here produced less disruption of the balance of contra- and ipsilateral excitation and inhibition than ketamine, barbiturate, and α-chloralose that have been used in previous studies.

Anesthesia was used in the present study to facilitate comparison with the majority of studies of cortical spatial sensitivity in other species and for ease of data collection. Our research group previously has studied spatial sensitivity in area A1 of cats under anesthetized conditions (e.g., Middlebrooks and Pettigrew, 1981; Stecker et al., 2003) and, in other cats, awake conditions (Mickey and Middlebrooks, 2003) and awake/behaving conditions (Lee and Middlebrooks, 2011, 2013). Across those studies, we observed prominent differences in the temporal firing patterns of spikes and some differences in spatial sensitivity. Nevertheless, all of those conditions showed similar distributions of omnidirectional and spatially sensitive units, with the spatially sensitive units most often favoring contralateral locations. Given the general stability of distributions of spatial sensitivity across a wide range of experimental conditions in cats, we think it is unlikely that the use of anesthesia in the present study would have masked basic characteristics of spatial tuning in the rat.

2.5.3 *Species Differences in Spatial Representation Correlate with Spatial Acuity*

Rats can discriminate locations of sound sources on either side of the frontal midline with acuity comparable to that of other rodents, carnivores, and primates. Reported psychophysical thresholds around the midline are 11–14° for rats (Heffner and Heffner, 1985; Ito et al., 1996; Kavanagh and Kelly, 1986), compared with 7–23° for gerbils (Carney et al., 2011; Heffner and Heffner, 1988b; Lesica et al., 2010; Maier and Klump, 2006), 15–19° for ferrets (Kavanagh and Kelly, 1987), 3–4° for cats (Heffner and Heffner, 1988a; Martin and Webster, 1987; Moore et al., 2008), 2–10° for monkeys

(Recanzone and Beckerman, 2004), and around 3° for humans (Middlebrooks and Onsan, 2012; Recanzone et al., 1998). Discrimination of near-midline locations by the most sensitive single- and multiple- unit cortical recordings in the present rat experiment was comparable in scale with psychophysical thresholds. That is, the 10th percentile of spatial acuity for sources near the midline was ~16° across a 30-dB range of sound levels.

Psychophysical discrimination of sound sources within a hemifield (e.g., pairs of sources centered on 60°) is strikingly worse in rat than in carnivores and primates. Carnivores and primates can successfully discriminate lateral sounds, with discrimination thresholds that average 28.8° for ferrets (Kavanagh and Kelly, 1987), range from 3° to 10° for monkeys (Heffner and Heffner, 1990; Populin, 2006; Recanzone and Beckerman, 2004), and range from 2° to 4° for humans (Middlebrooks and Onsan, 2012; Recanzone et al., 1998); also, cats can correctly localize sounds from among loudspeakers separated by 15° (Malhotra et al., 2004). The psychophysical ability to discriminate or localize lateral sounds is matched by cortical spatial sensitivity, such that spike rates of single neurons in cats (Stecker and Middlebrooks, 2003) and of populations of neurons in monkeys (Miller and Recanzone, 2009) can identify a lateral sound source with considerable accuracy. In contrast to carnivores and primates, rats are essentially unable to discriminate source locations within a hemifield. Rats could not reach criterion psychophysical discrimination of sources separated by 60° when the pair of sources was centered on 60° (Kavanagh and Kelly, 1986). Consistent with rats' poor psychophysical discrimination of lateral sounds, the present cortical recordings in rats showed substantially worse discrimination of lateral sources than of near-midline sources. For instance, median discrimination thresholds were >53° for pairs of sources located >40° from the midline.

We note that the parallels between spatial sensitivity of rat cortical neurons and localization/discrimination psychophysics do not demonstrate that psychophysical acuity is necessarily a product of the cortical activity. Indeed, contrary to such a claim of causality, bilateral lesions of rat auditory cortex have little or no impact on midline sound location discrimination (Kelly, 1980; Kelly and Glazier, 1978; Kelly and Kavanagh, 1986). In carnivores and primates, bilateral auditory cortex lesions or inactivation results

in profound sound localization deficits (Heffner and Heffner, 1990; Jenkins and Masterton, 1982; Jenkins and Merzenich, 1984; Kavanagh and Kelly, 1987; Malhotra and Lomber, 2007; Thompson and Cortez, 1983). Even in carnivores and primates, however, discrimination between sound hemifields is largely preserved after bilateral lesion or inactivation. In that sense, the main difference between rats and other studied species is that auditory cortex lesions in carnivores and primates disrupt discrimination of lateral sources whereas rats cannot discriminate lateral sources even with the auditory cortex intact. Although it is difficult to attribute rat auditory psychophysics to cortical function, we can say with some confidence that spike activity of A1 cortical neurons appears to follow the same principles of spatial sensitivity as rat sound localization psychophysics.

Several recent studies have raised the possibility that sound locations are represented by the relative activity of as few as two “opponent” neural populations (McAlpine and Grothe, 2003; Phillips, 2008; Salminen et al., 2009; Stecker et al., 2005b). Nevertheless, unilateral cortical lesions in carnivores and nonhuman primates result in strictly contralesional sound localization deficits (see, e.g., Jenkins and Masterton, 1982; Thompson and Cortez, 1983). For that reason, our group has argued that an opponent model of cortical representation must include both contra- and ipsilaterally tuned neurons within the same cortical hemisphere (Stecker et al., 2005b). Our present results in rats demonstrate the requisite hemifield spatial sensitivity of neurons but fail the requirement for contra- and ipsilateral tuning within the same cortical hemisphere. The absence of diverse patterns of contra- and ipsilateral spatial tuning in the rat’s auditory cortex, and presumably elsewhere in its auditory pathway, might leave the rat without a mechanism for discrimination of lateral sound sources. A failure to discriminate such sources, however, is exactly what is seen in the rat’s psychophysics. In light of the present cortical results, with consideration of previous rat psychophysical studies, we are inclined to think about sound location coding in the rat auditory cortex simply in terms of strong activity in one cortical hemisphere or the other, depending on the left or right location of the sound source, which might be sufficient to permit the rat to turn toward the sound of a desired target or turn away from a possible predator. Thus, whereas the absence of frontal-tuned, ipsilateral-tuned, and

omnidirectional sensitive neurons in the rat is striking, we have found that the rat's single class of contralateral-tuned neurons represents a physiological counterpart to its sound localization psychophysics and, seemingly, to its ecological niche.

2.5.4 *Concluding Remarks*

Cortical neurons in area A1 in the rat lack the diversity of spatial sensitivity that is seen in carnivores and primates and lack the ability to code nonmidline sound source locations with great acuity. This might make the rat seem uninteresting for future study of spatial representation. On the other hand, the homogeneity of spatial sensitivity in the rat auditory cortex lends itself to future studies regarding the cortical mechanisms of hemifield spatial tuning, which is the most common pattern of spatial sensitivity seen in more sophisticated auditory cortices. That is, in studies employing *in vitro*, pharmacological, or optogenetic procedures, one could be assured that any neuron encountered in cortical area A1 would show contralateral-hemifield spatial tuning, even in situations in which that tuning could not be confirmed with *in vivo* recording with calibrated free-field stimulation. We hope to take advantage of this characteristic in future experiments.

2.6 Acknowledgements

We thank Zekiye Onsan for administrative support, and Elizabeth McGuire and Lauren Javier for surgical preparation and assistance. This work was supported by National Institute on Deafness and Other Communication Disorders Grants R01-DC000420 and T32-DC010775 (Interdisciplinary Training Program in Hearing Research).

CHAPTER 3: Transformation of Spatial Sensitivity along the Ascending Auditory Pathway

This work has been published in J Neurophysiol 113: 3098–3111, March 5, 2015.

3.1 Summary

Locations of sounds are computed in the central auditory pathway based primarily on differences in sound level and timing at the two ears. In rats, the results of that computation appear in the primary auditory cortex (A1) as exclusively "contralateral hemifield" spatial sensitivity, with strong responses to sounds contralateral to the recording site, sharp cutoffs across the midline, and weak, sound-level-tolerant, responses to ipsilateral sounds. We surveyed the auditory pathway in anesthetized rats to identify the brain level(s) at which level-tolerant spatial sensitivity arises. Noise-burst stimuli were varied in horizontal sound location and in sound level. Neurons in the central nucleus of the inferior colliculus (ICc) displayed contralateral tuning at low sound levels, but tuning was degraded at successively higher sound levels. In contrast, neurons in the nucleus of the brachium of the inferior colliculus (BIN) showed sharp, level-tolerant spatial sensitivity. The ventral division of the medial geniculate body (MGBv) contained two discrete neural populations, one showing broad sensitivity like the ICc and one showing sharp sensitivity like A1. Dorsal, medial, and shell regions of the MGB showed fairly sharp spatial sensitivity, likely reflecting inputs from A1 and/or the BIN. The results demonstrate two parallel brainstem pathways for spatial hearing. The tectal pathway, in which sharp, level-tolerant spatial sensitivity arises between ICc and BIN, projects to the superior colliculus and could support reflexive orientation to sounds. The lemniscal pathway, in which such sensitivity arises between ICc and the MGBv, projects to the forebrain to support perception of sound location.

3.2 Introduction

Spatial hearing permits a listener to determine the locations of sound sources based spatial cues derived from the interaction of sound with the head and external ears. Those cues are processed in specialized brainstem nuclei, and the output of those nuclei converges in the central nucleus of the inferior colliculus (ICc) (Grothe et al., 2010). Multi-synaptic pathways from the ICc reach two structures in which neurons exhibit spatial sensitivity: the superior colliculus (SC) and the auditory cortex. It is

unknown from the published literature whether spatial sensitivity arises *de novo* at the levels of the SC and auditory cortex by convergence of pathways representing individual spatial cues or whether that spatial sensitivity is inherited from such a convergence at a lower level of the auditory pathway.

The *tectal* pathway projects from the ICc to the SC by way of the nucleus of the brachium of the inferior colliculus (BIN) (Jiang et al., 1993; King et al., 1998; Nodal et al., 2005; Slee and Young, 2013). Note that the BIN is the *nucleus* of the brachium, which is a cell group that lies adjacent to the brachium itself; the brachium of the inferior colliculus is the major fiber bundle containing the axons of ICc principal cells. Topographical representations of auditory space based on space-tuned neurons have been described in the SC of anesthetized guinea pigs, cats, and ferrets (Palmer and King, 1982; Middlebrooks and Knudsen, 1984; King and Hutchings, 1987). The *lemniscal* pathway projects by way of the medial geniculate body (MGB) to the primary auditory cortex, area A1. Area A1 in carnivores and primates exhibits a variety of spatial sensitivity, including spatially insensitive “omnidirectional” responses, contralateral “hemifield” tuning, and, in a minority of neurons, frontal and ipsilateral tuning (King and Middlebrooks, 2011).

In anesthetized rats, essentially all neurons in A1 studied with free-field stimulation show level-tolerant contralateral-hemifield spatial sensitivity consisting of strong responses to sounds contralateral to the recording site, a sharp cutoff in responses across the midline, and weak responses to ipsilateral sounds (Yao et al., 2013). Consistent with the finding of exclusively hemifield spatial sensitivity, a study in rat A1 using dichotic stimulation found primarily excitatory/inhibitory (EI) responses (Kyweriga et al., 2014). That study concluded that the EI responses were inherited from sub-cortical processing, consistent with our findings in the present study. The Kyweriga group also studied a second class of binaural responses: predominantly binaural. Those neurons were found primarily in the rat's suprarhinal auditory field, and their responses were determined to reflect intracortical processing.

The rat lacks the variety of spatial sensitivity that is seen in primates and carnivores. For that reason, it is an ideal animal model for study of the most common form of spatial sensitivity observed across species, contralateral hemifield tuning,

because in examining sub-cortical structures in the rat one can be confident of the spatial sensitivity of target neurons in area A1. We also note that the spatial tuning seen in the rat's area A1 coincides with the rat's performance in psychophysical tasks, in which it discriminates sounds on the left from those on the right of the midline with reasonable spatial acuity but fails to discriminate locations within one hemifield (Kavanaugh and Kelly, 1986).

The present study surveyed spatial sensitivity in the auditory pathway of the anesthetized rat with the goal of identifying the first location(s) of level-tolerant spatial sensitivity. We quantified the spatial sensitivity of neurons in the ICc, the BIN, and structures of the MGB including the ventral (MBGv), medial (MGBm), and dorsal (MGBd) divisions and the shell nucleus (MGBs), and we compared those data with our previous data from area A1 (Yao et al., 2013). The results show that level-tolerant contralateral hemifield spatial sensitivity arises independently in tectal and lemniscal pathways. Surprisingly, we found two distinct populations of neurons in the MGBv, distinguished only by their spatial sensitivity. It remains to be tested whether those MGBv populations represent two stages in a progression from broad to sharp spatial sensitivity or whether they are components of parallel broadly- and sharply-sensitive pathways.

3.3 Materials and Methods

We recorded from IC and MGB neurons in 14 adult male Sprague-Dawley rats (median age: 11.1 wk; Charles River Laboratories, Hollister, CA) weighing 265–475 g (median weight: 380 g) and compared these data with previously reported data from cortical area A1 in 15 other rats (Yao et al., 2013). All procedures were performed with the approval of the University of California at Irvine Institutional Animal Care and Use Committee according to the National Institutes of Health guidelines and were largely identical to those of a previous report from our lab (Yao et al., 2013). In what follows we briefly describe the procedures with an emphasis on differences between our previous cortical and the current subcortical recordings.

3.3.1 *Animal Surgery*

Surgical anesthesia was induced with urethane (1.5 g/kg ip) and xylazine (10 mg/kg ip) and supplemented as needed to maintain an areflexive state. To reduce the

viscosity of bronchial secretions and to prevent brain edema we administered atropine sulfate (0.1 mg/kg ip) and dexamethasone (0.25 mg/kg ip), respectively, at the beginning of surgery and every 12 h thereafter. Core body temperature was maintained at ~37°C.

Surgery began with a midline scalp incision and the exposure of the underlying skull. We cemented an inverted machine screw to the skull on the midline, rostral to bregma, to serve as a head-holder. The skull was opened as needed to access the right IC and MGB. Prior to recordings, the scalp was partially closed and the positions of the pinnae were adjusted to minimize any alteration the surgical procedure may have caused. Recordings were made with multi-site recording probes (described below). The right ICc and BIN were accessed with vertical probe placements (14 placements in 5 animals) approximately ~2–3 mm lateral to the midline and ~7–9 mm caudal to bregma. Two approaches were used to access the right MGB. The vertical approach (22 probe placements in 8 animals) used vertical probe placements ~3–4 mm lateral to the midline and ~5–6 mm caudal to bregma. The lateral approach (18 probe placements in 6 animals) used a dorso-lateral to ventro-medial trajectory, ~30–50° from the sagittal plane, ~4–6 mm caudal to bregma.

3.3.2 *Experimental Setup, Stimulus Generation*

The animal was positioned in the center of a darkened double-walled sound-attenuating chamber (Industrial Acoustics; inside dimensions 2.6 x 2.6 x 2.5 m) that was lined with 60-mm-thick absorbent foam (SONEXone, Seattle, WA). The animal's head was supported by a 10-mm-diameter rod attached to the skull screw. The rod was held by a thin metal frame positioned behind the animal. The area around the head and ears was unobstructed.

We used Tucker-Davis Technologies System 3 equipment (TDT, Alachua, FL) controlled by a personal computer running custom MATLAB (MathWorks, Natick, MA) scripts for stimulus generation and data acquisition. Sounds were presented one at a time from 18 two-way coaxial loudspeakers (8.4 cm diameter; Pioneer Electronics, Long Beach, CA) that were located 1.2 m from the rat's head. The loudspeakers were positioned in the horizontal plane aligned to the interaural axis of the animal and were spaced 20° apart. We express loudspeaker locations in degrees of azimuth relative to

the loudspeaker directly located in front of the animal's head (0°). Negative values indicate locations on the animal's left, contralateral to the recording side located on the animal's right. We calibrated the loudspeakers individually to flatten and equalize their frequency responses (Zhou et al., 1992) using a precision microphone positioned in the center of the sound chamber at the normal position of the rat's head; the rat was absent during the calibration. The addition of the rat's ear-canal resonance added some gain at the level of the tympanic membrane relative to the level in the sound field (average gain of 24.1±3.3 dB at 17.2 kHz; Koka et al., 2008), and there was an additional gain of ~10 dB attributed to diffraction by the rat's head and pinna at the particular speaker location of –40° at which thresholds were measured. The reported minimum thresholds of –10 dB SPL at specific CFs, therefore, is equivalent to ~20 dB SPL in the ear canal, depending on frequency.

We recorded extracellular spike activity with single-shank silicon-substrate multisite recording probes from NeuroNexus Technologies (Ann Arbor, MI, USA) using high-impedance head stages and multichannel amplifiers from Tucker-Davis Technologies (TDT, Alachua, FL). The probes had either 16 recording sites spaced at 100 μm intervals or 32 sites spaced at 50 μm intervals; recording-site areas were 177-μm^2. Neural waveforms were digitized at 24.4 k samples/s and stored on computer disk for off-line analysis.

3.3.3 *Experimental Procedure*

The vertical approach to the IC typically encountered sound-evoked unit activity at a depth 3–6 mm below the surface of the occipital cortex. The probe depth was adjusted to maximize the number of recording sites with stimulus-evoked spiking activity. Typically, sustained or strong onset neural spike activity was seen on all sites. In the vertical approach to the MGB, we typically encountered stimulus-evoked activity at a depth of ~5–6.5 mm below the cortical surface. In the lateral approach to the MGB, we first encountered neural spiking activity at depths of ~1 mm as the probe first advanced through auditory cortical fields. This initial auditory activity ceased at a depth of ~2 mm. Stimulus-evoked activity returned at a depth of about 5–6.5 mm indicating that the electrode had reached the MGB. We adjusted the probe depth to maximize the number of recording sites with stimulus evoked spiking activity. Following probe placement, the

exposed brain tissue was covered with warmed 2% agarose dissolved in Ringers' solution. The agarose cooled to form a gel that reduced brain pulsations and kept the exposed brain surface moist.

At each probe placement, we first recorded frequency response areas (FRAs) with pure tones presented from the loudspeaker at –40°. Tones were 80 ms in duration with 5-ms raised-cosine onset and offset ramps. Tones varied in frequency from 0.2 to 40 kHz in 1/3- or 1/6-octave steps and in level in 10-dB steps, typically from –10 to 60 or 70 dB SPL with 10 repetitions per frequency-level combination. Next, we recorded mean-spike-rate-versus-azimuth functions (RAFs) to 80-ms Gaussian noise bursts across 360° in azimuth in 20° steps and at levels ranging from –10 to 70 dB SPL in 10-dB steps (20 repetitions per combination). All stimuli were presented at a repetition rate of 1 or 1.25/s. Data collection for the present study took ≤75 min at each probe placement. Additional stimuli needed for another study also were tested, extending the recording session at a single probe placement to between ~2–5 h, with experiments lasting ~18–20 h.

3.3.4 *Assignment of Units to IC and MGB Subdivisions*

Units were localized to ICc and BIN based on stereotaxic coordinates of probe placements and response properties. Localization of probe placements was confirmed histologically in a subset of cases. Units localized in the ICc typically displayed sustained responses to pure tones and broad-band noise, sharp frequency tuning, and a dorsal-to-ventral low-to-high gradient of characteristic frequency (Malmierca et al., 2008). BIN units were typically encountered when probe placements were made at more rostral (~1–2 mm) and slightly lateral (< ~1 mm) sites relative to ICc penetrations and caudal (~2 mm) from the probe placements made in the MGB. The BIN was studied with one probe placement in each of 3 rats and with two placements, separated rostrocaudally by 0.5 to 1 mm, in each of 2 other rats. Consistent with published reports in other species, units localized in the BIN displayed first-spike latencies comparable to those of ICc units, strong onset responses but rarely sustained firing, relatively broad frequency tuning, and a lack of a clear tonotopic gradient (Schnupp and King, 1997; Slee and Young, 2013).

Unit localization within the subdivisions of the MGB was based on physiological criteria of spike patterns, latency, and frequency response properties that were consistent with previous reports in small mammals (rat: Bordi and LeDoux, 1994a, 1994b; Edeline et al. 1999; guinea pig: He, 2001; He and Hu, 2002; Anderson et al. 2007; mouse: Anderson and Linden, 2011; Hackett et al. 2011; gerbil: Bäuerle et al. 2011); again, locations of a subset of probe placements were confirmed histologically. A total of 363 MGBv units were studied: 193 from vertical probe placements and 170 from lateral placements. Sharp "primary-like" or V-shaped frequency tuning and a lateral-to-medial increase in CFs (lateral approach) were taken as signatures of the MGBv. The MGBm was accessed exclusively using the lateral approach (41 units). The functional boundary from the MGBv to the MGBm was given by an increase in frequency bandwidth and a reversal in the CF gradient upon entering MGBm. The MGBd and MGBs were encountered most often using vertical probe placements (83/98 MGBd units; 48/60 MGBs units). The boundary from the MGBd to the MBGv was marked by a reduction in first-spike latency and a sharpening of frequency tuning. MGBs units were distinguished by their long first-spike latency and were typically encountered when probe placements were made at more lateral sites relative to MGBv penetrations.

The positions of 11 of the 54 probe placements (6 IC and 11 MGB) were verified histologically in 10 rats. For that purpose, the rear side of the silicon probes was coated with 4-(4-(dihexadecylamino)styryl)-N-methylpyridinium iodide (DiA), which is a lipophilic aminostryl dye (DiCarlo et al., 1996). The DiA inserts itself readily into cell membranes and exhibits a strong fluorescence (~580 nm). After the conclusion of these experiments, animals were perfused with 4% paraformaldehyde and the brains sectioned on a vibratome. Sections were counterstained with DAPI (D-1306; Invitrogen, Carlsbad, CA). Fluorescent images were photographed, stored, and adjusted for brightness and contrast using Adobe Photoshop. We were able to recover 11 electrode tracks (4 in IC and 7 in MGB) from a total of 17 coated probe placements (Fig. 3.1). The locations of probes seen in the histology agreed well with the locations inferred from stereotaxic coordinates and response properties.

3.3.5 *Data Analysis*

Spike sorting. All quantitative analyses are based on neuronal action potentials identified with an off-line spike-sorting procedure that is similar to the one previously used in our lab (Middlebrooks, 2008). First, a denoising procedure was applied to simultaneously recorded analog waveforms to attenuate signals that were common to multiple recording sites (Bierer and Anderson, 1999). Next, putative action potentials were extracted using a root-mean-squared-based threshold crossing procedure. The selected peaks then were sorted using an algorithm based on k-means clustering of the first three principal components of the putative action potentials. Visual inspection of waveforms and measures of mean spike counts verified the stability of recordings during the ≤75 min needed to collect the FRA and the RAF. We report spike times corrected for the 3.5-ms acoustic travel time between the loudspeaker and the animal's head (Yao et al., 2013), and latencies based on responses to CF at highest level. For units with unclear CFs (80 total), latencies were taken as the shortest first-spike latencies across all tested frequencies at the highest level.

Responses were classified as well-isolated single units when they showed: 1) uniform waveform appearance upon visual inspection; 2) inter-spike intervals that revealed a clear refractory period greater than 1 ms; and 3) stability of spike amplitude during the ≤75 min recording period. According to that classification, our sample of well-isolated single units consisted of 31 units in the IC and 55 in the MGB. An additional 246 recordings in the IC and 507 recordings in the MGB were classified as multiple units consisting of unresolved spikes from two or more neurons. Analysis of relative spike times on adjacent pairs of electrode sites showed little or no indication of spikes being recorded on multiple sites. We did not observe differences between properties calculated from the single compared to multiple units across any measure of spatial sensitivity at any suprathreshold level ($K = 0.17–0.35$, $P = 0.09–0.78$, 2-sample Kolmogorov-Smirnov test). The lack of differences between single and multiple units suggests that the variance in stimulus sensitivity among neurons recorded as a multiple unit was small enough that there was no broadening of apparent sensitivity compared to that of single neurons. In summary illustrations, the range and percentiles of distributions of multi-unit responses are represented by boxes and whiskers and well-isolated single units are represented by individual symbols. By every measure, every

single-unit response fell within the range of multi-unit responses. For those reasons, we combined single- and multiple-unit data in statistical tests of populations and we use the term “unit” to refer to both well-isolated and unresolved recordings. The unit count did not include the 75 units in the IC and 135 in the MGB that we excluded from the analysis because they responded with less than an average of one spike per trial to their most effective stimulus or with a maximum spike rate less than 2 standard deviations above their spontaneous rates.

Frequency response area, characteristic frequency, spectral bandwidth, and noise-burst threshold. We extracted frequency tuning curves (FTCs) from the measured FRAs using procedures described in signal detection theory (Green and Swets, 1966; Macmillan and Creelman, 2005; Middlebrooks and Snyder, 2007). For each frequency-level combination and all repetitions we accumulated the trial-by-trial distributions of spike counts and constructed an empirical receiver-operator-characteristic (ROC) curve for the stimulus condition versus a non-stimulus condition (i.e., versus a silent interval of the same duration) as a measure of spontaneous rate. The area under the ROC curve gave the proportion of trials in which one condition elicited more spikes than the other one. We expressed this proportion as a *z*-score multiplied by $\sqrt{2}$ to yield the discrimination index, d'. A d' of 1 indicates a one-standard- deviation separation of the means of the two distributions (stimulus versus silent). A stimulus thus elicited activity above spontaneous rate if it yielded a $d' \geq 1$.

For each unit, the matrix of d' values across all tested frequencies and levels was screened to eliminate isolated values of $d' > 1$ for which all neighboring values were <1; this eliminated isolated values lying outside the FRA. Then, the FTC (i.e., the border of the FRA) was found by interpolating the d' values across all tested sound levels in 1-dB steps at each tested frequency and finding the minimum sound level at which d' was ≥1. The characteristic frequency (CF) was given by the frequency of the lowest-level tip of the FTC. The filter bandwidth was estimated by fitting a rounded symmetrical exponential filter (roex-filter; Patterson, 1976) to the FTC as follows:

$$|H(f)|^2 = (1 + pg)e^{-pg}, \qquad \text{(Eq. 3.1)}$$

where g is the normalized deviation of the frequency from the CF, p is the slope parameter, and $|H(f)|^2$ represents the squared magnitude of the filter. The slope parameter p can be used to calculate the equivalent rectangular bandwidth (ERB) as:

$$ERB = 4CF/p. \quad \text{(Eq. 3.2)}$$

ERB represents the bandwidth of a rectangular filter whose area is equal to that of the FTC and takes the entire FTC into account. The Q_{ERB} (Verschooten et al., 2012) was computed to provide a value of sharpness of tuning normalized across CFs:

$$Q_{ERB} = CF/ERB. \quad \text{(Eq. 3.3)}$$

The thresholds for detection of neural activity elicited by noise bursts were computed by ROC analysis of trial-by-trial spike counts on trials in which a noise burst was or was not present. The minimum noise level eliciting $d' > 1$, interpolated in 1-dB steps, was taken as the noise-burst threshold.

Measures of spatial sensitivity. An ROC procedure also was used to quantify discrimination between pairs of stimulus locations based on spike counts. Based on responses to noise bursts at a fixed sound level, we found the trial-by-trial distribution of spike counts to noise bursts at a particular source location and compared that with the corresponding distribution for every other source location. The ROC analysis yielded a value of d' for each of the 153 unique combinations of 18 source locations. A "discrimination index" (DI) was given by the number of pair-wise comparisons yielding $d' \geq 1$ divided by 153. A DI of 0.5, for example, would indicate that half of the pair-wise comparisons of source locations could be discriminated significantly by the spike rate of a neuron.

The breadth of spatial sensitivity by each unit was represented by the width of its equivalent rectangular receptive field (ERRF) (Lee and Middlebrooks, 2011; Yao et al. 2013). The ERRF width was computed by integrating the area under a unit's RAF, forming a rectangle having peak height and area equal to that of the RAF, and measuring the resulting width.

The preferred stimulus location of each unit was represented by its spatial centroid (Middlebrooks et al., 1998; Yao et al., 2013). Spatial centroids were computed

only for neurons that showed ≥50% modulation of their mean spike rates by sound-source location across a 360° range. To obtain the spatial centroid, we first identified the peak of the RAF by finding the range of one or more contiguous locations that elicited spike rates ≥75% of the maximum spike rate; we also included the two neighboring locations having rates below that criterion. The spatial centroid was given by the orientation of the spike-rate-weighted vector sum across source locations within the peak.

The location in azimuth at which a neuron's response was most strongly modulated by source location was given by the steepest slope of its RAF. The steepest slope location of each neuron was computed by convolving its RAF with a 40° boxcar window, calculating the first derivative of mean spike rate with azimuth, and then finding the azimuth at which the slope was maximal.

Many units showed a broadening of their spatial sensitivity with increasing sound level. We quantified that for each unit by fitting a least-squares regression line to its ERRF widths in degrees versus sound levels in dB. The slope of each such fit was taken as a measure of level dependence.

Measures of distinct patterns of spatial sensitivity in MGBv. We noted fairly uniform spatial sensitivity properties within the ICc and within A1, whereas there were marked differences between ICc and A1. The population of recordings from MGBv, in contrast, exhibited a variety of spatial sensitivity, with some units showing broad spatial sensitivities like that seen in the ICc and others showing sharp spatial sensitivity like that seen in A1. We tested whether the similarity to ICc versus similarity to A1 formed a continuum or whether there were functionally distinct populations. That test consisted of comparing the RAF of each MGBv unit to templates of RAFs of ICc and A1 units; all the comparisons used responses to sounds 40 dB above unit thresholds. The templates were formed by normalizing the RAF of each ICc or A1 unit by its peak value and then computing the mean across all ICc units (using data from the present study) or across all A1 units (using data from our previous study: Yao et al., 2013). The RAF of each MGBv unit was compared to the two templates by computing the Euclidean distance (ED):

$$ED_T = \sqrt{\sum_{\theta}^{n} (R_\theta - T_\theta)^2}, \qquad \text{(Eq. 3.4)}$$

where R is the RAF of one MGBv unit, T is the ICc or A1 template, θ is the source location in azimuth, and n is the number of tested source locations (18). We then computed for each MGBv unit a similarity index (SI):

$$SI = ED_{ICc}/(ED_{ICc} + ED_{A1}), \qquad \text{(Eq. 3.5)}$$

where ED_{ICc} and ED_{A1} indicate the *EDs* from the ICc and A1 templates, respectively. An *SI* value close to 1 indicates that the individual test unit is more similar to the A1 template, and an SI value close to 0 indicates greater similarity to the ICc template.

The template-matching procedure demonstrated distinct populations of ICc-like and A1-like units in the MGBv, as presented in the RESULTS. We tested whether there was any anatomical segregation of those populations, analogous to the segregation in other species that has been demonstrated using connectional techniques (cat: Middlebrooks and Zook, 1983; Read et al., 2008; rabbit: Cetas et al., 2002). We used a permutation analysis to test for a nonrandom distribution of units in MGBv with similar spatial sensitivity (Ernst, 2004; Middlebrooks and Bremen, 2013). For each multi-site recording-probe placement, we counted the number of adjacent pairs of recording sites at which units showed similar spatial sensitivity. For example, a run of A1-like responses at 3 consecutive sites would be counted as two matched pairs. We then totaled the number of recording sites yielding A1-like and ICc-like responses across all recordings in the MGBv. We also formed a list of the number of recording sites in the MGBv on each of the 34 probe placements. For each permutation, we distributed all the MGBv units randomly across virtual probes having the same number of sites as the actual probe placements and counted the number of matching adjacent pairs of units. That procedure was repeated for 100,000 permutations, each time with a different random distribution of response types across virtual probes. The actual number of matching adjacent recordings was compared with the distribution of numbers of matching pairs across the permutations. If the actual recorded number of matching pairs was greater than the maximum value obtained across all permutations, the probability of obtaining that actual number by chance was taken as $<10^{-5}$.

Tests of statistical hypotheses. We used custom-written MATLAB scripts (MathWorks) that incorporated the MATLAB Statistics Toolbox when appropriate. All *post hoc* multiple comparisons used the Bonferroni correction. We used a goodness-of-fit measure (D'Agostino's K^2 test) to test if a given data set was normally distributed. We report median and interquartile values, and used nonparametric statistical tests on data sets for which a given measure was not normally distributed. In addition, we used the 2-sample Kolmogorov-Smirnov goodness-of-fit hypothesis test to check for statistically significant difference between two population samples. In the text, distributions are summarized by 25th, 50th, and 75th percentiles, written as –/–/–.

3.4 Results

We present data from a total of 839 single- and multi-unit recordings in 14 animals: 277 units in 14 probe placements in the IC and 562 units in 40 probe placements in the MGB. Of the 277 IC units studied, 146 (53%) were localized to the ICc and 131 (47%) were localized to the BIN. Of the 562 MGB units, 363 (65%) were localized to the MGBv, 98 (17%) to the MGBd, 41 (7%) to the MGBm, and 60 (11%) to the MGBs. Figure 3.1 depicts coronal sections through the MGB (Fig. 3.1*A*–*B*) and the IC (Fig. 3.1*C*–*D*) from four animals. The dashed white lines indicate the approximate borders of the subdivisions of each structure based on the appearance of the tissue and on stereotaxic coordinates (Paxinos and Watson, 2005). The orange-red fluorescent DiA traces indicate the electrode tracks. The sections in Fig. 3.1*A* and 3.1*B* were taken ~5.5 and ~5.8 mm posterior to bregma, respectively. The labeled tracks are seen passing through the MGBv (Fig 3.1*A*–*B*), and entering the MGBm (Fig. 3.1*B*). The section in Fig. 3.1*C* was taken ~8.8 mm posterior to bregma and contains the ICc. The section in Fig. 3.1*D* was taken ~7.5 mm posterior to bregma and contains the SC and BIN. The labeled track in Fig. 3.1*C* passes through the ICc, whereas the labeled track in Fig. 3.1*D* is located in the region designated as the BIN.

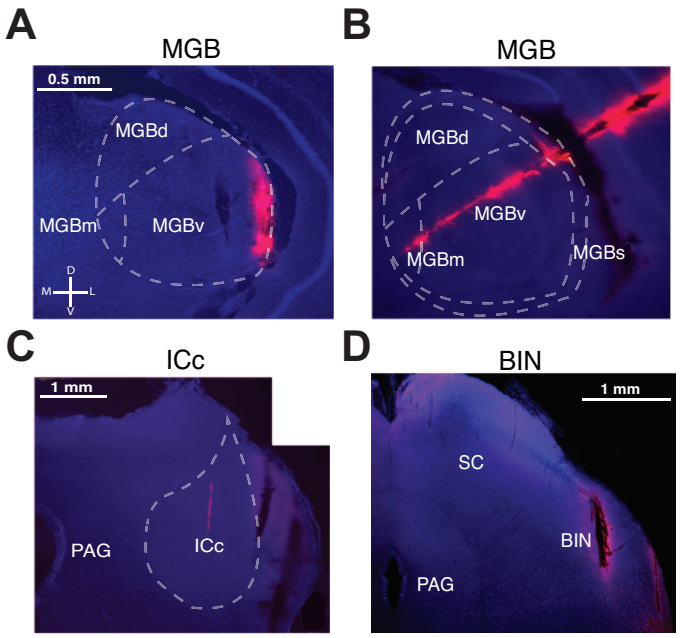

Figure 3.1. Histological reconstruction of recording sites in four animals (coronal view). *A*, Vertical approach to the MGB (FF1309). *B*, Lateral approach to the MGB (FF1402). *C* Vertical approach to the IC (FF1401). *D,* Vertical approach to the BIN (FF1403). The rear sides of the recording probes were coated with DiA (red) in order to determine their anatomical position. Sections were counterstained with DAPI (blue). MGBv, ventral division of the MGB; MGBd, dorsal division; MGBm, medial division; MGBs, shell division; ICc, central nucleus of the IC; SC, superior colliculus, PAG, periaqueductal gray; BIN, brachium of the inferior colliculus.

3.4.1 *Frequency Tuning*

Across our samples of ICc and BIN units, CFs ranged from 1 to >32; ">32" denotes instances in which CFs were higher than the 32-kHz maximum tested frequency. The quartiles of the CF distribution in the ICc were 7.17/12.7/26.7 kHz and in the BIN were 11.1/27.3/>32 kHz. The distribution of CFs in the BIN was shifted significantly toward higher frequencies than that in the ICc ($K = 0.32$, $P < 10^{-6}$; 2-sample Kolmogorov-Smirnov test). Units localized to the ICc typically displayed sharp frequency tuning (Fig. 3.2A; ICc_{QERB}: 0.74/1.00/1.24), whereas frequency tuning of BIN units was significantly broader (Fig. 3.2D; BIN_{QERB}: 0.61/0.93/1.13; $K = 0.15$, $P = 0.038$; 2-sample Kolmogorov-Smirnov test). We overestimated Q_{ERB} (i.e., underestimated bandwidths) in some cases because many FRAs appeared to extend to frequencies higher than 32 kHz, which was the highest that we tested; that was a greater problem in BIN than ICc because of the higher-frequency FRAs in BIN. The ICc displayed a tonotopic frequency gradient, with low and high CFs located dorsally and ventrally, respectively. The

quartiles of CF-range between the most superficial and deepest electrode sites along individual vertical probe placements in the ICc were 2.15/2.70/4.10 oct. The tonotopic gradient was less pronounced within the BIN; CF ranges between the most superficial and deepest electrode sites were distributed with quartiles of only 0.35/1.09/1.65 oct and there was no evident progression of CFs among recording sites on individual probes. The observation in the rat of broader frequency tuning in the BIN than in the ICc generally agrees with previous observations in the ferret (Schnupp and King, 1997) and marmoset (Slee and Young, 2013).

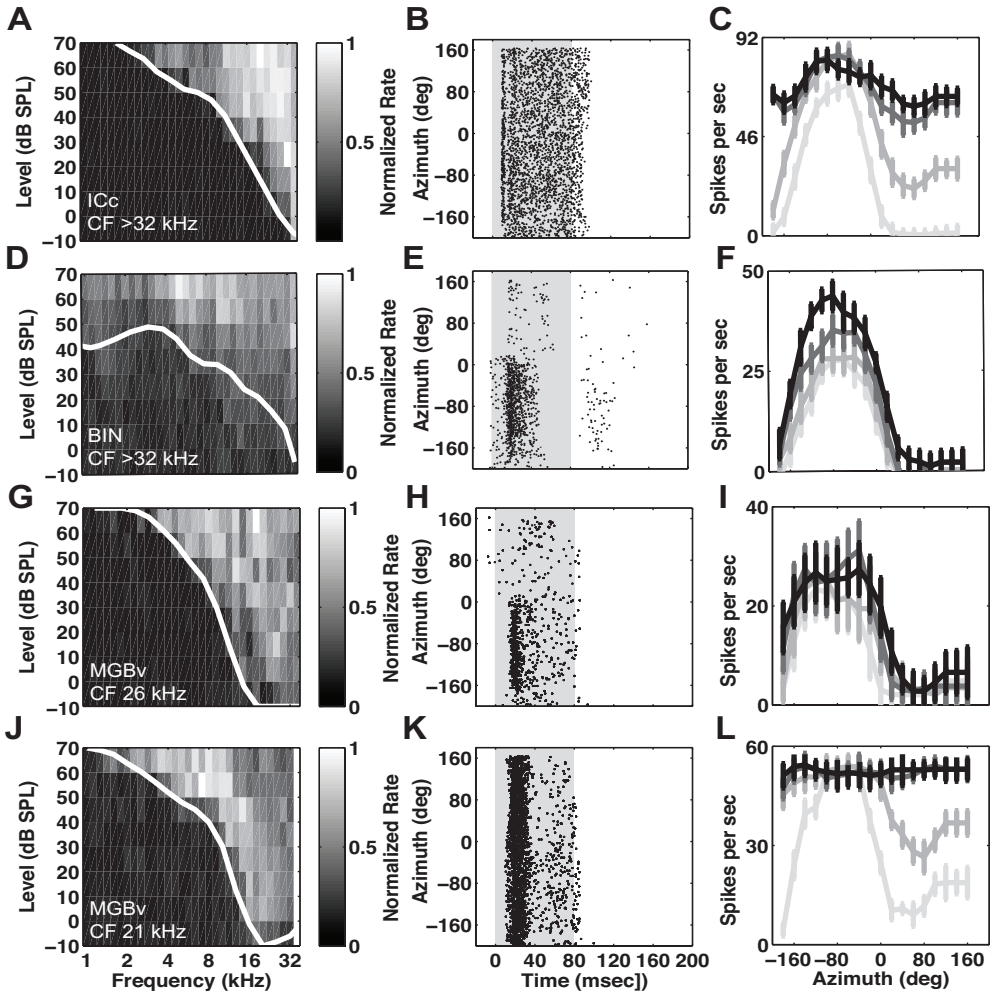

Figure 3.2. Examples of neural responses from well-isolated single units in rat ICc (*A–C*) (1403.5.31), BIN (*D–F*) (1404.7.32), and MGBv (*G–L*) (1312.4.21 and 1404.5.5). The left column (*A, D, G, and J*) displays frequency response areas (FRA) plotted as the normalized spike rate in response to pure-tone stimulation varying in frequency (x-axis) and sound level (y-axis). White lines represent extracted frequency tuning curves (3-point running average for visual purposes). The middle column (*B, E, H, and K*) displays dot rasters of spike times (x-axis) elicited by noise stimuli at 40 dB above the unit's threshold,

varying in azimuth (y-axis). Each dot represents 1 spike. Gray shading represents the stimulus duration. The right column (*C, F, I, and L*) displays rate-azimuth functions (RAFs) of spike rate (spike count per second) plotted against stimulus azimuth locations at levels 10, 20, 30, and 40 dB above threshold and corrected for spontaneous rate. Error bars indicate standard error of the mean. Characteristic frequencies (CFs) are indicated for each example unit.

Figures 3.2*G* and 3.2*J* show FRAs from two isolated single units in the MGBv with CFs of 26 and 21 kHz, respectively. Across our sample of MGBv units, CFs ranged from 1 to >32 kHz (10.2/20.4/>32 kHz). Frequency tuning in our sample of MGBv units was slightly but significantly broader than that observed in the ICc ($MGBv_{Q_{ERB}}$: 0.85/0.98/1.12; MGBv versus ICc $K = 0.16$, $P = 0.010$; two-sample Kolmogorov-Smirnov test) and sharper than that in the BIN ($K = 0.17$, $P = 0.0044$; 2-sample Kolmogorov-Smirnov test). The three non-lemniscal MGB nuclei all showed broad, non-primary-like frequency tuning (Fig. 3.3*A*, *D*, *G*; $MGBd_{Q_{ERB}}$: 0.59/0.73/1.01; $MGBm_{Q_{ERB}}$: 0.51/0.86/1.03; $MGBs_{Q_{ERB}}$: 0.50/0.85/1.06). Q_{ERB} values differed significantly among MGB subdivisions ($X^2_{(3,546)} = 22.6$, $P < 10^{-5}$; Kruskal-Wallis). Bonferroni-corrected multiple comparisons indicated significant differences between MGBv and MGBd, MGBv and MGBm, and MGBv and MGBs ($P < 0.05$) with MGBm displaying the broadest frequency tuning (proportion of $Q_{ERB} < 1$, MGBv: 40%; MGBd: 56%; MGBm: 69%; MGBs: 58%). The calculation of CF and Q_{ERB} was difficult in the non-lemniscal nuclei, especially in the MGBd, because of the non-primary-like FTCs (e.g., Fig. 3.3*A*). For that reason, we were able to compute these measures in only 58% of MGBd units and 33% of MGBs units. For the non-lemniscal units where calculation of CF was successful, values ranged from 1 to >32 kHz ($MGBd_{CF}$: 10.1/12.3/25.2; $MGBm_{CF}$: 7.17/10.1/22.3; $MGBs_{CF}$: 11.7/24.4/>32).

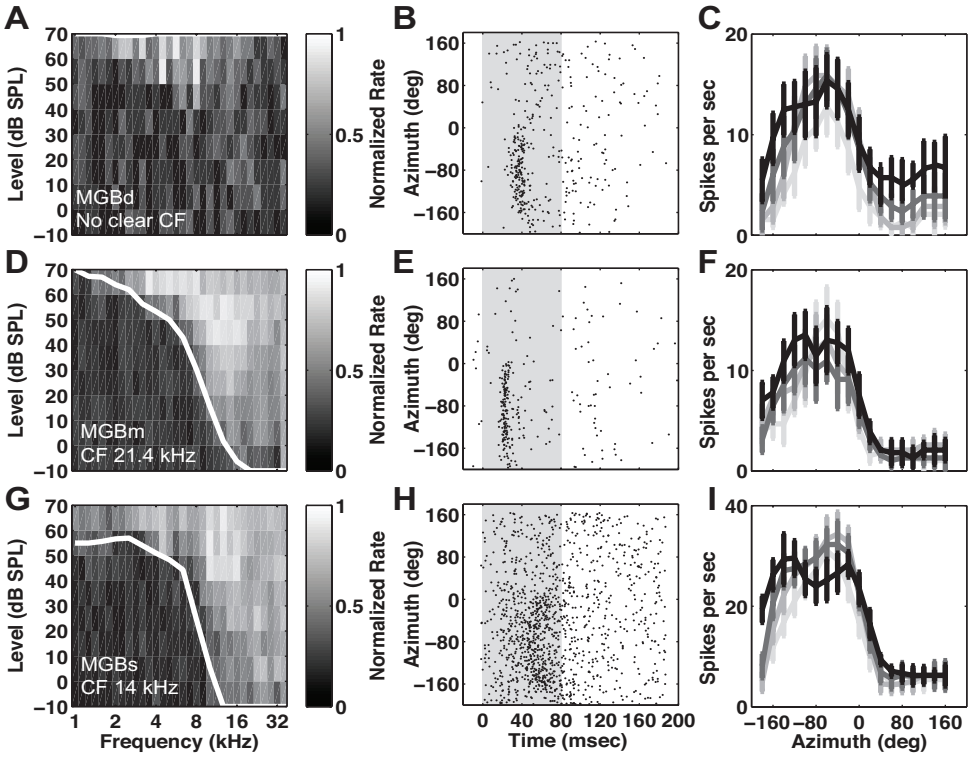

Figure 3. Examples of neural responses of well-isolated single units in rat MGBd (*A–C*) (1403.7.12), MGBm (*D–F*) (1302.6.15), and MGBs (*G–I*) (1404.1.32). All conventions as in Figure 3.2.

3.4.2 *First-Spike Latencies*

We measured first-spike latencies of all units using stimuli at the highest sound level tested at unit CF. In units for which we were not able to extract a CF (1 ICc, 8 BIN, 72 MGBd, and 22 MGBs), we recorded the shortest latency observed across all tested frequencies at the highest level. First-spike latencies in the BIN (8.62/9.27/10.2 ms) were slightly but significantly longer than those in the ICc (8.49/8.86/9.81 ms): $K = 0.15$, $P = 0.047$; 2-sample Kolmogorov-Smirnov test. The small median latency difference (<0.50 ms) between these structures is somewhat unexpected given that the ICc is presynaptic to the BIN (Nodal et al., 2005), but we note that similarly small differences have been reported previously in the marmoset (Slee and Young, 2013). In general, the short latencies seen among our sampled midbrain units suggest that we did not record from other nuclei within the IC, such as the dorsal cortex, which contains units with much longer latencies (Syka et al., 2000; Lumani and Zhang, 2010).

Significant differences in first-spike latencies were seen among MGB subdivisions ($X^2_{(3,579)} = 375$, $P < 10^{-6}$; Kruskal-Wallis). Consistent with being post-

synaptic from the ICc, MGBv and MGBm showed roughly 1 ms longer first-spike latencies compared to the ICc (MGBv: 9.60/9.93/10.7 ms; MGBm: 9.77/10.2/11.6 ms). Those latency distributions (MGBv versus MGBm) were not statistically different from each other ($P > 0.05$, Bonferroni-corrected for multiple comparisons). First-spike latencies of MGBd (28.1/33.5/40.2 ms) and MGBs (36.3/42.5/45.1 ms) units, however, were substantially longer compared to those of MGBv and MGBm units ($P < 10^{-6}$; Bonferroni-corrected), consistent with their classification as being part of non-lemniscal and/or corticofugal pathways.

3.4.3 *Spiking Patterns*

Examples of the various spiking patterns that were encountered are given in the middle column of panels in Figures 3.2 and 3.3. Each of these dot raster plots represents responses to noise bursts at 40 dB above unit thresholds. The vertical axis of each plot represents the full range of tested sound-source azimuth. As illustrated by the example in Fig. 3.2B, units in the ICc displayed a strong onset and sustained spiking pattern. In contrast, BIN units responded phasically and typically lacked the sustained component seen among ICc units (Fig. 3.2E). Spike patterns for each ICc and BIN unit were quantified with the same response index used by Slee and Young (2013) in which the difference in spike rate between the first (0–40 ms) and second half (41–80 ms) of the stimulus duration is divided by the sum of both halves. This index ranges from –1 (build up response) to 1 (purely phasic response). An index value of 0 indicates a purely sustained response. Index response values for all BIN units were greater than 0 (5th percentile, 0.25) and typically clustered around 0.80 (median, 0.78), whereas ICc units possessed index response values near 0 (median, 0.18; significantly different from BIN units, $P < 10^{-6}$; rank sum). The prevalence of phasic responses in the BIN compared to the ICc is consistent with findings in the BIN of anesthetized ferrets (Schnupp and King, 1997), although the majority of units in the BIN in awake marmosets (Slee and Young, 2013) show sustained responses. This difference might be attributable to the use of anesthetics in the ferret and present study.

MGBv and MGBm units typically responded phasically to the onsets of the stimuli (Fig. 3.2*H*, *K* and 3.3*E*). MGBd units responded selectively to sound-source locations within the contralateral hemifield and responded phasically to these locations (Fig.

3.3*B*). Units localized in the MGBs exhibited strong onset responses, with some units showing additional sustained or offset responses (Fig. 3.3*H*).

3.4.4 *Offset Responses*

We noticed weak location-specific offset responses in 19 of 146 (13%) units in the ICc and 23 of 131 (18%) units in the BIN; offset responses typically occurred >10 ms after stimulus offset (ICc: 10.5/11/13.7 ms; BIN: 11/11.5/17.9 ms). For ICc units with offset responses, 13/19 (68%) responded only to +80° (among the locations tested in 20° increments) whereas the rest (6/19, 32%) were specific to –60°. Offset responses from all BIN units (23/23, 100%) were specific to +80°. The distribution of units showing offset responses along each probe placement within the ICc and BIN tended to be random, with no instance of more than 2 neighboring sites showing offset responses.

We observed offset responses in a small proportion of MGBv units (25/363; 7%). These offset responses typically occurred ~20 ms after stimulus offset (17.1/20.5/22.1 ms) and were seen across multiple azimuth locations. Of these units, 80% (20/25) were driven by ipsilateral locations, whereas the remaining units (5/25) showed stronger offset responses to contralateral locations. Only 2 units in the MGBm (4.8%) displayed offset responses. Those responses were to ipsilateral locations and occurred ~15–20 ms after stimulus onset. A greater number of offset responses were seen within the MGBd (38/98; 38.8%) with latencies typically occurring ~21 ms after stimulus offset (10/21/35.5 ms). Of the 38 units, 3 (7.9%) showed equal responses to all locations, 26 (68.4%) showed stronger responses to ipsilateral locations, and 9 (23.7%) showed stronger responses to contralateral locations. Within the MGBs, 33.3% (20/60) of units displayed offset responses. These offset responses occurred ~20 ms (20/20.8/22 ms) with 80% (16/20) of these units showing stronger offset responses to ipsilateral locations and the rest showing stronger responses to contralateral locations.

Units exhibiting offset responses tended to form clusters within specific MGB subdivisions. Of the 15 adjacent pairs of sites across 12 multisite probe placements that displayed offset responses in the MGBv, 14 (93.3% of pairs) showed matching responses. Of the 27 pairs of sites in the MGBd with offset responses, 26 (96.3%) showed matching responses. In the MGBs, 10/12 (83.3%) adjacent pairs of sites showed matching offset responses. Our results are consistent with the offset response

pathways seen in the MGB of the guinea pig, where neurons with offset responses typically formed clusters along the outer edges of the MGBv and within neighboring subdivisions like the MGBd and MGBs (He, 2001).

3.4.5 *Examples of Spatial Sensitivity*

The spatial sensitivity of units from various IC and MGB subdivisions are represented by well-isolated single units shown in the right column of panels in Figures 3.2 and 3.3. Spike rates (spikes/s) as a function of azimuth location (rate-azimuth functions; RAFs) are plotted for sound levels 10, 20, 30, and 40 dB above unit threshold (shades of gray, darkness increasing with sound level); error bars indicate standard errors of the mean. The example ICc unit (Fig. 3.2*C*), showed spatial sensitivity primarily for contralateral sources when sound levels were only 10 dB above unit threshold. That spatial sensitivity was markedly degraded, however, at higher sound levels, primarily due to increases in the responses to ipsilateral sound sources. In contrast to ICc units, units in the BIN exhibited sharp spatial sensitivity across all levels tested. This can be seen in the example BIN unit in Figure 3.2*F*, which responded selectively to contralateral sound sources and showed little or no response to ipsilateral sources, regardless of sound level. The example MGBv unit depicted in Figure 3.2*I* also responded in a level-tolerant manner, responding selectively to sources in the contralateral hemifield. Spatial sensitivity of the second example MGBv unit (Fig. 3.2*L*) was much more vulnerable to increasing sound levels, similar to responses of ICc units. Units in the other MGB subdivisions (Fig. 3.3*C*, *F*, and *I*) generally showed sharp, sound-level-tolerant contralateral tuning similar to that shown by BIN units (Fig. 3.2*F*) and by the more spatially sensitive MGBv units (Fig. 3.2*I*).

3.4.6 *Two Physiologically Distinct Subpopulations in the MGBv*

We observed two patterns of spatial sensitivity among units in the MGBv. One pattern consisted of sharp, level-tolerant contralateral specificity like that illustrated in Figure 3.2*I* and like we have encountered in cortical area A1 (Yao et al., 2013), and the other consisted of broader spatial sensitivity that degraded with increasing sound levels like that illustrated in Figure 3.2*L* and like we observed in the ICc. We tested whether the two patterns of spatial specificity, sharp versus broad, represented extremes of a continuum or whether they were characteristic of two functionally distinct neural

populations. For that purpose, we developed a template-matching procedure in which we compared the RAF of each MGBv unit with two templates: one based on a grand mean of RAFs of cortical area A1 units measured in our previous study (Yao et al., 2013) and the other based on a grand mean of RAFs of ICc units measured in the present study; the template-matching procedure is detailed in Materials and Methods. All of the RAFs used for that analysis were those measured at the highest tested sound level, 40 dB above unit thresholds. Figure 3.4*A* illustrates the A1 template (thick line and filled circles), the ICc template (thick line and x's) and an RAF of one MGBv unit (thin line and open circles).

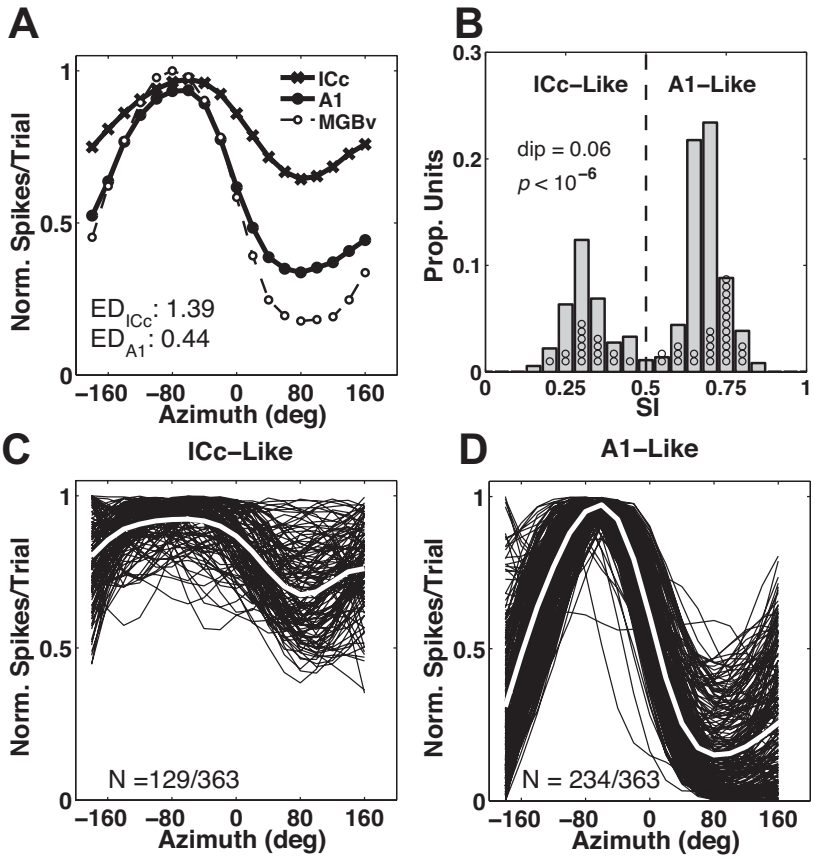

Figure 3.4. Classifying distinct classes of spatial sensitivity in MGBv. *A*, Normalized RAF at 40 dB above unit threshold from one example MGBv unit (thin line and open circles) overlaid with RAF templates constructed from all ICc (thick line and x's) and A1 (thick line and filled circles) units. Euclidean distance (ED) values between the example MGBv RAF and templates are indicated in the panel. ED values were used to calculate the "Similarity Index" (SI). These metrics were used to determine how closely each MGBv unit matches either template. *B*, Distribution of SI values for all MGBv units. Circles represent data from single units. Vertical dashed line represents the boundary at 0.50. Dip-statistics and corresponding *p*-value are indicated in the panel. *C* and *D*, Individual MGBv RAFs assigned as "ICc-Like" (*C*) and "A1-Like" (*D*). White lines represent the grand means.

Our template-matching procedure yielded a "similarity index" (SI) that could range from 0 to 1, where numbers nearer 0 indicate greater similarity to the ICc and numbers nearer 1 indicate greater similarity to A1. The distribution of *SI* values from all MGBv units is plotted in Figure 3.4*B*. There was a clear bimodal distribution (dip = 0.06, $P < 10^{-6}$; Hartigan's dip test) with peaks at around 0.30 and 0.70, consistent with the view that MGBv consists of two classes of units distinguished by their spatial sensitivity. We classified units having *SI* values < 0.50 or ≥ 0.50 as "ICc-like" or "A1-like", respectively. The individual normalized RAFs of MGBv units that were classified in that way are illustrated in Figure 3.4*C* (*N* = 129 ICc-like units) and Figure 3.4*D* (*N* = 234 A1-like units). We also compared the RAF of each BIN unit with the two A1 and ICc templates. Consistent with our impressions of BIN spatial tuning, the distribution of *SI* values from all BIN units was unimodal, with each of 131 units possessing an *SI* value > 0.50 (median, 0.63).

We tested whether the two populations of MGBv that were distinguished by their spatial sensitivity differed in other response properties; specifically, we compared distributions of CF, breadth of frequency tuning (i.e., Q_{ERB}), and 1st-spike latency. Figure 3.5*A* and *B* display frequency bandwidth (Q_{ERB}) and 1st-spike latency of the two populations as a function of unit CF in 1-octave bins. Within each ICc-like or A1 group, the Q_{ERB} increased (i.e., frequency tuning narrowed) with increasing CF (ICc-like: $X^2_{(5,123)} = 31.9$, $P < 10^{-5}$; A1-like: $X^2_{(5,228)} = 83.8$, $P < 10^{-6}$; Kruskal-wallis). Within each 1-oct CF band, however, there was no significant difference between ICc-like and A1-like groups ($P = 0.15–0.97$; rank sum). Neither ICc-like nor A1-like groups showed a significant dependence of 1st-spike latency on CF (ICc-like: $X^2_{(5,123)} = 10.1$, $P = 0.07$; A1-like: $X^2_{(5,228)} = 3.99$, $P = 0.55$; Kruskal-wallis). All but one of the 1-oct CF bands showed no significant difference between groups ($P = 0.26–0.88$, rank sum). The exception was the band centered on 4 kHz ($P = 0.04$, rank sum), but we doubt the importance of that difference given the small numbers of units in those groups.

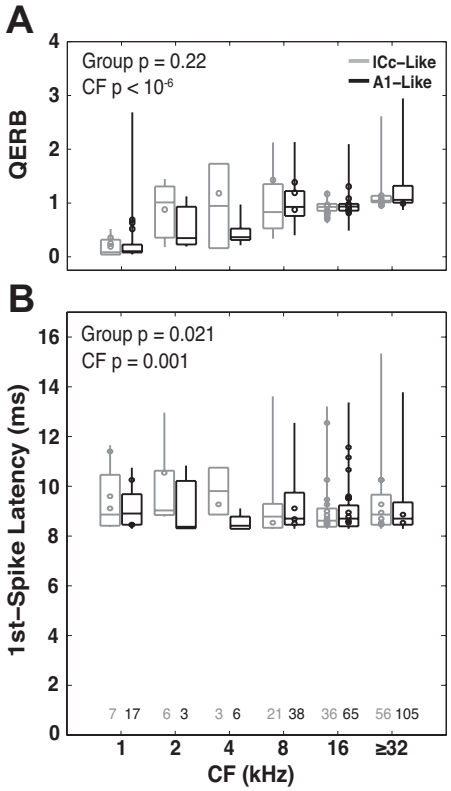

Figure 3.5. Distribution of Q_{ERB} values (*A*) and First-spike latencies (*B*) from ICc-Like (gray) and A1-Like (black) units in the MGBv plotted as a function of unit CF binned at 1 octave bands. Horizontal lines forming the boxes indicate the 25th, 50th, and 75th percentiles of multi-unit responses. Vertical lines indicate the full range from multi-unit responses. Circles represent data points from well-isolated single units. *P*-values (Kruskal-wallis) are indicated in the panel. The row of numbers above the horizontal axis indicates the total number of units represented in each bin.

We tested for a correlation between *SI* and unit CF by performing a Spearman rank correlation analysis with 10,000 bootstrapped replications. For each replication we randomly drew with replacement an equal number of units per 1-octave CF bin from the MGBv population. Confidence intervals (CIs) were calculated from each distribution of correlation coefficients (empirical two-tailed). No relationship was seen between *SI* and unit CF (correlation coefficient CI = [–0.20 0.29], $p > 0.05$; Spearman rank correlation). To summarize, the two unit populations that formed such a strikingly bi-modal distribution on the basis of similar spatial sensitivity to ICc or A1 units showed little or no systematic difference in CF, sharpness of frequency tuning, or 1st-spike latency.

Within a single recording-probe placement in the MGBv, units at contiguous sequences of recording sites tended to fall within the same spatial sensitivity class. This led to the hypothesis that units that differed in spatial sensitivity were segregated

anatomically within the MGBv. We tested that hypothesis by using a permutation test, which is detailed in Materials and Methods. We examined 363 units along 40 multisite probe placements and counted 290 instances for which units at the 312 pairs of adjacent recording sites displayed matching spatial sensitivity classes. One hundred thousand random distributions of ICc- and A1-like units along 40 virtual recording probes yielded a median of 178 and a maximum of only 213 adjacent matching pairs. That the actual number of adjacent pairs was larger than the maximum across 100,000 permutations indicates a nonrandom distribution of response classes among recording sites at a level of $P < 10^{-5}$. There were 28 runs of 3–23 consecutive matching pairs of unit spatial sensitivity, spanning 150–1,150 μm. The distribution of the lengths of runs of recording sites showing matching spatial sensitivity had quartiles of 200/350/600 μm.

3.4.7 *Transformation of Spatial Sensitivity in the Ascending Pathway*

We quantified the breadth of spatial sensitivity by calculating ERRF widths (Fig. 3.6A) at all tested supra-threshold stimulus levels. Figure 3.6*A* and *B* plot data from all the studied brain regions plus the previously obtained data from cortical area A1 (Yao et al., 2013). Across all regions and levels tested, ERRF widths ranged from around 120° to around 300°, i.e., from somewhat less than a hemifield to covering nearly all azimuth locations. Generally, MGBv-A1-like units showed the narrowest ERRF widths, those in ICc and the MGBv-ICc-like population were broadest, and those of A1 units, BIN, and non-lemniscal MGB subdivisions were intermediate. The magnitudes of ERRF-width differences between regions varied with tested level, but the ranking in spatial sensitivity across regions remained nearly constant. Note that the difference in spatial sensitivity between MGBv-A1-like and MGBv-ICc-like units is expected, given that units in those groups were selected based on spatial tuning. Similarly, it is not surprising that median ERRF widths in A1 are broader than those in the MGBv-A1-like population given that the A1 population includes all A1 units that were encountered, whereas the MGBv-A1-like units were selected for sharp spatial tuning.

We found that all regions showed some variation in ERRF width with increasing level (Fig. 3.6*A*). ERRF widths for ICc and MGBv-ICc-like units increased most markedly with increasing level, with a median increase of 123° and 98°, respectively, between 10 and 40 dB above unit thresholds. All other regions were less susceptible to

increasing levels, with median differences ranging from ~24° to ~34° between 10 and 40 dB above unit threshold for A1, MGBv-A1-like, and non-lemniscal MGB nuclei. BIN units showed a slightly greater change in ERRF width with increasing level, possessing a median increase of 69° between 10 and 40 dB above unit threshold. We fitted regression lines to the ERRF-width versus sound level above threshold functions on a unit-by-unit basis and used the slopes to quantify the dependence of sound level on spatial sensitivity. We present the cumulative distributions of slopes for all regions in Figure 3.6*B*; this includes 168 units from A1 reported previously (Yao et al. 2013). We found slopes differed significantly among all regions ($X^2_{(7,999)} = 379.9$, $P < 10^{-6}$; Kruskal-wallis). Specifically, ICc and MGBv-ICc-like units were most vulnerable to increasing levels, possessing the highest slopes ($P < 10^{-6}$; post-hoc multiple comparison, Bonferroni-corrected), whereas A1 and non-lemniscal MGB units were least vulnerable. BIN units were slightly, but significantly more vulnerable to increasing levels than A1 and non-lemniscal MGB units, but less vulnerable (i.e., more level-tolerant) than ICc and MGBv-ICc-like units ($P < 10^{-6}$; post-hoc multiple comparison, Bonferroni-corrected). Overall, the most remarkable differences were between the ICc and its projection sites along the lemniscal (MGBv-A1-like) and tectal (BIN) pathways. These comparisons showed the greatest contrast in spatial sensitivity and level dependence. Thus, the findings suggest that spatial sensitivity transforms along two independent pathways along the ascending auditory system with sharp, level-tolerant spatial sensitivity arising between the ICc and BIN as well as between the ICc and MGBv.

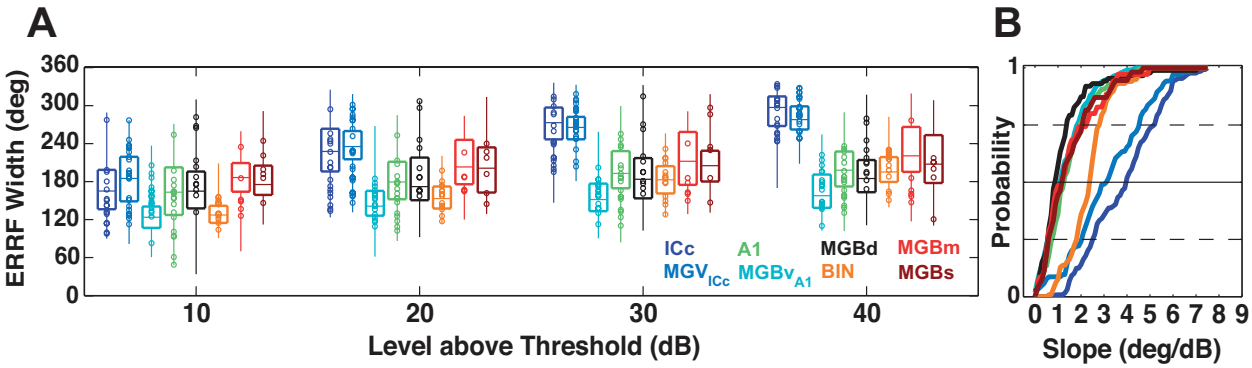

Figure 3.6. Breadth of spatial sensitivity and level dependence. *A*, Distributions of ERRF Width grouped by the four tested sound levels above threshold for all sampled populations, as indicated by color. Horizontal lines forming the boxes indicate the 25th, 50th, and 75th percentiles of multi-unit responses. Vertical lines indicate the full range from multi-unit responses. Circles represent data points from well-isolated single units. *B*, Cumulative distributions of linear fit slopes.

We compared our sampled populations across additional measures of spatial sensitivity, including preferred azimuth (represented by centroids) and steepest slope locations. Centroids were computed only for units that showed more than 50% modulation of their spike rates throughout 360° of azimuth; units showing less than that criterion for spike-rate modulation were classified as having no centroid (NC). The interquartile range from those centroids lay within 7.4 to 29.2° (left and right) of contralateral 60°, regardless of anatomical region or sound level. The percentage of NC units was highest among ICc and MGBv-ICc-like units at suprathreshold levels greater than 10 dB, and the percentages of NC units in those regions increased dramatically with increasing sound level. Steepest slope locations for BIN, A1, and units in all MGB nuclei except the MGBv-ICc-like units typically clustered within ~20° (interquartile range = –20 to 20°) of the midline across all levels. Steepest slope locations for MGBv-ICc-like and ICc units were vulnerable to increasing level, tending to shift ipsilaterally from the midline with increasing sound levels (interquartile range at 40 dB above threshold = –20 to 40°).

3.4.8 *Discrimination of Sound-Source Locations*

We tested how well individual units could distinguish between azimuth locations on the basis of trial-by-trial distributions of spike counts (described in Materials and Methods and Yao et al., 2013). Figures 3.7*A*-*H* show examples from individual units as matrices of *d′* for all possible comparisons between azimuth locations at 40 dB above threshold; the examples correspond to the 7 single units represented in Figures 3.2 and 3.3 plus one area-A1 unit from our previous paper (Yao et al., 2013). Values of $d' \geq 1$ indicate significant discrimination between the compared azimuth locations. These matrices are representative in that most BIN (Fig. 3.7*A*), MGBv-A1-like (Fig. 3.7*B*), A1 (Fig. 3.7*C*), MGBd (Fig. 3.7*D*), MGBm (Fig. 3.7*G*), and MGBs (Fig. 3.7*H*) units could readily discriminate between locations in differing hemifields, as indicated by high *d′* values in the upper left and lower right quadrants of the matrices, but could not discriminate well within a hemifield. In contrast, most ICc (Fig. 3.7*E*) and MGBv-ICc-like (Fig. 3.7*F*) units could not discriminate reliably between any of the locations.

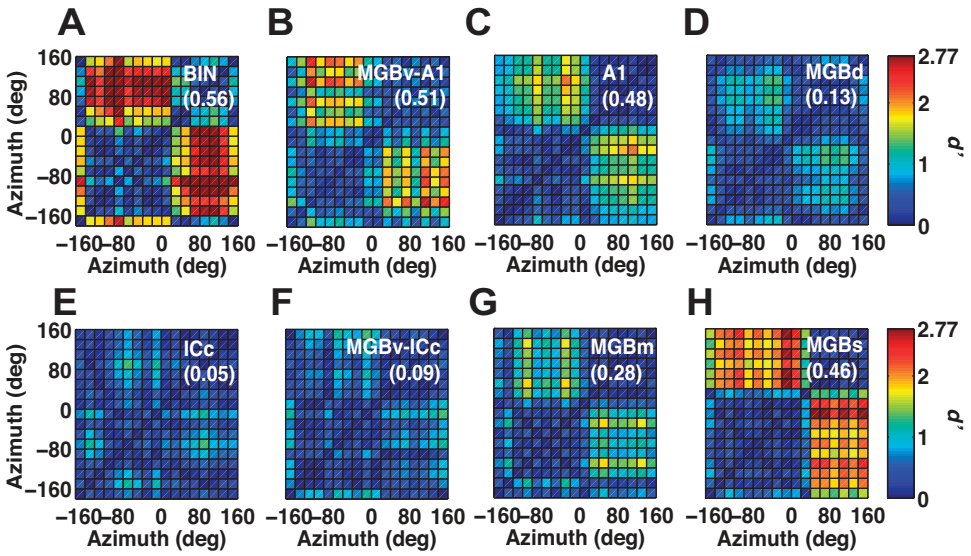

Figure 3.7. Pairwise *d′* matrices for corresponding pairs of stimulus locations at 40 dB above threshold from the single units shown in Figures 2 and 3. *A*, BIN; *B*, MGBv-A1-Like; *C*, A1; *D*, MGBd; *E*, ICc; *F*, MGBv-ICc-Like; *G,* MGBm; *H,* MGBs. Stimulus locations were separated by 20°. Significant discriminations among paired locations are indicated by $d' \geq 1$.

The overall accuracy of location discrimination by each unit was quantified by the percentage of location pairs that could be discriminated with $d' \geq 1$. In principle, this percentage could range from 0, meaning no locations discriminated, to 100, meaning all pairs of locations discriminated. Based on the typical sinusoidal shape of the RAFs of the most spatially-sensitive units, however, one would expect the maximum percentage of discriminated location pairs to be closer to 50%, indicating discrimination of most between-hemifield location pairs and few discriminations within hemifields. Figure 3.8 plots the median and interquartile ranges of the percentages of discriminated location pairs from the various sampled regions as a function of level above threshold. The comparisons between sampled populations mirror the trends of ERRF-width measures in Figure 3.6A. For instance, consistent with displaying the sharpest spatial sensitivity, MGBv-A1-like and BIN units possessed the highest percentages (~50%) across all sound levels. In addition, units from the remaining sampled regions consistently maintained effective discrimination of many source locations across levels, except for ICc and MGBv-ICc-like units, which showed a dramatic decrease in percentages with increasing levels (Fig. 3.8).

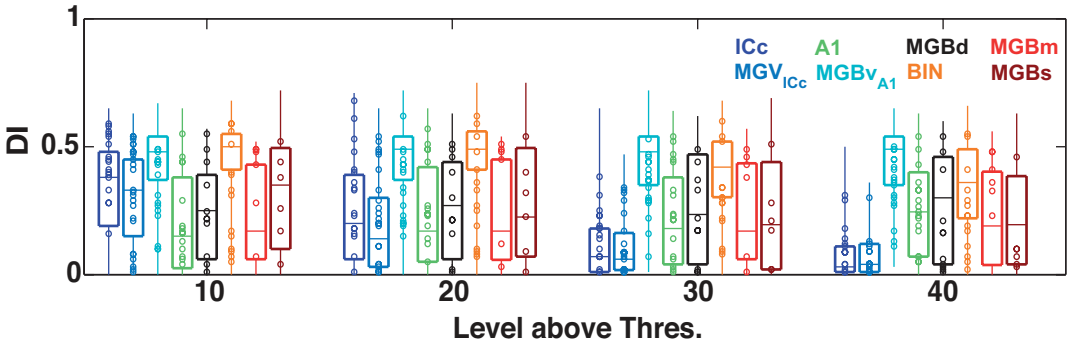

Figure 3.8. Distributions of percentages of discriminated location pairs for all sampled populations as a function of level above threshold. Similar convention as in Figure 3.6*A*.

3.5 Discussion

The present results demonstrate a transformation of spatial sensitivity along the ascending tectal and lemniscal auditory pathways, with RAFs dramatically sharpening and becoming more level tolerant from the ICc to the BIN and from the ICc to the MGBv. Neurons within non-lemniscal MGB subdivisions displayed spatial sensitivity that largely reflect putative inputs from A1 or BIN. Unexpectedly, we observed that the MGBv, the major thalamic structure in the lemniscal pathway, contains two distinct classes of neurons distinguished by their spatial sensitivity. These two classes might be related to known neuron classes described in the literature (e.g., Hashikawa et al. 1991; de Venecia et al. 1995, 1998) and need to be further examined.

3.5.1 *Two Parallel Pathways for Auditory Space Processing*

The schematic diagram in Figure 3.9 summarizes a tentative circuit for spatial processing observed in the present study, commencing at the level of the ICc. The circuit is based on reported anatomical connections and on the present observations of spatial sensitivity. Spatial sensitivity in each brain region is represented by grand-mean RAFs at four sound levels.

All of the non-lemniscal MGB structures in the present study showed fairly sharp, level-tolerant spatial sensitivity. The short-latency space-sensitive responses in the MGBm could reflect its reported inputs from the BIN (Kudo et al., 1984). The longer-latency responses in the MGBd could reflect descending input via corticofugal projections from A1 (Rouiller and Welker, 1991; Shi and Cassell, 1997; Bartlett et al., 2000; Winer et al., 2001; Hazama et al., 2004). The MGBs has primarily been

characterized in guinea pigs (Anderson et al., 2007; He, 2001; He and Hu, 2001; Redies et al., 1989) and is thought to receive direct input from the rostral half of the MGBv; we omit that connection in our drawing because of the relative lack of anatomical evidence available in the rat. The spatial sensitivity in MGBs is similar to that of the sharply tuned units in MGBv, although a direct projection from MGBv to MGBs would not account for the long latency of neurons in the shell nucleus.

We find evidence for two parallel pathways showing sharp, level-tolerant spatial tuning, both originating with neurons showing broad spatial sensitivity in the ICc. Neurons in the ICc showed contralateral spatial sensitivity at low sound levels that degraded rapidly at increasing levels, primarily due to level-dependent increases in responses to ipsilateral locations. The lack of spatial sensitivity at moderate sound levels was reflected in the inability of ICc units to discriminate between azimuth locations (Fig. 3.8). The presence of broad, level-dependent spatial tuning in our sample of ICc units matches the omnidirectional and level-dependent class of ICc units reported in other animals (e.g., cat: Aitkin et al., 1984; rabbit: Kuwada et al., 2011), although those same studies also report subpopulations of sharply-tuned, level-tolerant units. The difference between species might be due to differences in the underlying anatomical circuitry of converging inputs to the IC. In rats, the commissure of the IC is thought to provide intensity-dependent excitatory and inhibitory input to most ICc neurons (Malmierca et al., 2005). Whether or not input from the intercollicular commissure varies between species remains to be seen. Despite the degraded spatial sensitivity in the ICc at higher sound levels, its two ascending targets showed sharp, level-tolerant spatial sensitivity. We hypothesize that the advent of level invariance in those targets represents changes in the balance of contralateral excitation and ipsilateral inhibition, but tests of that assumption must wait for future intracellular studies. The present extracellular data indicate that sharp spatial sensitivity arises in two distinct pathways: the tectal pathway through the BIN and the lemniscal pathway through the MGBv.

The BIN has been reported to receive direct projections from the ICc (Jiang et al., 1993; King et al., 1998; Nodal et al., 2005; Slee and Young, 2013). All of our BIN units exhibited relatively sharp, level-tolerant spatial sensitivity that was biased to the

contralateral hemifield (Fig. 3.9). As a result, these units were capable of discriminating nearly half of all azimuth locations across our tested sound levels (Fig. 3.8). Preference for contralateral azimuth locations is typically seen in the few studies that examined the spatial sensitivity of this structure (ferret: Schnupp and King, 1997; awake marmoset: Slee and Young, 2013), however, we found spatial sensitivity in the rat to be much sharper than that seen in awake marmosets, and more level-tolerant than in the ferret. The absence of BIN units showing broad spatial sensitivity in the present study suggests that the transformation to sharp spatial sensitivity in the BIN is complete at or before the level of synapses of ICc axons onto BIN neurons in the rat. In anesthetized ferrets, Schnupp and King (1997) found a rather indistinct topography of spatial tuning as a function of BIN location. We observed no such topography in the rat BIN, which is not surprising given the very limited range of spatial centroids in the rat BIN. Previous studies have shown that the BIN projects to the SC (ferret: Jiang et al., 1993; King et al., 1998). In the SC of the rat, neurons showed predominantly contralateral hemifield spatial sensitivity, and there was only a somewhat poorly defined spatial topography (Gaese and Johnen, 2000). That is consistent with the notion that the spatial sensitivity seen in the SC is inherited largely from the BIN.

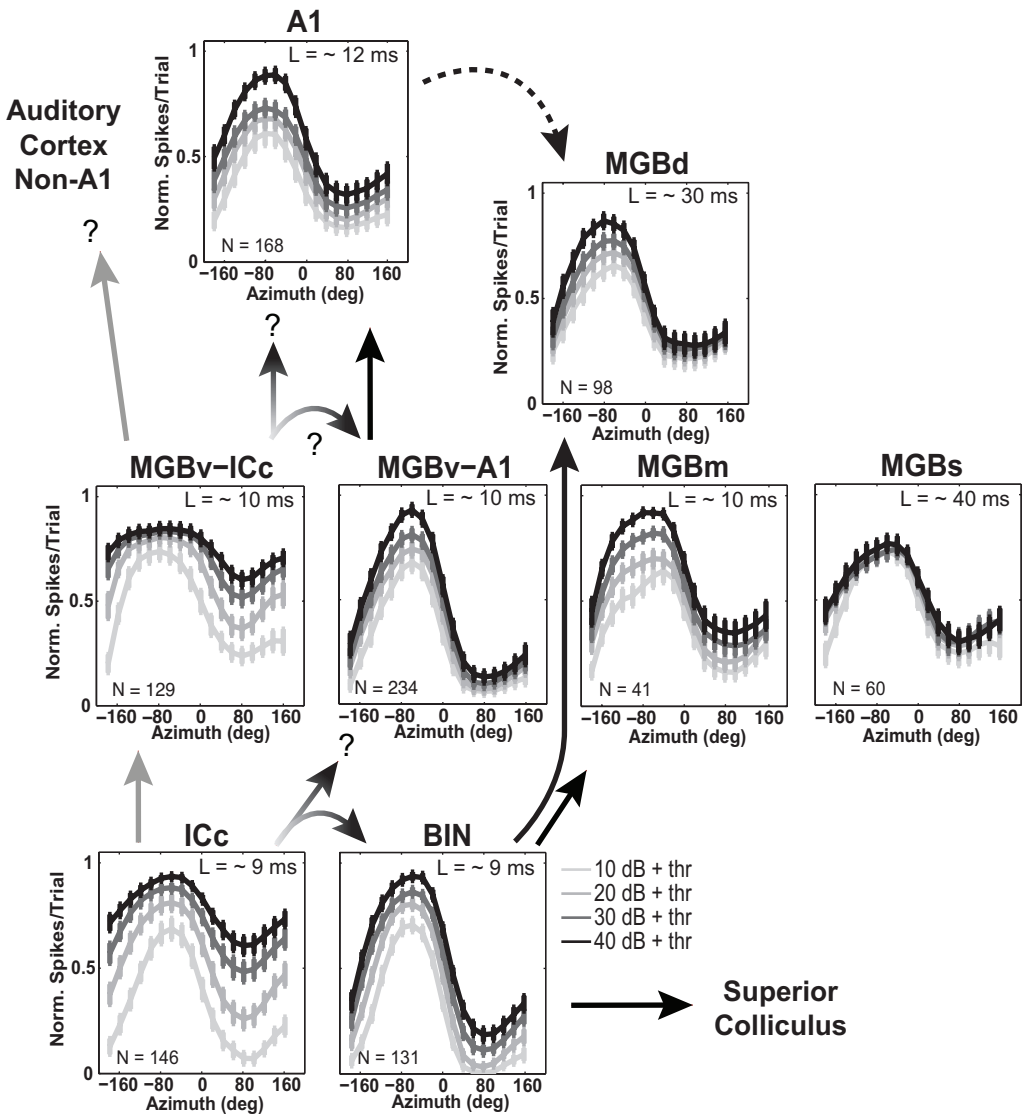

Figure 3.9. Grand mean rate azimuth functions (RAFs) across 10, 20, 30, and 40 dB above threshold from all units within each subdivision sampled. RAFs are normalized to each unit's maximum spike rate location and highest level. Data are presented along the ascending (solid lines) and descending (dashed lines) circuitry of the IC-MGB-A1 axis with possible inheritance and/or transformations from circuitry projections based on latency (L). Notice the transformation of azimuth representation as it ascends from the ICc to MGBv, and from the ICc to BIN.

About 65% of the units in our sample of the MGBv units, the "A1-like units", showed sharp, level-tolerant spatial sensitivity, whereas the other 35% showed broader spatial sensitivity (ICc-like), vulnerable to increasing sound level, like that observed in the ICc. The MGBv is well known to receive its ascending input from the principal cells in the ICc (Calford and Aitkin, 1983). At present, it is not clear whether the sharply-tuned A1-like MGBv units that we studied were directly post-synaptic to ICc axons or whether

they received their input by way of the MGBv-ICc-like neurons. That issue is considered in the following section.

3.5.2 *Two Populations of Neurons Within the MGBv*

An unexpected finding was that of the two distinct populations of neurons within the MGBv. The populations differed markedly in their spatial sensitivity while showing little or no differences in other physiological measures that we evaluated. We also observed a conspicuous nonrandom distribution of these two classes of neurons in the MGBv. The organization of adjacent units with similar spatial sensitivity is reminiscent of the complex banded organization of binaural sensitivity in the cat MGBv, where neurons that project to cortical neurons that are excited by either ear (EE) are segregated from those that project to cortical neurons that are inhibited by the ipsilateral ear (EI) (Middlebrooks and Zook, 1983). EE and EI characteristics could be similarly compared with the broad spatial sensitivity of MGBv-ICc-like and the sharp spatial sensitivity of MGBv-A1-like units, respectively.

We consider two hypotheses for the origin of such distinct unit classes within the MGBv. One hypothesis is that MGBv-ICc-like units lie on a pathway between the ICc and MGBv-A1-like units, first receiving direct input from the ICc and then projecting to MGBv-A1-like units. If A1-like units received direct input from ICc-like units, then their response latencies would be longer than those of ICc-like units. Contrary to that prediction, first-spike latencies of the MGBv-A1-like population were not significantly different from those of the MGBv-ICc-like population, arguing against such an anatomical substrate. An alternative hypothesis involves two distinct functional pathways, with MGBv-A1-like units resulting from a transformation of spatial sensitivity across the colliculo-thalamic synapse and MGBv-ICc-like units directly inheriting spatial sensitivity from the ICc.

One might raise the hypothesis that the ICc already contains both broadly and sharply tuned unit classes, but that our use of multi-unit recording obscured the sharp tuning by recording simultaneously from putatively intermingled broadly and sharply tuned units. That hypothesis seems unlikely in that not one of the 17 well-isolated single units recorded in the ICc showed sharp, level-tolerant spatial sensitivity like that shown by the MGBv-A1-like units.

The anatomical projection sites of the two distinct classes of MGBv units are largely unknown. Our previous observations of sharp level-tolerant spatial tuning in rat A1 units would be consistent with the view that rat A1 spatial sensitivity is inherited exclusively from MGBv-A1-like units and that the MGBv-ICc-like units either project elsewhere in the cortex or do not project out of the MGB. Alternatively, it might be that A1-like and ICc-like projections are somehow combined but that the A1-like inputs dominate the spatial sensitivity seen in A1. One possible cortical projection target for MGBv-ICc-like units could be auditory areas anterior and posterior to A1, where units showing excitatory inputs from both ears have been reported (Kelly and Sally, 1988). Future work involving anatomical and physiological methodology are needed to explore these hypotheses.

3.5.3 *Potential Behavioral Relevance for Parallel Pathways for Auditory Space Processing*

Previous studies suggest distinct roles of tectal and lemniscal pathways in auditory spatial behavior and perception. The tectal pathway provides auditory input to the SC for its role in directing reflexive orienting movements of the eyes, head, and external ears to auditory and multisensory stimuli (Sparks and Groh, 1995; King, 2004). Unilateral lesions of the SC in cats result in lengthening of the latencies of behavioral orientations to contralateral sounds (Thompson and Masterton, 1978) and reduce the multisensory enhancement of orientation responses to spatially coincident auditory and visual targets (Burnett et al., 2004). In contrast, the lemniscal pathway has been shown in cats and ferrets to be essential for operant localization of sound sources, including responses to remembered locations. For example, unilateral lesions (Jenkins and Merzenich, 1984) or inactivation by cortical cooling (Malhotra and Lomber, 2007) of auditory cortex disrupts the ability of a cat to walk to the remembered location of a brief sound presented from the side contralateral to the lesion or inactivation. Similar dissociations of reflexive orientation and localization of remembered targets have been demonstrated in homologous tectal and lemniscal pathways in the barn owl (Knudsen et al., 1993; Knudsen and Knudsen, 1996). Severe impairments in left-versus-right discrimination ability were seen in rats when lesions were made within the tectal pathway (Kelly and Judge, 1985), suggesting left-versus-right orientation ability requires

an intact tectal pathway. Consistent with these findings, our recorded BIN units could accurately discriminate between-hemifield source-locations, possessing percentages of discriminated location pairs around 50% (Fig. 3.8). It remains to be tested how transformation of spatial sensitivity along the lemniscal pathway aids in the perception of sound-source locations. Optogenetic and chemical genetic approaches may provide a means to directly assess this in future studies.

3.6 Acknowledgements

We thank Zekiye Onsan for administrative support, and Elizabeth McGuire and Lauren Javier for technical and administrative assistance. We also thank Minhan Dinh and Dr. Karina Cramer for generously providing advice, facilities, and supplies for histology. This work was supported by National Institute on Deafness and Other Communication Disorders Grants R01-DC000420 and F31 DC013013 (Ruth L. Kirschstein Predoctoral Individual National Research Service Award to promote diversity in health-related research).

CHAPTER 4: Emergence of Spatial Stream Segregation in the Ascending Auditory Pathway

This work is currently under review at J Neurosci (2015).

4.1 Summary

Stream segregation enables a listener to disentangle multiple competing sequences of sounds. A recent study from our laboratory demonstrated that cortical neurons in anesthetized cats exhibit spatial stream segregation (SSS) by synchronizing preferentially to one of two sequences of noise bursts that alternate between two source locations. Here, we examine the emergence of SSS along the ascending auditory pathway. Extracellular recordings were made in anesthetized rats from the inferior colliculus (IC), the nucleus of the brachium of the IC (BIN), the medial geniculate body (MGB), and the primary auditory cortex (A1). Stimuli consisted of interleaved sequences of broadband noise bursts that alternated between two source locations. At stimulus presentation rates of 5 and 10 bursts per second, at which human listeners report robust SSS, neural SSS is weak in the central nucleus of the IC (ICC), it appears in the nucleus of the brachium of the IC (BIN) and in about two thirds of neurons in the ventral MGB (MGBv), and is prominent throughout A1. The enhancement of SSS at the cortical level reflects both increased spatial sensitivity and increased forward suppression. We demonstrate that forward suppression in A1 does not result from synaptic inhibition at the cortical level. Instead, forward suppression might reflect synaptic depression in the thalamocortical projection. Taken together, our findings indicate that auditory streams are increasingly segregated along the ascending auditory pathway as distinct mutually-synchronized neural populations.

4.2 Introduction

In the complex auditory scenes experienced in everyday life, listeners can disentangle competing sound sequences from multiple sources, a phenomenon known as “stream segregation” (Bregman, 1990). There is a robust spatial component to this phenomenon, with as little as 8° spatial separation between competing sound sources resulting in successful perceptual segregation of streams (Middlebrooks and Onsan, 2012). Moreover, neurons in the auditory cortex of anesthetized cats exhibit a correlate of spatial stream segregation (SSS) by synchronizing preferentially to one of two

sequences of noise bursts that alternate in location (Middlebrooks and Bremen, 2013). Here, we examine in rats the emergence of SSS among four levels of the ascending auditory pathway: the central nucleus of the inferior colliculus (ICC), the nucleus of the brachium of the inferior colliculus (BIN), the ventral division of the medial geniculate body (MGBv), and primary auditory cortex (area A1). The rat is a suitable experimental model for these experiments because it shows good spatial acuity in psychophysical tests, at least across the frontal midline (Heffner and Heffner, 1985; Kavanagh and Kelly, 1986; Ito et al., 1996), because neurons in cortical area A1 show homogeneous patterns of spatial sensitivity (Yao et al., 2013), and because midbrain, thalamic, and cortical levels of the ascending auditory system are readily accessible for study (Yao et al., 2015).

It is known that both spatial tuning (Yao et al., 2015) and the ability of neurons to synchronize to sound envelopes (Creutzfeldt et al., 1980; Joris et al., 2004; Wang et al., 2008) undergo pronounced transformations along the ascending auditory pathway. In the rat, for example, spatial tuning of neurons sharpens and becomes increasingly level-tolerant at successive levels of the pathway from the ICC to a subpopulation of neurons located in the MGBv to essentially all neurons studied in cortical area A1 (Yao et al., 2015). Moreover, the maximum frequencies at which neurons synchronize to stimulus envelopes decrease at successive levels of the pathway, from up to 340 Hz in the IC (rat: Rees and Møller, 1987), to ~100 Hz in MGB (guinea pig: Creutzfeldt et al., 1980; marmoset: Bartlett and Wang, 2007) to 18 Hz or less in cortical neurons (rat: Gaese and Ostwald, 1995; Kilgard and Merzenich, 1999).

We hypothesized that sharpening of spatial sensitivity and decreases in the maximum frequency for envelope synchrony result in enhanced segregation of sequences of sounds from multiple sources, thereby rendering the individual sound streams accessible for subsequent perceptual selection. Accordingly, we tested the hypothesis that SSS strengthens along the ascending auditory pathway and can be attributed to a gradual increase in spatial sensitivity and a decrease in a low-pass envelope filter cutoff between area A1 and its subcortical input.

We found that, at temporal scales at which SSS is seen behaviorally (Middlebrooks and Onsan, 2012), neurons in the ICC showed little evidence of SSS, but

that SSS emerges in the BIN and in about two thirds of neurons in the MGBv, and is prominent among all neurons in A1. The SSS observed among neurons in the MGBv and BIN could be explained largely by the sharp spatial tuning of those neurons, whereas the SSS observed in cortical area A1 also reflected a low-pass envelope filter resulting from forward suppression. To further elucidate the mechanism of cortical SSS, we tested the hypothesis that forward suppression observed in the cortex results from GABA-ergic inhibition at the level of thalamocortical synapses. Contrary to that hypothesis, topical application of $GABA_A$ and $GABA_B$ receptor antagonists in the auditory cortex gave no relief from forward suppression, despite producing an overall increase in spike rate. We conclude that the forward suppression that we observe in the auditory cortex is due to synaptic depression rather than synaptic inhibition or intrinsic biophysical properties of A1 neurons and that forward suppression combined with the sharpened spatial sensitivity seen at cortical levels result in a neural correlate for SSS in the auditory cortex.

4.3 Materials and Methods

The data reported here were obtained from the population of neurons from which data were presented in previous reports (Yao et al., 2013, 2015). The previous reports focused on frequency sensitivity measured using tonal stimuli and on spatial sensitivity measured using single broadband noise bursts. The present study focuses on segregation of interleaved sequences of broadband noise bursts from paired sources.

4.3.1 *Animal Preparation*

All procedures were performed with the approval of the University of California at Irvine Institutional Animal Care and Use Committee according to the National Institutes of Health guidelines and were similar to those of previous reports from our lab (Middlebrooks and Bremen, 2013; Yao et al., 2013, 2015). Data presented here were obtained from 37 adult male Sprague-Dawley rats (median age: 10.7 wk; Charles River Laboratories, Hollister, CA) weighing 265–475 g (median weight: 370 g). The IC and MGB were studied in 15 rats and cortical area A1 was studied in 22 rats. Surgical anesthesia was induced with urethane (1.5 g/kg ip) and xylazine (10 mg/kg ip) and supplemented as needed to maintain an areflexive state. To reduce the viscosity of bronchial secretions and to prevent brain edema we administered atropine sulfate (0.1

mg/kg ip) and dexamethasone (0.25 mg/kg ip), respectively, at the beginning of surgery and every 12 h thereafter. Core body temperature was maintained at ~37°C. Surgery began with a midline scalp incision and the exposure of the underlying skull. We cemented an inverted machine screw to the skull on the midline, rostral to bregma, to serve as a head holder. The skull was opened to access the right auditory cortex, IC, and MGB. Prior to recordings, the scalp was partially closed and the positions of the pinnae were adjusted to minimize any alteration that the surgical procedure may have caused.

4.3.2 *Experimental apparatus, stimulus generation, and data acquisition*

The animal was positioned in the center of a darkened double-walled sound attenuating chamber (Industrial Acoustics; inside dimensions 2.6 x 2.6 x 2.6 m) that was lined with 60-mm-thick absorbent foam (SONEXone, Seattle, WA). The animal's head was supported by a 10-mm-diameter rod attached to the skull screw. The rod was held by a thin metal frame positioned behind the animal. The area around the head and ears was unobstructed. A circular hoop, 1.2 m in radius, supported 8.4 cm coaxial loudspeakers (Pioneer Electronics, Long Beach, CA) in the horizontal plane aligned with the rat's interaural axis, 1.2 m above the floor. The loudspeakers were spaced at 20° increments from left to right 80° relative to the rat's midline. Left and right loudspeaker locations are given as contralateral (C) and ipsilateral (I), respectively, with respect to the side of the recording sites, which were all in the right hemisphere.

We used Tucker-Davis Technologies System 3 equipment (TDT, Alachua, FL) controlled by a personal computer. Custom MATLAB (MathWorks, Natick, MA) scripts controlled the stimulus sequences, acquired the neural waveforms, and provided on-line monitoring of responses at the 16 or 32 recording sites. Sounds were generated with 24-bit precision at a 100 kHz sampling rate. Loudspeakers were calibrated using a precision microphone positioned in the center of the sound chamber at the normal position of the rat's head; the rat was absent during the calibration. Golay codes (Zhou et al., 1992) were used for calibration of broadband sounds. The broadband frequency responses of the loudspeakers were flattened and equalized such that for each loudspeaker the standard deviation of the magnitude spectrum across the 0.2 to 25kHz

was <1 dB. The stimulus spectrum was rolled off by 10 dB from 25 to 40 kHz. Tonal stimuli were calibrated with tone bursts from 0.2 to 40 kHz.

We recorded extracellular spike activity with single-shank silicon-substrate multisite recording probes from NeuroNexus Technologies (Ann Arbor, MI, USA) using high-impedance head stages and multichannel amplifiers from Tucker-Davis Technologies (TDT, Alachua, FL). The probes had either 16 recording sites spaced at 100 μm intervals or 32 sites spaced at 50 μm intervals; recording-site areas were 413-μm^2 and 177-μm^2 for 16 and 32 site probes, respectively. Neural waveforms were digitized with 16-bit-precision at 25k samples/s, filtered, and stored on computer disk for off-line analysis.

4.3.3 *Experimental Procedure*

Extracellular recordings were performed in area A1 with 16-channel probes, and in the MGB and the IC with 32-channel probes. Recording procedures are identical to those of previous studies from our lab (Yao et al., 2013, 2015). For recordings in A1, the probe was aligned to be approximately orthogonal to the cortical surface and was adjusted in depth to maximize the number of recording sites in active cortical layers. Neural spike activity was encountered along probe segments spanning around 1,000 μm in length (median; 5^{th} and 95^{th} percentiles: 500 and 1,400 μm). Inasmuch as the thickness of the rat auditory cortex has been reported to average 1,100 μm (Games and Winer, 1988), that means that our cortical recordings consistently sampled the thalamocortical-recipient (granular) layers as well as substantial portions of infra- and supra-granular layers. Cortical area A1 was identified by brisk short-latency responses to noise bursts (first-spike latencies ~10–15 ms), V-shaped frequency tuning curves, and a caudal-to-rostral increase in CFs (Polley et al. 2007). The borders of A1 were defined by reversals in tonotopy and increases in latencies (Doron et al. 2002; Rutkowski et al. 2003). Our previous findings demonstrated uniform contralateral hemifield spatial tuning in this neural sample (Yao et al., 2013). Higgins and colleagues (2010) showed sensitivity to interaural level differences (ILDs) in A1 consistent with contralateral spatial tuning, whereas they found ILD sensitivity consistent with tuning to the spatial midline in neighboring areas VAF and caudal SRAF. That our neural sample showed consistently contralateral sensitivity uncontaminated by neurons showing

midline sensitivity supports the view that our cortical data sample was limited to area A1. After each probe was in position, the cortical surface was covered with a warmed 2% solution of agarose in Ringer's solution, which cooled to a firm gel that reduced brain pulsations and prevented the cortical surface from drying.

The right IC was accessed with vertical probe placements (14 placements in 5 animals) approximately ~2–3 mm lateral to the midline and ~7–9 mm caudal to bregma. Two approaches were used to access the right MGB. The vertical approach (22 probe placements in 8 animals) used vertical probe placements ~3–4 mm lateral to the midline and ~5–6 mm caudal to bregma. The lateral approach (18 probe placements in 6 animals) used a dorso-lateral to ventro-medial trajectory, ~30–50° from the sagittal plane, ~4–6 mm caudal to bregma. Unit localization within the ICC, the brachium of the IC (BIN), and the MGBv were based on stereotaxic coordinates and physiological criteria and further confirmed histologically (see Yao et al., 2015). Recordings from the ICC were characterized by monotonically increasing CFs along the dorsal to ventral trajectories, with ranges of CFs in individual probes spanning 2.2/2.7/4.1 octaves (25^{th}/ 50^{th}/ 75^{th} percentiles). Recordings from the MGBv were characterized by a lateral to medial increase in CF. The border with the medial division of the MGB was marked by an increase in frequency bandwidth and a reversal in tonotopy.

Study of responses at each probe position consisted of measurements of frequency response areas, of mean-spike-rate-versus-azimuth functions (RAFs), of excitation thresholds for broadband noise bursts, and of spatial stream segregation. Measurements were based on single- and multiple unit responses, as defined in Data Analysis). Frequency response areas (FRAs) were measured with pure tones, 80 ms in duration with 5-ms raised-cosine onset and offset ramps, at a repetition rate of 1 or 1.25 s^{-1} presented from the loudspeaker located 40° contralateral to the right-sided recording site (C40°). Tones varied in frequency from 0.2 to 40 kHz in 1/3- or 1/6- octave steps and in level in 10-dB steps, typically from –10 to 60 or 70 dB SPL with 10 repetitions per frequency-level combination. The range of CFs across the entire sample was 1 to >32 kHz (25/50/75th percentiles, A1: 6.70/12/>32; MGBv: 11.2/18/>32; ICc: 8/12.7/>32; BIN: 12.7/32/>32 kHz). We recorded RAFs for 80 ms Gaussian noise bursts across 360° in azimuth in 20° steps at levels ranging from –10 to 70 dB SPL in 10-dB steps (20

repetitions per combination). All stimuli were presented at a repetition rate of 1.00 or 1.25 s^{-1}. We have quantified the spatial tuning characteristics of the neurons reported here in a previous report (Yao et al., 2015). Noise thresholds were measured using 80-ms Gaussian noise bursts at a 1 or 1.25 s^{-1} repetition rate from the C40° loudspeaker, varied in level in 5–10 dB steps, with 20 repetitions per level; a silent condition also was included. Noise thresholds along each recording probe were estimated on-line, and a modal value was selected. Stimulus levels for subsequent measurements were set 40 dB or more above that modal value. Off-line, noise thresholds were measured using a receiver-operating characteristic (ROC) procedure (see below, Data analysis), and stimulus levels were computed relative to those thresholds. Across 481 unit recordings in ICC, BIN, MGBv, and A1, the distribution of stimulus levels relative to threshold had a 5^{th}, 50^{th}, and 95^{th} percentiles of 25.3, 39.7, and 56 dB, respectively. Along the 72 individual probe placements in those structures, thresholds varied by a median of only 16 dB (5^{th} and 95^{th} percentiles: 3.3 and 28 dB).

The stimulus conditions for the study of spatial stream segregation were identical to those used in a previous study in our lab (Middlebrooks and Bremen, 2013). In the "competing-source" conditions, stimuli consisted of sequences of independent Gaussian noise bursts, 5 ms in duration with 1 ms cosine-squared on and off ramps. Sequences alternated between A and B sources in an ABAB... pattern comprising 15 A and 15 B bursts. Aggregate "base rates" (i.e., presentation rates) of 5, 10, 20, and 40 bursts per second (bps) were tested, such that the difference in onset times between an A burst and that of the following B burst was 200 to 25 ms for base rates of 5 to 40 bps, respectively. The duration of the sequences was 6400 to 800 ms for base rates of 5 to 40 bps, with an additional silent period of ≥700 ms between the offset of one sequence and the onset of the next. The A bursts were presented from C40°, 0°, and ipsilateral 40° (I40°), and the B bursts were presented from C80° to I80° in 20° steps, which included conditions of A and B colocated at C40°, 0°, and I40°. In every case, we also tested B-alone conditions in which the rate of the B stimuli was equal to that in the A-B condition (i.e., half the stated base rate) and in which the rate of B stimuli was equal to that of the aggregate A-B base rate. Every combination of A location (or B alone) and B location was tested once in a random order, then every combination was tested again in

a different random order, and so on until every stimulus combination was presented 10 times.

4.3.4 *Pharmacological Procedures*

We applied pharmacological agents topically, via a microliter syringe (Hamilton), over the surface of cortical area A1 in 6 rats to assess the consequences of GABA receptor blockage on responses of A1 neurons. We tested 3 different types of GABA receptor antagonists. 1) Gabazine (2 rats; 4 probe placements) is a selective post-synaptic $GABA_A$ receptor antagonist (Heaulme et al., 1986; Kotak et al., 2008); 2) CGP 36216 hydrochloride (2 rats; 4 probe placements) is a selective $GABA_B$ antagonist that is most active at pre-synaptic receptors (Ong et al., 2001); and 3) 2-Hydroxysaclofen (2 rats; 6 probe placements) is a selective $GABA_B$ antagonist that is effective on post-synaptic receptors (Kerr et al., 1988; Metherate and Ashe, 1994). All drugs were freshly dissolved on the day of the experiment. We performed pilot experiments to determine the appropriate drug concentration to be used as well as the time course of their effect on A1 neurons. We found that drug concentrations of ~20–25 μM at a volume of ~4–6 μl could be applied without triggering epileptiform or seizure-like neuronal activity. In these conditions, there was an increase in stimulus-evoked activity starting <10 min after drug application that remained constant for ~45–60 min.

The test of each drug began with placement in the cortex of a multi-site recording probe and recording of baseline activity elicited by pulse-train stimuli. Stimuli for the drug tests consisted of sequences of independent Gaussian noise bursts, 5 ms in duration with 1 ms cosine-squared on and off ramps similar to the ABAB patterns used to assess stream segregation. Pulse trains were presented at 12 different repetition rates (1, 2–20, in steps of 2, 30, and 40 bps), 10 times for each rate, with each repetition rate presented once in a random order before repeating all the rates in a different random order. Stimulus levels were set at ≥40 dB above the on-line estimated modal value from all active channels. After baseline study, one of the GABA antagonists was applied to the cortical surface and the stimulus set was repeated at several post-application time points. After study in the drug condition, we washed out the drug with saline and waited ~45 min prior to shifting the recording probe to another cortical location to test the same or a different drug. In pilot studies, we found no significant

difference in spikes per burst between the pre-drug condition compared to the condition ~45 min after drug wash out (Gabazine, paired $t_{(21)} = 0.69$, $p = 0.69$; CGP 36216, paired $t_{(26)} = -0.81$, $p = 0.42$; 2-Hydroxysaclofen, paired $t_{(12)} = -0.90$, $p = 0.36$).

4.3.4 *Data Analysis*

All quantitative analyses are based on neuronal action potentials identified with an off-line spike-sorting procedure (see Yao et al., 2015 for more details). Responses were classified as well-isolated single units when they showed: 1) consistent waveform appearance upon visual inspection; 2) inter-spike intervals that revealed a clear refractory period greater than 1 ms; and 3) stability of spike amplitude throughout the recording period. According to that classification, our sample of well-isolated single units consisted of 17 ICC, 13 BIN, 35 MGBv, and 15 A1 neurons. An additional 401 unit recordings (76 ICC, 52 BIN, 185 MGBv, 88 A1) were classified as multi-unit activity consisting of unresolved spikes from two or more neurons. Well-isolated single units are referred to as such, whereas “unit activity” or “units” refers to single- and/or multiple unit recordings from a single recording site. All statistics include combined single- and multiple-unit responses except when stated otherwise. Not all of the stimulus sets were tested for all of the units. Nearly all ICC (N = 93), BIN (N = 65), and MGBv (N = 220) units were tested under all stream segregation base rate conditions, whereas only a subset of A1 units were tested at rates of 20 bps (N = 24/103), and no A1 units were tested at 40 bps. In addition to these 481 units, 168 units in A1 were studied using the pharmacological procedures.

We have previously characterized spatial tuning in MGBv (Yao et al., 2015) and reported that neurons in this nucleus show a remarkably bimodal distribution of spatial tuning. About 2/3 of units showed contralateral hemifield spatial tuning, like that seen in A1 and 1/3 showed omnidirectional spatial tuning like that seen in the ICC. In that study and in the present work, we identified MGBv neurons as either “ICC-like” or “A1-like” using a template-matching procedure based on single-source rate azimuth functions (RAFs; Yao et al., 2015). Briefly, this procedure consisted of comparing the RAF of each MGBv unit to templates of RAFs of ICC and A1 units; all the comparisons used responses to single-burst 80 ms sounds 40 dB above unit thresholds. A similarity index was computed for each MGBv unit, which indicated whether the MGBv unit was more

similar to the ICC (“MGBv-ICC-like”, N = 69) or to the A1 (“MGBv-A1-like”, N = 151) template.

RAFs for competing-sound stimuli as used in the SSS paradigm expressed mean spike counts per 5 ms noise bursts as a function of loudspeaker location. Spikes tended to fall within ~25 ms after each noise-burst onset. For that reason, we counted spikes in the interval 0 to 25 ms after stimulus onset, which captured essentially all the spikes driven by each noise burst. With this procedure, spikes could be attributed to each A or B noise source sequence. Every stimulus set also included a condition in which the B sequence was presented in isolation either at half, or equal to, the aggregate A-B rate. Mean spikes per burst were computed across 10 trials.

The breadth of spatial sensitivity by each unit was represented by the width of its equivalent rectangular receptive field (ERRF) (Lee and Middlebrooks, 2011; Middlebrooks and Bremen, 2013; Yao et al., 2013, 2015). The ERRF width was computed by integrating the area under a unit’s RAF, forming a rectangle having a peak height and area equal to that of the RAF, and measuring the resulting width.

Procedures based on signal detection theory (Green and Swets, 1966; Macmillan and Creelman, 2005) were used to quantify the discrimination of sound-source location. We accumulated spike counts for all repetitions synchronized to each the A and B sources and formed an empirical receiver operating characteristic (ROC) curve based on the trial-by-trial distributions of spike counts elicited on all trials by each of the two stimuli. The area under the ROC curve gave the probability of correct discrimination of the stimuli. That probability was expressed as a z-score and was multiplied by $\sqrt{2}$ to obtain the discrimination index, d'. In some cases, 100% of the spike counts elicited by one stimulus were greater than any of those elicited by the other stimulus, the area under the ROC curve was 1.0, and the corresponding z-score was undefined. In those cases d' was written as ± 2.77, corresponding to 97.5% correct discrimination. The sign convention was that d' was positive when the more contralaterally located sound elicited more spikes.

We used two approaches to quantify spatial stream segregation. In one approach, we measured the difference in spikes per burst synchronized to the A source located at C40° corresponding to a shift in the B source from co-located at C40° to

spatially separated at I40°. This was quantified by the Spatial Release Index (SRI), which was:

$$SRI = (R_{I40} - R_{C40})/(R_{I40} + R_{C40}),$$

where R_{I40} and R_{C40} were the responses synchronized to the A stimulus when the B source was at ipsi- or contralateral 40°, respectively. Positive values of the SRI indicated that separation of A and B sources resulted in a release from masking of the A source.

In the other approach, the magnitude of spatial stream segregation in conditions of interleaved A and B noise bursts was quantified by computing d' for spikes synchronized to the A versus B bursts. Values of d' were plotted as a function of B-source location, and source-separation thresholds were taken as the corresponding interpolated separation at which the plot of d' versus azimuth crossed $d' = 1$.

The excitation thresholds (dB SPL) for detection of neural activity elicited by noise bursts were estimated by computing d' for pairs of noise bursts at successively increasing levels, plotting the cumulative d' versus sound level, and taking as threshold the minimum interpolated (1-dB steps) sound level at which $d' = 1$. To obtain each unit's characteristic frequency (CF), the matrix of d' values across all tested frequencies and levels was first screened to eliminate isolated values of $d' > 1$ for which all neighboring values were <1; this eliminated isolated values lying outside the FRA. The frequency tuning curve (FTC; i.e., the border of the FRA) was found by interpolating the d' values across all tested sound levels in 1-dB steps at each tested frequency and finding the minimum sound level at which d' was ≥ 1. The CF was given by the frequency of the lowest-level tip of the FTC.

The strength of stimulus synchrony of all units for single-source conditions across 2.5 to 40 bps was represented by vector strength (VS; Goldberg and Brown, 1969). The VS could range from 0 (no synchrony) to 1 (all spikes at identical phase). The statistical significance of the VS was evaluated by the Rayleigh test of uniformity (Mardia, 1972) at the level of $p < 0.001$.

Statistical procedures used custom-written MATLAB scripts (MathWorks) that incorporated the MATLAB Statistics Toolbox. *Post hoc* multiple comparisons used the

Bonferroni correction. Error bars in the illustrations indicate standard deviation (SD) unless stated otherwise.

4.4 Results

4.4.1 *Neural Responses to Competing Sound Sequences*

We tested an ABAB stimulus pattern consisting of sequences of noise bursts alternating between two source locations. Post-stimulus time histograms (PSTHs) from an isolated single unit in cortical area A1 in response to such stimuli are shown in Figure 4.1. In that example, the "base rate" was 5 bps, referring to the aggregate of A and B rates. Figures 4.1, *A*, *B*, and *C*, show conditions in which B was presented in the absence of A; we refer to this as the "single-source" condition, equivalent to 2.5 bps (half of the aggregate AB base rate of 5 bps). Note that this unit displays contralateral hemifield spatial tuning, with strong responses synchronizing to the single sound source at C40° (Fig. 4.1*A*), a decrease in overall spikes per burst to the sound source at 0° (Fig. 4.1*B*), and very weak responses to the sound source at I40° (Fig. 4.1*C*). Responses to the competing-source condition in which the A source was added at 0° are represented in Figure 4.1, *D*, *E*, and *F*. Under the condition when A and B sources were colocated at 0° (Fig. 4.1*E*), the presentation rate was equivalent to a 5 bps single-source condition. Note that the unit responded reliably only to the first sound burst and showed only weak responses to subsequent A (red) and B (blue) bursts. When the B source was shifted to C40° (Fig. 4.1*D*), the unit displayed robust responses synchronized to the B source in preference over the A source. Thus, the neural response was captured by the B source, relative to the A source. Under the condition when the B source was shifted to I40° (Fig. 4.1*F*), responses to both A and B sources were relatively weak, but responses synchronized to the A source were stronger than those synchronized to the B source.

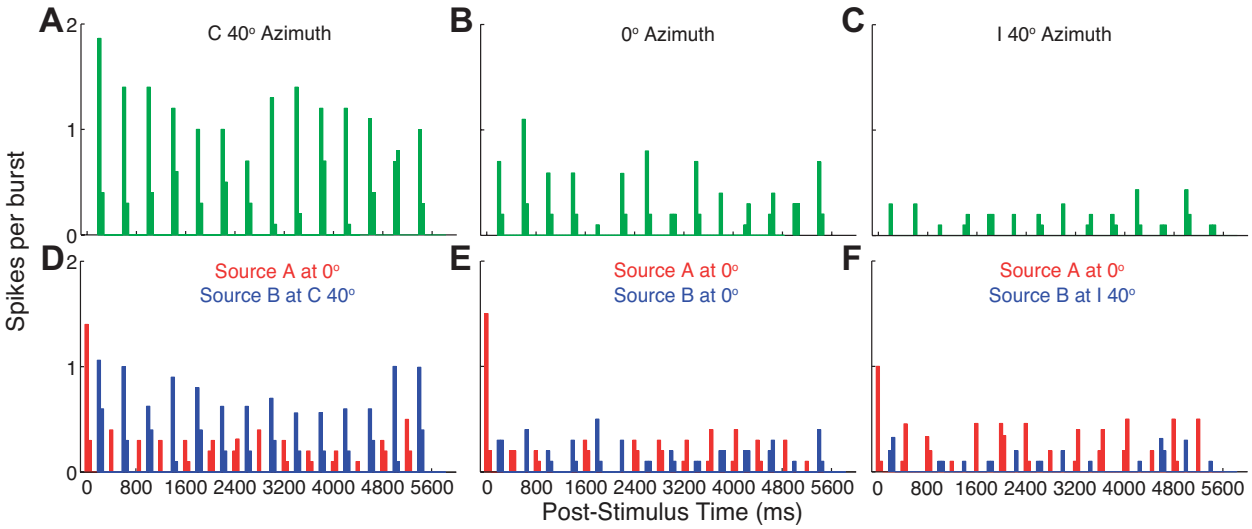

Figure 4.1. PSTH of a well isolated single unit from cortical area A1. Plotted are responses to sound sequences from a single-source location (top row, *A*, *B, C*) or to competing sequences from two locations (bottom row, *D, E, F*). Responses are spikes per sound burst in 100 ms bins, averaged over 10 trials. In the top row, the single sound-source was located at C40° (*A*), 0° (*B*), I40° (*C*). In the bottom row, red and blue color bars indicate spike rates synchronized to the A- and B-source, respectively. In those cases the A-source was fixed at 0°, whereas the location of the B-source varied from C40° (*D*), 0° (*E*), I40° (*F*). Unit 1216.2.4.

Synchronized mean spikes per burst from the same A1 single unit in Figure 4.1 are quantified for the full range of A and B location combinations in the right column of Figure 4.2; panels *E*, *J*, and *O* show conditions in which the A sources was fixed at locations C40°, 0°, and I40°, respectively. The green line replicated in all three panels shows the tuning to the location of a single sound source, which exhibited the contralateral hemifield pattern that was characteristic of all our recorded units in A1. This was consistent with the dominant contralateral hemifield tuning to single noise bursts seen in rat A1 units (Higgins et al., 2010; Yao et al., 2013). The location of the B source, plotted on the horizontal axis, influenced both the responses synchronized to the B source (blue lines) as well as those synchronized to the A source (red lines). Moreover, when A and B sources were co-located at the azimuths indicated by the vertical red lines, responses synchronized to A and B were roughly equal and the numbers of spikes per stimulus burst were reduced to about half of that seen for single sources, as indicated by the green lines at the corresponding azimuth. This reduction in response demonstrates forward suppression, in which responses of the A1 unit declined with increasing stimulus presentation rate. As A and B sources were moved apart, the

response to one of the sources increased and the other decreased or remained relatively weak. In that way, responses of the A1 unit were captured by one source over the other. The vertical distance between the blue (B-source) and red (A-source) curves at each azimuth of the B source represents the degree to which the sequences of sounds from A and B sources were segregated by the synchronized responses of this neuron.

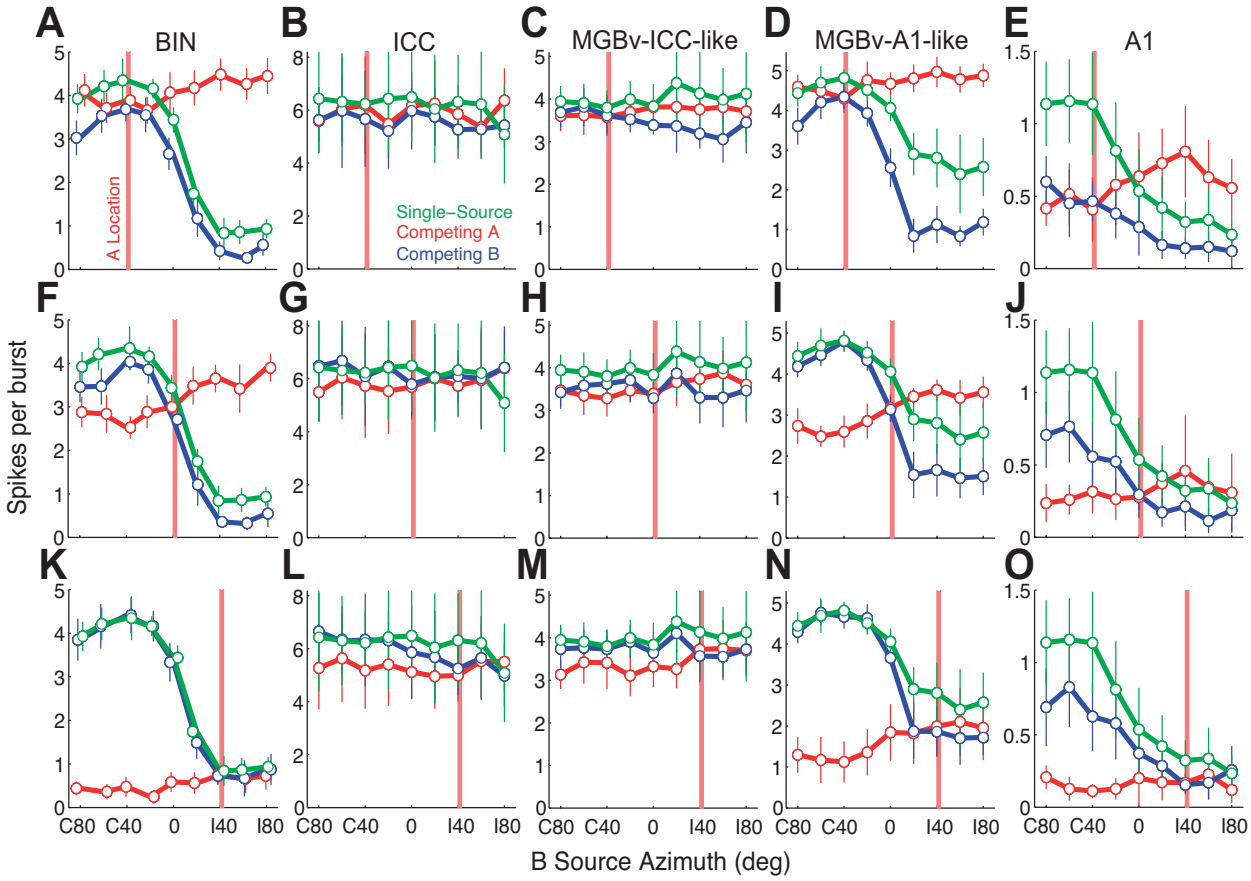

Figure 4.2. Responses to single-source and competing-source conditions. Mean spike rates (± 1 SD) are plotted as a function of B-source location from example single units from BIN (*A, F, K*; unit 1402.4.18), ICC (*B, G, L*, unit 1403.5.31), MGBv-ICC-like (*C*, *H, M*, unit 1312.2.15), MGBv-A1-like (*D, I, N*, unit 1311.2.13), and cortical area A1 (*E, J, O* same unit as Fig. 1). Green lines indicate spike rates synchronized to single-source sound sequences with a base rate of 2.5 bps. Red and blue indicate responses synchronized to A- and B-sound sources, respectively, in competing-source conditions; the base rate was 5 bps. B-source locations were as plotted, whereas A sources were fixed at the locations indicated by the vertical red lines (*A–E,* C40°; *F–J,* 0°; *K–O,* I40°). Variation in A responses reflected the effect of changing B-source locations.

We examined whether neural responses from subcortical levels displayed SSS similar to that seen in cortical area A1. Responses from one single unit in the ICC (Fig. 4.2, *B*, *G*, *L*) is representative of our population of ICC units in that it displayed little or

no spatial sensitivity to single sources. Unlike the case of cortical recordings (e.g., Fig. 4.2, *E*, *J*, and *O*), rates spikes per burst in this ICC unit to the co-located A and B conditions were similar to those seen under single-source conditions presented from the same location. That is, there was little reduction in responses seen between the 2.5 bps single-source and 5 bps competing-source conditions, which demonstrates an absence of forward suppression. Also, the location of the B source had relatively little influence on the responses to the A source. Figure 2 also displays responses from one single unit in the BIN (Fig. 4.2, *A*, *F*, *K*), which lies in the tectal pathway from the ICC to the superior colliculus. Spatial sensitivity for this particular unit and all BIN units showed sharp contralateral hemifield tuning under the single-source condition. As in the ICC, spikes per burst to the co-located A and B competing sources resembled those seen under single-source conditions presented from the same locations. However, responses under the competing A and B condition preferentially synchronized to either the A or B source, depending on the spatial configuration. Note that with the A source located at I40°, responses synchronized to the B source were indistinguishable from single-source responses. Accordingly, the A source did not influence the neuronal response to the B source.

We previously encountered two subpopulations of units in the MGBv, with one subpopulation showing spatial sensitivity similar to that seen in A1 and another one with spatial tuning characteristics similar to ICC (Yao et al., 2015). Those unit populations were denoted as “MGBv-A1-like” and “MGBv-ICC-like” and were distinguished by a quantitative procedure described in the METHODS; in the present study, about a third of units were classified as MGBv-ICC-like and two thirds were MGBv-A1-like. The differences in spatial sensitivity seen between the two subpopulations of units can be seen in their responses to the single source sound sequences in Figure 4.2. The MGBv-A1-like unit (Fig. 4.2, *D*, *I*, *N*) displays contralateral hemifield tuning similar to the single source condition seen in the A1 unit (Fig. 4.2, *E*, *J*, *O*), whereas the MGBv-ICC-like unit (Fig. 4.2, *C*, *H*, *M*) displays omnidirectional spatial tuning similar to that seen in the ICC unit (Fig. 4.2, *B*, *G*, *L*). Overall, we found that responses from the MGBv-A1-like unit showed some SSS by preferentially synchronizing to either the A or B competing source whereas responses to competing A and B sources from the MGBv-ICC-like unit were

undifferentiated. Note that this difference in SSS is consistent with their differences in spatial sensitivity. Similar to the ICC and BIN, both MGBv units displayed little evidence of forward suppression at the illustrated stimulus base rates, meaning that there was little difference in spike count between co-located competing A and B sources versus the single-source sequence presented from the same location. That is, doubling the stimulus rate by adding sounds from a co-located source had little effect on the rate of spikes per sound burst.

4.4.2 *Quantification of Spatial Stream Segregation*

One measure of the magnitude of SSS is the effect of B source location on the response to a fixed A source. Specifically, we measured the difference in spikes per bursts synchronized to the A source located at C40° corresponding to a shift in the B source from co-located at C40° to I40°. This was quantified by the Spatial Release Index (SRI; see METHODS). Positive values of the SRI indicated that separation of A and B sources resulted in a release from masking of the A source. The magnitudes of the SRI tended to vary with stimulus presentation rate. All ICC units and nearly all MGB units were tested at base rates of 5, 10, 20, and 40 bps. No A1 units responded to the fastest rate, so A1 units were not routinely tested at 40 bps and few were tested at 20 bps.

Distributions of SRI from all tested units in each population are shown in Figure 4.3 across base rates of 5, 10, 20, and 40 bps. Generally, spatial release tended to be high among A1 units and lowest among ICC units. At each base rate, the distributions of SRI varied significantly across unit populations (MU: $X^2 = 138–207.4$, $p < 10^{-6}$; SU: $X^2 = 24.4–35.9$, $p < 10^{-5}$; Kruskal-Wallis) with ICC units displaying the lowest SRIs ($p < 0.005$; Bonferroni-corrected). In A1, SRIs were significantly highest at 10 bps ($p < 0.0001$, Bonferroni-corrected), whereas at 5 and 20 bps, SRIs of A1 units were not significantly different from those of BIN and MGBv-A1-like units ($p > 0.05$, Bonferroni-corrected); A1 units were not tested at 40 bps. SRIs were higher among MBGv-A1-like units than among MGBv-ICC-like units at 5 and 10 bps ($p < 0.0001$, Bonferroni-corrected), whereas there was no significant difference between those populations at 20 and 40 bps. Units in A1 typically showed greater spatial release with increasing stimulus rates. For example, the SRIs more than doubled between base rates of 5 and 10 bps;

SRIs in A1 declined again at 20 bps, which might reflect the generally poorer responses of A1 neurons to high-rate stimuli. Subcortical units in the BIN and MGBv also displayed progressively greater spatial release across increasing stimulus rates (SRI medians across 5 to 40 bps rates: BIN = 0.08, 0.13, 0.23, 0.30; MGBv-A1-like: 0.11, 0.18, 0.20, 0.19; MGBv-ICC-like: 0.05, 0.08, 0.14, 0.26). Median SRI values for ICC units were ~0 across all bps conditions, although a small proportion of ICC units (10/93; 8 MUs, 2 SUs) at the 40 bps condition exhibited a high degree of spatial release (SRI > 0.20) that was similar to the other unit populations. These trends indicate a strong relationship between presentation rate and the magnitude of SSS, possibly reflecting the time scale of forward suppression. We examine forward suppression in a later section.

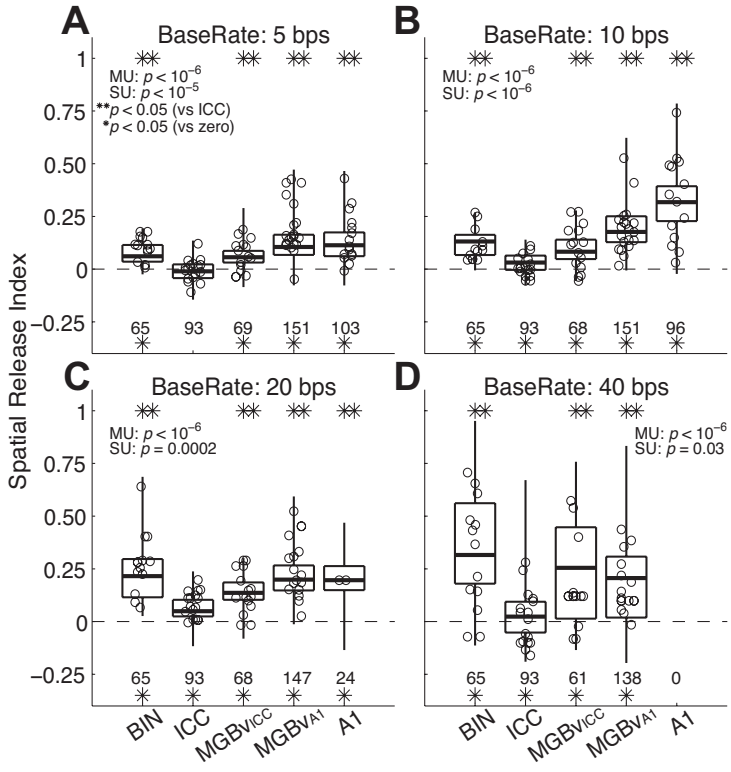

Figure 4.3. Distribution of the spatial release index (SRI) values across each unit population for each base rate tested (*A*, 5-bps; *B*, 10-bps; *C*, 20-bps; *D*, 40-bps). Horizontal lines forming the boxes indicate the 25th, 50th, and 75th percentiles of multi-unit responses. Vertical lines indicate the full range from multi-unit responses. Circles represent data point from well-isolated single units. The *p* values in each subplot indicate results of a non-parametric analysis of variance (Kruskal-Wallis) test across the unit populations; MU and SU indicate statistics from multiple- and single-unit recordings. Double asterisks indicate significant difference in distribution versus ICC (Bonferroni-corrected multiple comparisons), whereas single asterisks indicate significant difference for a mean different from 0 (*t* test, Bonferroni-corrected multiple comparisons). The listed numbers under each unit distribution correspond to the number of units in each population.

We quantified the discrimination between sound source locations with a discrimination index, *d′*. Specifically, *d′* quantified the acuity with which sound sequences from the A versus B sources could be discriminated on the basis of trial-by-trial spike rates synchronized to the A or B source (Fig. 4.4; same example units as in Fig. 4.2). The blue lines indicate discrimination between A and B competing sources at a given A-source location (indicated with the vertical red line). The green and black lines indicate single-source conditions compared to the three fixed A-source locations (C40°, Fig. 3*A–C*; 0°, *F–J*; I40°, *K–O*); black and green lines represent stimulus rates equal to the aggregate A-B rate (5 bps) or half that rate (2.5 bps), respectively. Similar to the trends in the responses seen in Figure 2, significant source segregation indicated by magnitudes of $d' \geq 1$ was typically seen for most non-zero A and B source separations among BIN, MGBv-A1-like, and A1 units. Specifically, significant source segregation was achieved at the minimum A and B source separations that were tested (i.e., 20° separation) when the A-source was fixed at C40° (Fig. 4.4*A*, *D*, *E*) and 0° (Fig. 4.4*F*, *I*, *J*). In essentially all conditions, the *d′* for spatial segregation was greater for the competing-source (blue line) than for the single-source condition at either base rate (green and black lines). Significant source segregation among MGBv-ICC-like (Fig. 4.4*C*, *H*, *M*) and ICC (Fig. 4.4*D*, *I*, *N*) units was seen only at the extreme source separations (~80° separation). The trends seen for these example units are quantified below for the population.

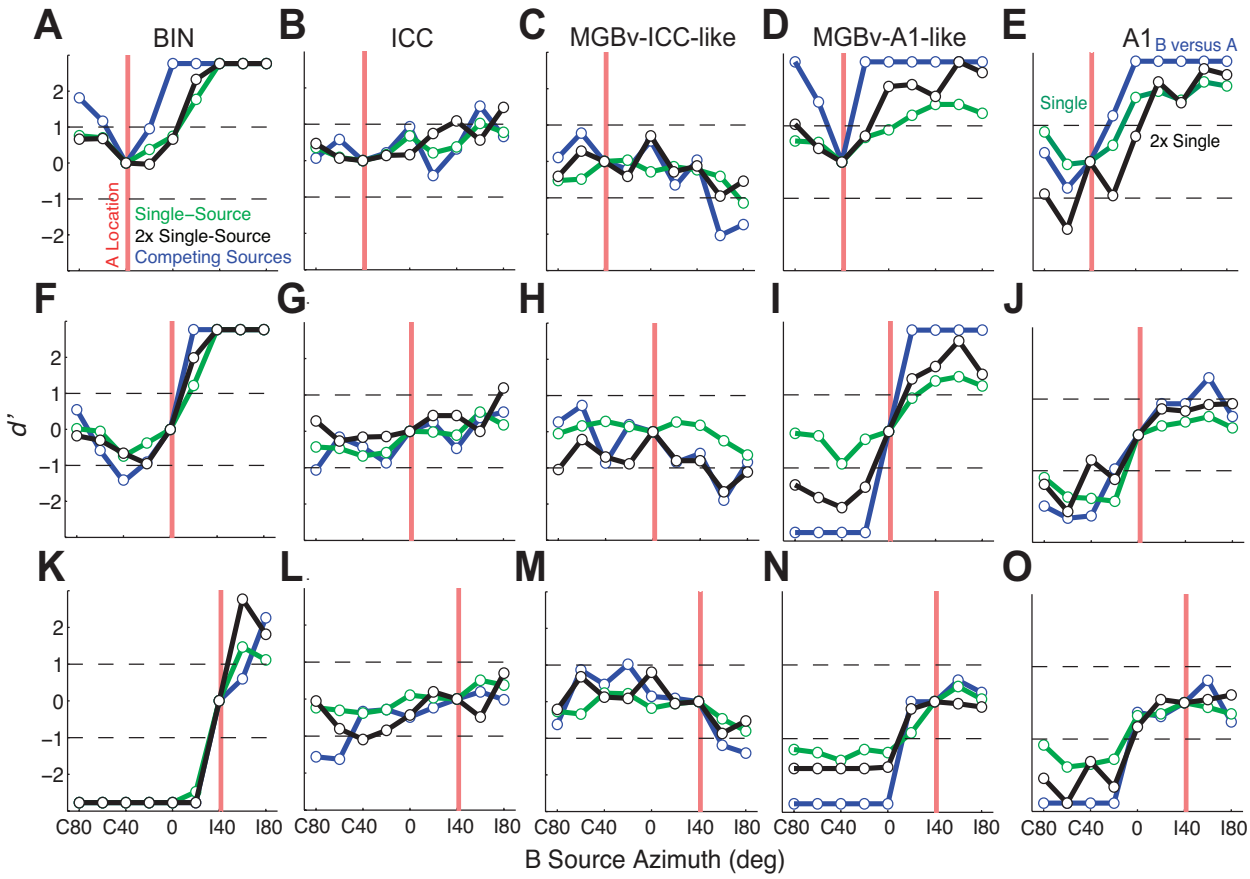

Figure 4.4. Discriminating competing sources. Blue lines indicate *d'* values for discrimination of trial-by-trail spike counts elicited by A versus B sources. Green and black lines indicate discrimination of spikes per burst elicited from the plotted location versus those elicited in separate trials from the fixed location indicated by the vertical red line at 2.5 and 5 bps single-source rates, respectively. Similar convention and same units as in Figure 2.

We used the source separation at which *d'* crossed ±1 (dashed lines) as the spatial threshold for significant segregation between competing A and B sources; values were interpolated in 1°-steps. We then selected for each unit the minimum threshold across conditions of A source at C40°, 0°, and I40°; distributions of those minimum thresholds across all unit populations are shown in Figure 4.5. We found a significant difference in thresholds across all unit populations at 5 (Fig. 4.5*A*) and 10 (Fig. 4.5*B*) bps conditions (MU: $X^2 = 108–130$, $p < 10^{-6}$; SU: $X^2 = 25–26$, $p < 0.0001$; Kruskal-Wallis). Generally, thresholds were narrowest (i.e., highest-acuity segregation) for BIN and MGBv-A1 units, intermediate for A1 units, and broadest (i.e., worst) for MGBv-ICC and ICC units. *Post-hoc* multiple comparisons indicated that, at 5 and 10 bps, thresholds were narrower for BIN and MGBv-A1 units than for those of A1 units ($p <$

0.05; Bonferroni-corrected), and that thresholds of A1 units were narrower than those of MBGv-ICC and ICC units ($p < 0.05$; Bonferroni-corrected). Median values of the distribution of thresholds were very similar among A1, MGBv-A1-like, and BIN units, whereas the cumulative distributions diverge among the units having broader minimum thresholds.

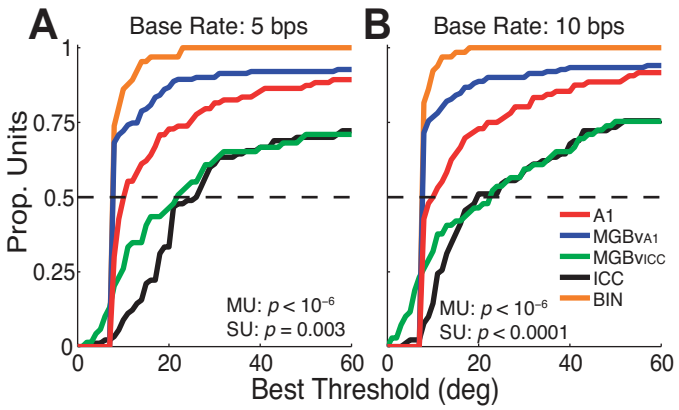

Figure 4.5. Cumulative distributions of best thresholds (minimum interpolated separation (°) at which *d′* crosses ±1 across the 3 conditions of A sources at C40°, 0°, and I40°) for segregating competing A and B sources at 5 (*A*) and 10 (*B*) base rates. Horizontal dashed line indicates the 50th percentile. Statistics from a non-parametric analysis of variance (Kruskal-Wallis) test across the multi- and single-unit populations are shown in each subplot.

Spatial segregation for various A-source locations was quantified by computing the *d′* for discrimination of A or B sources that were separated by 20°. In Figure 6, each box displays the distribution of *d′* for discrimination of A and B sources across every combination of A-source location at C40° (Fig. 4.6*A*, *D*), 0° (Fig. 4.6*B*, *E*), or I40° (Fig. 4.6*C*, *F*) and base rate (5 bps: Fig. 4.6*A–C*; 10 bps: Fig. 4.6*D–F*). For each unit at each A location, the B location resulting in the greater magnitude of *d′* for a B location 20° to the left or right of the A source was selected and represented in the distribution by its absolute value. Similar to the spatial release (SRI) results (Fig. 4.3), A1, MGBv-A1-like, and BIN units showed the greatest segregation between competing A and B sources across all conditions. In addition, spatial stream segregation was strongest when the A-source location was fixed on the midline (Fig. 4.6*B*, *E*). For midline A-source locations, >70% of A1, >85% of MGBv-A1-like units, and >94% of BIN units showed significant spatial stream segregation ($d' \geq 1$) whereas only slightly more than half of MGBv-ICC-like units (54%) and roughly one-third (34%) of ICC units showed significant spatial

stream segregation. Overall, these findings indicate that spatial stream segregation was strongest among A1, MGBv-A1-like, and BIN units and weakest for MGBv-ICC-like and ICC units.

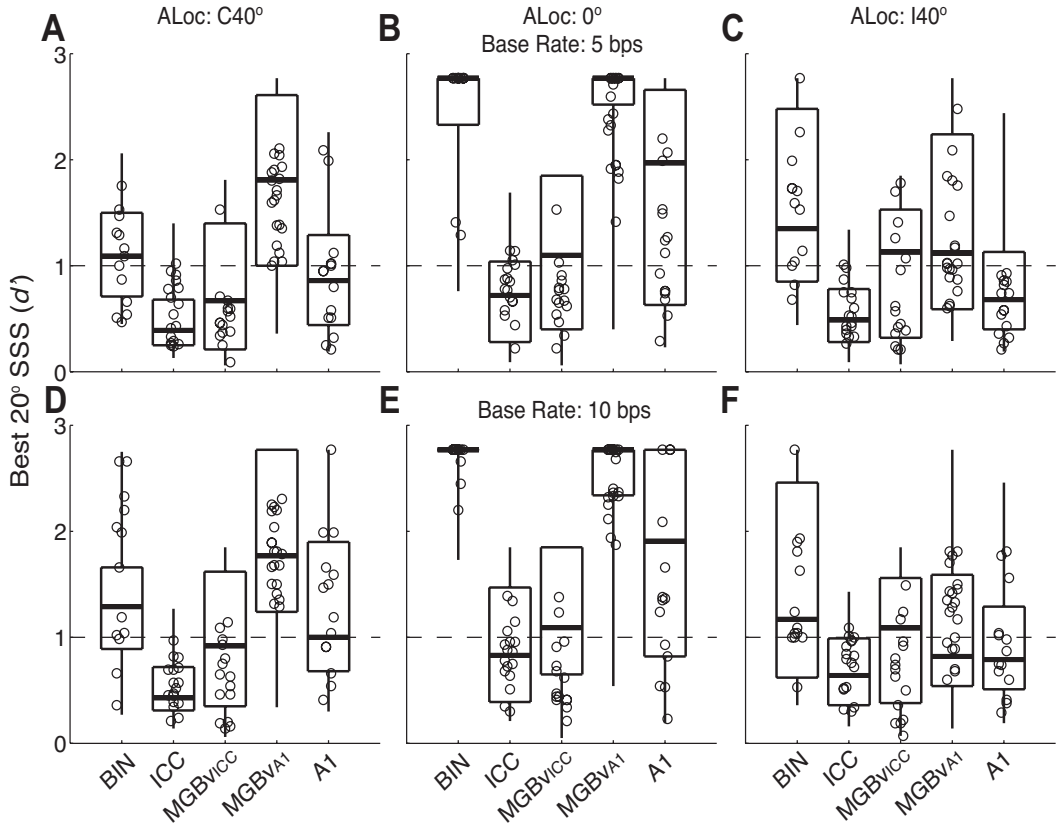

Figure 4.6. Distribution of *d′* for discrimination of A and B sources. Each *d′* in the distributions represents for one unit the greater absolute value of *d′* for discrimination of A and B sources across locations 20° to the left or right of A sources at C40° (*A*, *D*), 0° (*B*, *E*), and I40° (*C*, *F*). Rows represent 5 bps (*A*–*C*) and 10 bps (*D*–*F*) base rates. Each subplot shows boxplot distributions for each unit population. Horizontal lines forming the boxes indicate the 25th, 50th, and 75th percentiles of multi-unit responses. Vertical lines indicate the full range from multi-unit responses. Circles represent data points from well-isolated single units.

The tendency of MGBv-A1-like units to show stronger and higher-acuity SSS than units in A1 must reflect to some degree the procedure by which were selected. That is, the MGBv-A1-like units were a subpopulation of MGBv units selected for similarity to the average of A1 responses, which showed hemifield tuning. The A1 population, in contrast, included the entire A1 sample, which had an approximately Gaussian distribution of sharpness of tuning. The experimentally induced bias toward sharper tuning among MGBv-A1-like units presumably would have introduced a bias

toward stronger, higher-acuity SSS among MGBv-A1-like units compared to A1. The greater across-unit variation in SSS among A1 units compared to MBGv-A1 units is evident in distributions shown in Figures 4.5 and 4.6.

The trends in distributions of SSS magnitude among neural populations and base rates were largely constant across ranges of frequency tuning of units, represented by their CFs. We tested for a correlation between the accuracy of SSS and unit CF by performing a Spearman rank-correlation analysis with 10,000 bootstrapped replications. SSS accuracy was taken as the greatest d' magnitude across all A-B separations of 20° to the left or right of A sources at C40°, 0°, and I40° (i.e., maximum d' across 6 A–B locations, all within 20° within A and B). For each replication, we randomly drew with replacement an equal number of units per one-octave CF bin from each unit population and across all bps conditions. Confidence intervals (CIs) were calculated from each distribution of correlation coefficients (empirical 2-tailed). We found a weak but significant positive relationship between d' and CF among BIN units at 5 bps (correlation coefficient confidence interval, CI = [0.08, 0.92], $p < 0.05$; Spearman-rank correlation) and MGBv-ICC-like units across 10 (CI = [0.18, 0.95]), 20 (CI = [0.04, 0.91]), and 40 (CI = [0.13, 0.89]) bps ($p < 0.05$; Spearman-rank correlation), which we regard as of little practical importance. No significant CF dependence of d' was seen among A1, MGBv-A1-like, and ICC unit populations across all tested bps conditions (CIs = [–0.11 to –0.87, 0.34 to 0.95], $p > 0.05$; Spearman-rank correlation).

4.4.3 *Contribution of Forward Suppression to SSS*

Many neurons, particularly in A1, showed a substantial decrease in spikes per sound burst under conditions of colocated A and B sources at C40° compared to a single-source at C40°; we refer to this as “forward suppression” as a neutral term that could encompass a number of mechanisms including refractoriness, forward inhibition, and/or synaptic depression. This can be seen in the example shown in Figure 2*E*. For all units, we quantified the amount of forward suppression by the fractional reduction in spikes per sound burst between single-source and co-located competing-sources at C40°; values approaching 0 and 1 indicate weak and strong forward suppression, respectively. The cumulative distributions of forward suppression for all unit populations at each bps condition are shown in Figure 4.7. At base rates of 5, 10, and 20 bps, we

found a significant difference in forward suppression across all unit populations (MU: X^2 = 66.1–195.2, $p < 10^{-6}$; SU: X^2 = 24.9–32.3, $p < 10^{-5}$; Kruskal-Wallis). *Post-hoc* comparisons indicated that forward suppression was greatest among A1 units at all base rates at which A1 units were tested, 5-20 bps ($p < 0.0001$, Bonferroni-corrected). The stronger forward suppression among A1 units was also evident in their reduced capability to synchronize to trains of sound bursts from single sources. Figure 4.8*A* plots the median values of vector strength for phase locking to trains of bursts at 2.5 to 40 bps, and Figure 4.8*B* plots the percentage of neurons showing statistically significant phase locking to those rates. By both measures, it is clear that the ability of neurons to synchronize to sequences of noise bursts is dramatically decreased between subcortical regions and A1.

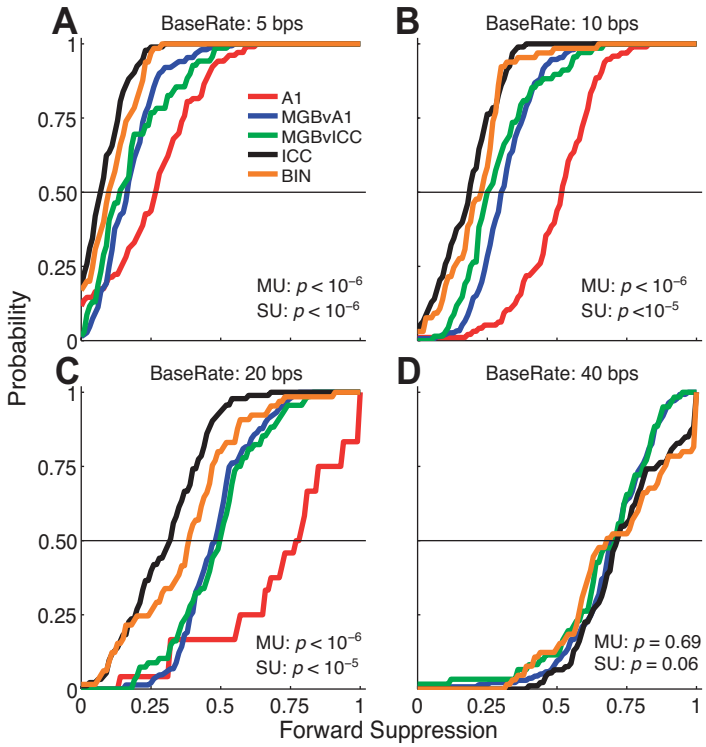

Figure 4.7. Cumulative distribution of forward suppression across each unit population for each tested base rate (*A*, 5 bps; *B*, 10 bps; *C*, 20 bps; *D*, 40 bps). Statistics from a non-parametric analysis of variance (Kruskal-Wallis) test across the multi- and single-unit populations are shown in each subplot.

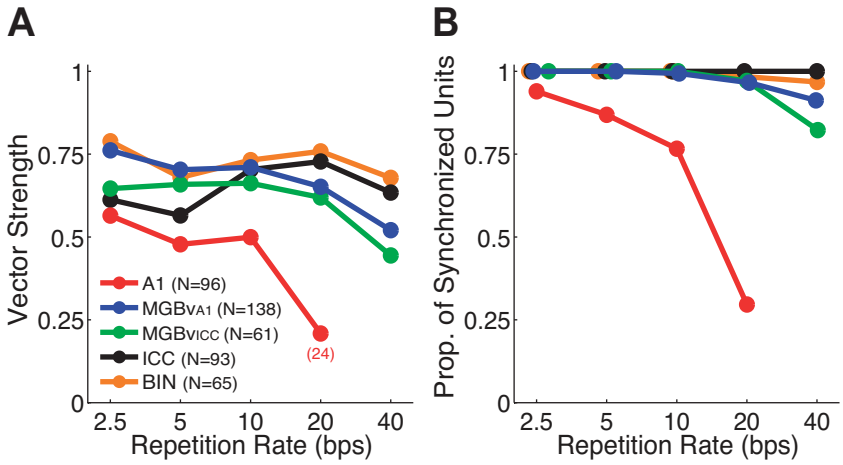

Figure 4.8. Median vector strength (*A*) and the proportion of synchronized units (*B*) for each unit population (color coded) at varying repetition rates (bps; horizontal axis). The x-coordinates are was slightly offset for visual purposes. Total number ("N") of each unit population is shown. Only 24 A1 units were tested at the 20 bps rate.

The addition of a competing source tended to sharpen the spatial tuning of units. This effect tended to increase with increasing stimulus base rate and was stronger among A1 units than among subcortical units. We quantified the sharpening of spatial tuning by calculating the ERRF width (defined in Methods) for each unit under single- and competing-source conditions (Fig. 4.9). The reduction in ERRF width (in degrees) between conditions varied significantly across unit populations at all base rates (MU and SU: $X^2 = 30.4–299.7$, $p < 0.001$; Kruskal-Wallis). *Post-hoc* analysis showed that addition of a competing sound produced substantial sharpening among A1 units at all tested base rates ($p < 0.0001$, Bonferroni-corrected), whereas considerable sharpening was only evident among ICC, BIN, and MGBv units at faster base rates. This accords with the observation that only A1 units showed substantial forward suppression at base rates as low as 20 bps and suggests that A1 units, but not sub-cortical units, show a sharpening of spatial tuning that includes a major contribution from forward suppression.

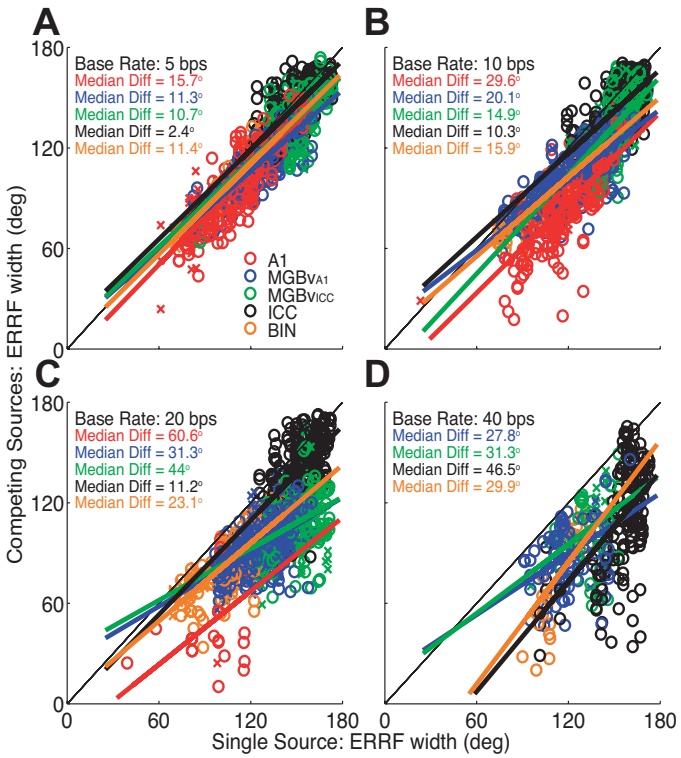

Figure 4.9. Breadth of spatial sensitivity for the single-source (horizontal axis) versus the competing-source (vertical axis) condition across all unit populations for each tested base rate (*A*, 5 bps; *B*, 10 bps; *C*, 20 bps; *D*, 40 bps). Data points below the diagonal line indicate sharper spatial tuning in the presence of a competing sound. Circles represent multiple units whereas "x" symbols represent single-units. The diagonal black line represents the unity line. Thick colored lines represent linear regression fits for corresponding ERRF widths for each unit population.

4.4.4 *Forward Suppression in A1 is not due to Synaptic Inhibition*

Our measures of spatial stream segregation at multiple levels of the auditory pathway demonstrate a dramatic increase in forward suppression between subcortical regions and A1. We hypothesized that forward suppression represents either synaptic inhibition within the cortex or some other biophysical property of A1 neurons that limits the following rates in A1. We explored the putative inhibitory mechanism by recording extracellular neural responses from A1 neurons while applying GABA antagonists to the cortical surface (see Experimental Procedures for more details). Three GABA antagonists were used: 1) Gabazine, an antagonist of post-synaptic $GABA_A$ inhibition, and 2) CGP 36216, an antagonist of pre-synaptic $GABA_B$ inhibition; and 3) 2-Hydroxysaclofen, an antagonist of post-synaptic $GABA_B$ inhibition. We measured responses to pulse train stimuli presented at various repetition rates before and after drug application. The repetition rate cutoff was taken as the maximum repetition rate

(Hz) at which responses were ≥ 50% of the maximum response across all tested repetition rates. If forward suppression in A1 was due to synaptic inhibition, we would expect application of GABA antagonists to lead to an increase in the stimulus repetition rate to which A1 neurons synchronize. In addition, the targeted receptor specificity of the agents would potentially indicate the source of intracortical synaptic inhibition. Surprisingly, we found that none of the GABA antagonists produced the hypothesized relief from forward suppression (Fig. 4.10*A*–*C*). Specifically, no significant change in repetition rate cutoffs were seen between pre- and post-application of any of the 3 agents (Gabazine, $p = 0.19$; CGP 36216, $p = 0.49$; 2-Hydroxysaclofen, $p = 0.75$; sign test). A similar lack of effect on repetition rate cutoff was seen at all cortical depths. That the drugs reached cortical neurons in effective concentrations was demonstrated by an overall increase in spikes per burst (Fig. 4.10*D*, Gabazine, paired $t_{(61)} = 6.47$, $p < 10^{-6}$; CGP 36216, paired $t_{(46)} = 7.86$, $p < 10^{-6}$; 2-Hydroxysaclofen, paired $t_{(58)} = 5.46$, $p < 10^{-6}$); again, this was seen at all cortical depths. These results are inconsistent with an explanation for forward suppression based on intracortical inhibition.

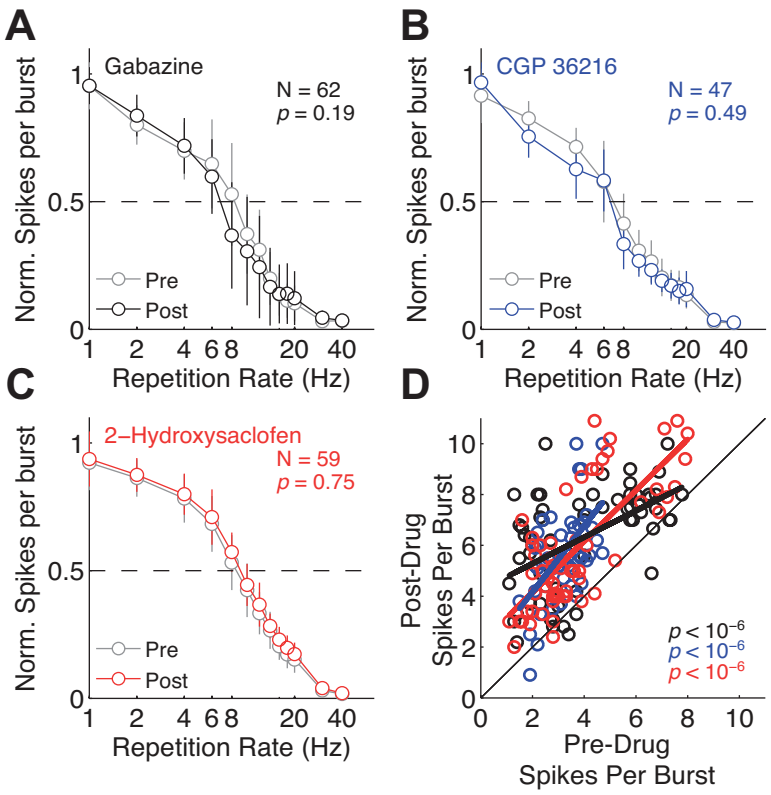

Figure 4.10. Effects of $GABA_A$ or $GABA_B$ antagonists on A1 responses. Normalized grand mean spikes per burst (± 1 SD) to pulse train stimuli presented at varying repetition rates (horizontal axis) are plotted pre- and post-application of Gabazine (*A*), CGP 36216 (*B*), and 2-Hydroxysaclofen (*C*). (*D*) Mean spikes per burst of each unit for pre- (horizontal-axis) and post-drug (vertical axis) application. The *p* values indicate results from comparing the mean repetition rate cutoffs (sign test) (*A*–*C*) or mean spikes per burst (*D*) between pre- and post-drug application samples (two-sample *t* test).

4.5 Discussion

We evaluated SSS at three levels of the ascending auditory system: midbrain (ICC and BIN), thalamus (two subpopulations of MGBv neurons), and cortical area A1. The results demonstrate that the degree to which neurons preferentially synchronize to sounds from one or the other of two sources is progressively enhanced along the ascending pathway, with robust SSS observed in essentially all A1 neurons that we sampled. The enhancement of SSS reflects the sharpened spatial sensitivity and strengthened forward suppression at higher levels of the auditory pathway. Moreover, we found that forward suppression within the auditory cortex was not due to intracortical synaptic inhibition.

4.5.1 *Stream Segregation Along the Ascending Auditory System*

Physiological studies of stream segregation based on differences in tone frequencies have demonstrated neural correlates within the mammalian auditory cortex (Fishman et al., 2001, 2004, 2012; Micheyl et al., 2005; Elhilali et al., 2009) and avian forebrain (Bee and Klump, 2004; Bee et al., 2010). Stream segregation based on differences in spatial location has been identified in the responses of cortical neurons (Middlebrooks and Bremen, 2013; the present study), and physiological correlates of stream segregation based on interaural time differences (ITDs) are observed in the auditory cortex of human listeners in studies using magnetoencephalography (MEG; Carl and Gutschalk, 2013) and functional magnetic imaging (fMRI; Schadwinkel and Gutschalk, 2010). Other studies have reported that stream segregation is present at subcortical levels, with tone-based stream segregation seen among single-unit responses from the cochlear nucleus (Pressnitzer et al., 2008), and ITD-based behavioral streaming linked with fMRI BOLD activity in the IC (Schadwinkel and Gutschalk, 2011). These reports, together with the present results, offer the view that some forms of stream segregation can be present throughout all levels of the ascending auditory pathway. Specifically with regard to spatial factors, however, we find that SSS begins with gradual sharpening of spatial sensitivity at successive levels of the brainstem and thalamus, and that SSS is enhanced by forward suppression between thalamic and cortical levels.

Our results are consistent with the failure to demonstrate location-based stream segregation at the level of the IC in guinea pigs (Shackleton et al., 2012). Although we encountered SSS among BIN and a subpopulation of MGBv neurons at faster base rates (Fig. 4.3), those presentation rates are considerably faster than the time-scale reported in psychophysical studies of stream segregation. Schadwinkel and Gutschalk's (2011) findings of associated fMRI BOLD activity in the IC with ITD-based streaming might be attributed to active engagement or attentional modulation. Kondo and Kashino (2009) report that feedforward and feedback processes along the thalamocortical loop are involved in the formation of auditory streaming percepts. Thus, further work should attempt to distinguish the roles of corticothalamic and corticotectal modulation that aid in auditory streaming.

4.5.2 *Segregating Streams Through Spatial Hearing and Forward Suppression*

In our rat animal model spatial sensitivity develops along the ascending tectal and lemniscal pathway, from level-dependent spatial sensitivity that broadens markedly with increasing sound levels within the ICC to level-tolerant contralateral hemifield spatial sensitivity within the BIN, a subpopulation of neurons in MGBv, and area A1 (Yao et al., 2015). Not surprisingly, SSS was most prominent among A1, MGBv-A1-like, and BIN units. BIN and MGBv-A1-like units displayed SSS by virtue of their dominant contralateral hemifield tuning, whereas SSS among A1 units was due to contralateral hemifield tuning enhanced by forward suppression at that level. These results give further evidence for two parallel pathways for auditory space processing: tectal, projecting to the superior colliculus; and lemniscal, projecting to the forebrain (Knudsen et al., 1993; Knudsen and Knudsen, 1996; Yao et al., 2015). Whether or not the representation of segregated streams along the tectal pathway plays a role in auditory scene analysis remains to be tested.

Despite the species differences in single-source spatial sensitivity, we encountered SSS results from A1 neurons in the anesthetized rat very similar to those observed among cortical neurons in anesthetized cats (Middlebrooks and Bremen, 2013). Specifically, we found that segregation of competing sources within cortical neurons was weakest when both sources were located within the contralateral hemifield and strongest when one of the two sources was located in the ipsilateral hemifield, as shown in Figures 4.2 and 4.6. This indicates that a cortical neuron's spatial sensitivity, which is derived from binaural computations within the brainstem and likely inherited from MGBv-A1-like units (Kyweriga et al., 2014), favors one of the two competing sound sources. That spatial bias is amplified by additional forward suppression. In particular, A1 neurons show strong suppression of responses in the condition when competing sounds are co-located and a strong release from suppression when one source is moved away from the other, yielding neural responses that are captured by one source. Our interpretation for such findings is that SSS begins in a subpopulation of neurons within the MGBv and is further enhanced along the thalamocortical synapse, becoming dominant at the cortical level.

4.5.3 *Potential Mechanisms of Forward Suppression*

Consistent with previous reports, our measures of SSS at multiple levels of the auditory pathway demonstrate a dramatic increase in forward suppression and corresponding decrease in upper rate cutoffs for synchrony to repeated stimuli between the MGBv and A1. Our results accord with observations of forward suppression in tone-based streaming studies (Fishman et al., 2001, 2004; Bee and Klump, 2004) and with measures of spatially-dependent forward suppression with leading and lagging sounds (Reale and Brugge, 2000; Mickey and Middlebrooks, 2005; Zhou and Wang, 2014). Also, the time scale of forward suppression that we measured in the context of SSS agrees with that of suppression observed in forward masking studies where the response to a probe stimulus is largely suppressed following a preceding masker stimulus (Calford and Semple, 1995; Brosch and Schreiner, 1997; Scholes et al., 2011). These findings suggest that similar cortical mechanisms could be involved in forward masking, forward suppression of temporal sequences, and segregating sequential sounds into discrete streams.

We used a pharmacological procedure to test the hypothesis that forward suppression in the auditory cortex is due to synaptic (GABAergic) inhibition. Interestingly, we found that cortical neurons did not display the hypothesized relief from forward suppression post-drug application, suggesting that forward suppression is not due to synaptic inhibition. Results from Wehr and Zador (2005) indicate that synaptic inhibition plays a small role in forward suppression. In that study, they conducted whole-cell recordings on neurons in the rat auditory cortex and found that inhibitory post-synaptic potentials elicited by forward masking stimuli were brief, lasting no more than 100 ms. Thus, the forward suppression that we observed on a >100 ms time-scale could not result from the brief synaptic inhibition of cortical neurons. Our negative results against intracortical synaptic inhibition, in addition with the findings from Wehr and Zador's (2005) study, refute the synaptic inhibition hypothesis for forward suppression.

Forward suppression seen within A1 could reflect various mechanisms. One hypothesis involves the biophysical property of post discharge adaptation (i.e., refractoriness). Middlebrooks and Bremen (2013), however, demonstrated that the probability of action potential firing in response to a sound was independent of firing

elicited by a preceding sound. This was particularly the case under the 5 bps condition, with some indication of intracortical adaptation in the 10 bps condition. The 10 bps value accords well with the time constant of forward masking in A1, evident in Figure 4.8 and in previous reports (e.g., Creutzfeldt et al., 1980; Schreiner and Urbas, 1988). This argues against cortical post discharge adaptation as a mechanism of forward suppression. Other potential sources of cortical forward suppression could be inheritance from thalamic inputs or synaptic depression at the thalamocortical synapse. It is unlikely that cortical neurons directly inherit their forward suppression from thalamic neurons since MGBv neurons can follow periodic stimuli at much higher repetition rates compared to their cortical inputs (Creutzfeldt et al., 1980). It is more likely that cortical forward suppression reflects synaptic depression of thalamocortical synapses. Findings from intracellular recordings suggest that the low-pass temporal filtering between the thalamic and cortical level is the result of an activity-dependent decrease in synaptic transmission (Chance et al., 1998; Fortune and Rose, 2000; Varela et al., 1997). Furthermore, results from computational modeling studies have demonstrated that cortical repetition rate suppression can be modeled by presynaptic depression and a small amount of facilitation (Eggermont, 1999; 2002). Recently, a study in mice by Bayazitov and colleagues (2013) demonstrated that synaptic depression along the thalamocortical synapse can explain the forward suppression seen in the auditory cortex. Specifically, they found that paired-pulse synaptic depression at thalamocortical projection sites is due to a switch between firing modes of thalamic neurons, which is dependent on $Ca_v3.1$ T-type calcium channels. Pharmacologically inhibiting or RNA-mediated knockdown of those calcium channels significantly diminished synaptic depression at thalamocortical projections and forward suppression in the auditory cortex.

Based on the available reports, we hypothesize that cortical SSS is due to synaptic depression at the thalamocortical synapse. We hope to directly explore the synaptic depression hypothesis in future experiments.

4.6 Acknowledgements

We thank Zekiye Onsan, Lauren Javier,and Elizabeth McGuire for technical and administrative assistance. We also thank Dr. Raju Metherate for expert advice regarding

pharmacological manipulations. This work was supported by National Institute on Deafness and Other Communication Disorders Grants R01-DC000420 and F31 DC013013 (Ruth L. Kirschstein Predoctoral Individual National Research Service Award to promote diversity in health-related research).

Chapter 5: Summary and Conclusions

In most everyday situations listeners are capable of disentangling multiple competing sequences of sounds that originate from distinct sources. This phenomenon, called “stream segregation”, is aided by differences in spatial location between the sources. A possible substrate of spatial stream segregation (SSS) has been described in the auditory cortex, but the mechanisms leading to those cortical responses are unknown. This dissertation investigated SSS at three levels of the ascending auditory pathway with extracellular unit recordings in anesthetized rats. We provide ample evidence in support of the hypothesis that neural SSS emerges within the ascending auditory pathway as a consequence of sharpened spatial sensitivity and increased forward suppression. Overall, this dissertation highlights possible mechanisms that underlie the role of spatial hearing that culminate in SSS at the level of the auditory cortex.

The overarching goal of this dissertation was to uncover the neural mechanisms involved in neural SSS. Cats are typically used as an experimental model for spatial hearing research. However, cats are not amenable, nor are they practical for the necessary experimental techniques required to test for potential neural mechanisms. Those techniques include pharmacological manipulations and extracellular recordings from multiple regions along the ascending auditory system. A rodent, such as the rat, is more practical for pharmacological manipulations and its midbrain, thalamus, and cortex are readily accessible for *in vivo* extracellular recordings. Thus, we utilized the rat as our model for conducting experiments that examine the neural substrates and mechanisms behind SSS.

This dissertation reports several novel findings regarding spatial sensitivity in the rat auditory system. The rat displays good spatial acuity in psychophysical tests, at least across the frontal midline (Heffner and Heffner, 1985; Kavanagh and Kelly, 1986; Ito et al., 1996), but are poor at discriminating between sounds located within a hemifield (Kavanagh and Kelly, 1986). In Chapter 2, we tested the hypothesis that those characteristics of the rat’s sound localization psychophysics are evident in the characteristics of spatial sensitivity of its cortical neurons. We assessed the spatial sensitivity of single- and multiple-neuron responses in area A1 of urethane-anesthetized

rats with free-field broadband noise bursts that varied throughout 360° of azimuth in the horizontal plane at sound levels from 10 to 40 dB above neural thresholds. All of our sampled neurons in A1, with characteristic frequencies that were distributed across the rat's audiogram, displayed contralateral-hemifield spatial tuning in that they responded strongly to contralateral sound source locations, their responses cut off sharply for locations near the frontal midline, and they showed weak or no responses to ipsilateral sources. Spatial tuning was level-tolerant such that it was quite stable across a 30-dB range of sound levels. Consistent with rat psychophysical results, a linear discriminator analysis of cortical spike counts exhibited high spatial acuity for near-midline sounds and poor discrimination for off-midline locations. The presence of a largely homogenous population of neurons in rat A1 might make the rat seem uninteresting for studying spatial hearing. However, the lack of diversity of spatial sensitivity enables itself useful for future studies regarding the mechanisms of hemifield spatial tuning, which is the most common pattern of spatial sensitivity seen in more sophisticated auditory cortices. In studies employing *in vitro*, pharmacological, or optogenetic procedures, one could be assured that any A1 neuron would show contralateral hemifield spatial tuning, even in situations where that tuning could not be confirmed with detailed *in vivo* recording with free-field stimulation.

The results from the study presented in Chapter 2 prompted to an interesting question: Where does level-tolerant hemifield tuning arise along the ascending auditory pathway? Is it generated within the auditory cortex, inherited from subcortical nuclei, or transformed along the ascending pathway? This was addressed in the study presented in Chapter 3. In that study, we surveyed the auditory pathway in anesthetized rats to identify the brain level(s) at which level-tolerant spatial sensitivity arises. Our experimental procedures were similar to the study presented in Chapter 2 in that we assessed the spatial sensitivity of single- and multiple-neuron responses at different levels of the ascending auditory system of urethane-anesthetized rats with free-field broadband noise bursts that varied throughout 360° of azimuth. We found that neurons in the ICC displayed contralateral tuning at low sound levels, but tuning was degraded at successively higher sound levels. In contrast, neurons in the BIN, which receives input from the ICC and projects to the SC along the tectal pathway, showed sharp,

level-tolerant spatial sensitivity. The MGBv contained two discrete neural populations, one showing broad and level-intolerant sensitivity like the ICC and one showing sharp and level-tolerant sensitivity like A1. The nonlemniscal dorsal, medial, and shell regions of the MGB showed fairly sharp spatial sensitivity that was level-tolerant, likely reflecting inputs from A1 and/or the BIN. These results suggest for two parallel brainstem pathways for spatial hearing: 1) the tectal pathway, in which sharp, level-tolerant spatial sensitivity arises between the ICC and the BIN, projects to the SC and could support reflexive orientation to sounds; 2) the lemniscal pathway, in which such sensitivity arises between the ICC and the MGBv, projects to the auditory cortex to support perception of sound location. It remains to be directly tested how transformation of spatial sensitivity along the tectal and lemniscal pathways aids in spatial hearing. Utilizing a sound localization paradigm with optogenetic and chemical genetic approaches may provide a means to directly assess this in future studies.

Rats have been a model system for research involving the neuroanatomy of the auditory system (Beyerl, 1978; Kelly, 1980; Kelly and Kavanagh, 1986; Kelly and Glazier, 1978), sound localization behavior (Kavanagh and Kelly, 1986; Heffner and Heffner, 1985), and the development of sound localization circuitry and mechanisms in the brainstem (see Kandler and Gillespie, 2005 for review). The studies presented in Chapters 2 and 3 contribute significantly to the field of auditory neuroscience, particularly with regards to auditory processing, and forms the foundation for the neurophysiological representation of acoustic space in the rat ascending auditory system. Overall, these data will support future study on the mechanisms of spatial hearing in a preparation that is amenable and practical to modern intracellular, pharmacological, optical imaging, and optogenetic methodologies.

We have established that midbrain, thalamic, and cortical levels of the ascending auditory system in the rat are readily accessible for study (Chapter 3). Thus, the study presented in Chapter 4 examines, in rats, the emergence of SSS among four levels of the ascending auditory pathway: the ICC, the BIN, the MGBv, and area A1. We hypothesized that sharpening of spatial sensitivity and decreases in the maximum frequency for envelope synchrony, which both occur along the ascending auditory pathway and most dominantly at the cortical level, result in enhanced segregation of

sequences of sounds from multiple sources, thereby rendering the individual sound streams accessible for subsequent perceptual selection. We found that at stimulus presentation rates at which human listeners report robust SSS, neural SSS is weak in the ICC, it appears in the BIN and in about two thirds of neurons in the MGBv, and is ubiquitous in A1. Consistent with our hypothesis, the enhancement of SSS at the cortical level reflects increased spatial sensitivity and increased forward suppression.

Our measures of SSS at multiple levels of the auditory system demonstrate a dramatic increase in forward suppression and a corresponding decrease in upper rate cutoffs for synchrony to repeated stimuli between the MGBv and A1. We utilized pharmacological procedures to examine the potential mechanisms of SSS at the cortical level (Chapter 4). Specifically, we tested the hypothesis that forward suppression in the cortex, a possible precursor to SSS, results from GABAergic inhibition. Contrary to that hypothesis, we found that topical application of $GABA_A$ and $GABA_B$ receptor antagonists in the auditory cortex gave no relief from forward suppression. This suggests that cortical forward suppression results from synaptic depression along the thalamocortical synapse. Whether or not forward suppression is activated or further enhanced during active engagement remains to be tested.

The findings presented in this dissertation reveal the characteristics and potential mechanisms behind SSS, which provide insights on how the auditory system successfully analyzes the auditory scene and solves the “cocktail party listening problem”. Of clinical relevance, our results, along with future work, can aid in the design of sound processing schemes for enhanced hearing in complex auditory scenes by users of hearing aids and cochlear implants.

Future Directions. The results from the presented studies in this dissertation reveal several avenues for future investigation. In chapter 2, I presented data that suggest cortical neurons in area A1 in the rat lack the diversity of spatial sensitivity that is seen in other animal models used for spatial hearing research for they only display contralateral hemifield tuning that is level tolerant. This homogeneity of spatial sensitivity lends itself to future studies regarding the cortical mechanisms of hemifield spatial tuning, which is the most common pattern of spatial sensitivity seen in other animal models and has been thought to be the source behind discriminating between

sounds on opposing sides of the midline. Future studies employing *in vitro*, pharmacological, or optogenetic techniques can be assured that any neuron sampled from rat area A1 would show contralateral-hemifield spatial tuning, even in situations in which that tuning could not be confirmed with *in vivo* recording with free-field stimulation.

In chapter 3, I presented work that suggest the representation of free-field acoustic space is transformed along two separate pathways of the ascending auditory system: from spatially insensitive neurons that are level intolerant within the ICC to contralaterally-tuned and level tolerant neurons in the BIN (tectal pathway) and area A1 (lemniscal pathway). It is thought that the tectal pathway is more involved in reflexive orientation to sounds, while the lemniscal pathway supports the perception of sound location. Future studies employing optogenetic or chemical genetic techniques could directly assess the role of each pathway in sound localization behavior and other types of operant learning that involves spatial hearing. By characterizing the spatial sensitivity of neurons along the ascending auditory pathway, we also found evidence that two discrete populations of neurons, displaying separate types of spatial sensitivity, exist within the MGBv. “A1-like” MGBv neurons displayed level tolerant contralateral hemifield tuning similar to neurons in area A1, whereas “ICC-like” neurons displayed broad spatial tuning that was level intolerant, similar to the neurons in the ICC. The anatomical projection sites of these two distinct classes of MGBv neurons are unknown. A1-like neurons may project directly to area A1 since we did not see any difference in spatial sensitivity across cortical depth, suggesting that level tolerant contralateral hemifield spatial tuning is already present at the thalamocortical input and does not undergo additional processing within the cortex. ICC-like MGBv neurons may undergo additional processing within the MGBv that would lead to contralateral hemifield tuning. By taking this additional computation step into consideration, A1-like neurons should possess longer spike latencies than ICC-like neurons. That was not the case since no difference in spike latencies were seen between the two neural populations. It is possible that ICC-like neurons project to cortical areas outside of area A1. Future work involving anatomical and physiological methodology is needed to reveal the true projection targets of these distinct classes of neurons.

In chapter 4, I presented data demonstrating that spatial stream segregation emerges along the ascending auditory pathway and is most dominant in cortical area A1. The enhanced segregation of competing sequences of sounds within area A1 was due to forward suppression. We found evidence contrary to the hypothesis that cortical forward suppression was due to synaptic (GABAergic) inhibition. It is more likely that cortical forward suppression is due to synaptic depression along the thalamocortical synapse. One particular study demonstrated that synaptic depression along the thalamocortical synapse can explain the forward suppression seen in the auditory cortex (Bayazitov et al., 2013). In that study, the authors found that paired-pulse synaptic depression at thalamocortical projection sites is due to a switch between firing modes of thalamic neurons, which is dependent on $Ca_v3.1$ T-type calcium channels. Pharmacological inhibition or RNA-mediated knockdown of those calcium channels within the MGB significantly diminished synaptic depression at the thalamocortical synapse and the subsequent forward suppression in the auditory cortex. Future studies involving the direct examination of the mechanism behind stream segregation would benefit from utilizing a similar pharmacological procedure to test whether $Ca_v3.1$ T-type calcium channels are also involved in the suppression of responses to competing sequences of sounds, leading to stream segregation. The hypothesis is that pharmacological inhibition or RNA-mediated knockdown of those calcium channels would release cortical neurons from forward suppression and would lead to a lack of stream segregation.

REFERENCES

Aitkin LM, Gates GR, Phillips SC (1984) Responses of neurons in inferior colliculus to variations in sound-source azimuth. J Neurophysiol 52:1–17.

Anderson LA, Wallace MN, Palmer AR (2007) Identification of subdivisions in the medial geniculate body of the guinea pig. Hear Res 228:156–167.

Anderson LA, Linden JF (2011) Physiological differences between histologically defined subdivisions in the mouse auditory thalamus. Hear Res 274:48–60.

Ashida G, Carr CE (2011) Sound localization: Jeffress and beyond. Curr Opin Neurobiol 21:745–751.

Bartlett EL, Stark JM, Guillery RW, Smith PH (2000) Comparison of the fine structure of cortical and collicular terminals in the rat medial geniculate body. Neurosci 100:811–828.

Bartlett EL, Wang X (2007) Neural representations of temporally modulated signals in the auditory thalamus of awake primates. J Neurophysiol 97:1005–1017.

Bauerle P, von der Behrens W, Kossl M, Gaese BH (2011) Stimulus-specific adaptation in the gerbil primary auditory thalamus is the result of a fast frequency-specific habituation and is regulated by the corticofugal system. J Neurosci 31: 9708–9722.

Bayazitov IT, Westmoreland JJ, Zakharenko SS (2013) Forward suppression in the auditory cortex is caused by the Ca(v)3.1 calcium channel-mediated switch from bursting to tonic firing at thalamocortical projections. J Neurosci 33: 18940–18950.

Bee MA, Klump GM (2004) Primitive auditory stream segregation: a neurophysiological study in the songbird forebrain. J Neurophysiol 92:1088–1104.

Bee MA, Micheyl C,Oxenham AJ, Klump GM (2010) Neural adaptation to tone sequences in the songbird forebrain: patterns determinants, and relation to the build-up of auditory streaming. J Comp Physiol A Neuroethol Sens Neural Behav Physiol 196:543–557.

Beyerl, BD (1978) Afferent projections to the central nucleus of the inferior colliculus of the rat. Brain Res 145:209–223.

Bidet-Caulet A, Bertrand O (2009) Neurophysiological mechanisms involved in auditory perceptual organization. Front Neurosci 3:182–191.

Bierer SM, Anderson DJ (1999) Multi-channel Spike Detection and Sorting using an Array Processing Technique. Neurocomputing 26-27:947–956.

Blauert J (1997) Spatial hearing: the psychophysics of human sound localization. MIT press.

Boudreau JC, Tsuchitani C (1968) Binaural interaction in the cat superior olive S segment. J Neurophysiol 31:442–454.

Bordi F, LeDoux JE (1994a) Response properties of single units in areas of rat auditory thalamus that project to the amygdala. I. Acoustic discharge patterns and frequency receptive fields. Exp Brain Res 98:261–274.

Bordi F, LeDoux JE (1994b) Response properties of single units in areas of rat auditory thalamus that project to the amygdala. II. Cells receiving convergent auditory and somatosensory inputs and cells antidromically activated by amygdala stimulation. Exp Brain Res 98:275–286.

Bregman AS (1990) Auditory scene analysis: the perceptual organization of sound. Cambridge, MA: MIT.

Bremen P, Joris PX (2013) Axonal recordings from medial superior olive neurons obtained from the lateral lemniscus of the chinchilla (Chinchilla laniger). J Neurosci 33:17506–17518.

Brosch M, Schreiner CE (1997) Time course of forward masking tuning curves in cat primary auditory cortex. J Neurophysiol 77:923–943.

Brown CH, Schessler T, Moody D, Stebbins W (1982) Vertical and horizontal sound localization in primates. J Acoust Soc Am 72(6):1804–1811.

Brugge JF and Merzenich MM (1973) Responses of neurons in auditory cortex of the macaque monkey to monaural and binaural stimulation. J Neurophysiol 36:1138–1158.

Brugge JF, Dubrovsky NA, Aitkin LM, and Anderson DJ (1969) Sensitivity of single neurons in auditory cortex of cat to binaural tonal stimulation; effects of varying interaural time and intensity. J Neurophysiol 32:1005–1024.

Brugge JF, Reale RA, Hind JE (1996) The structure of spatial receptive fields of neurons in primary auditory cortex of the cat. J Neurosci 16(14):4420–4437.

Burnett LR, Stein BE, Chaponis D, Wallace MT (2004) Superior colliculus lesions preferentially disrupt multisensory orientation. Neurosci 124:535–547.

Calford, MB (1983) The parcellation of the medial geniculate body of the cat defined by the auditory response properties of single units. J Neurosci 3:2350–2364.

Calford MB, Semple MN (1995) Monaural inhibition in cat auditory cortex. J Neurophysiol 73:1876–1891.

Carl D, Gutschalk A (2013) Role of pattern, regularity, and silent intervals in auditory stream segregation based on interaural time differences. Exp Brain Res 224:557–570.

Carney LH, Sarkar S, Abrams KS, Idrobo F (2011) Sound-localization ability of the Mongolian gerbil (Meriones unguiculatus) in a task with a simplified response map. Hear Res 275(1-2):89–95.

Cetas JS, Price RO, Velenovsky DS, Crowe JJ, Sinex DG, McMullen NT (2002) Cell types and response properties of neurons in the ventral division of the medial geniculate body of the rabbit. J Comp Neurol 445:78–96.

Chadderton P, Agapiou JP, McAlpine D, Margrie TW (2009) The synaptic representation of sound source location in auditory cortex. J Neurosci 29(45):14127–14135.

Chance FS, Nelson SB, Abbott LF (1998) Synaptic depression and the temporal response characteristics of V1 cells. J Neurosci 18:4785–4799.

Cherry CE (1953) Some experiments on the recognition of speech,with one and two ears. J Acoust Soc Am 25:975–979.

Clarey JC, Barone P, Irons WA, Samson FK, Imig TJ (1995) Comparison of noise and tone azimuth tuning of neurons in cat primary auditory cortex and medical geniculate body. J Neurophysiol 74:961–980.

Creutzfeldt O, Hellweg FC, Schreiner C (1980) Thalamocortical transformation of responses to complex auditory stimuli. Exp Brain Res 39:87–104.

Day ML, Semple MN (2011) Frequency-dependent interaural delays in the medial superior olive: implications for interaural cochlear delays. J Neurophysiol 106:1985–1999.

de Venecia RK, Smelser CB, Lossman SD and McMullen NT (1995) Complementary expression of parvalbumin and calbindin D-28k delineates subdivisions of the rabbit medial geniculate body. J Comp Neurol 359:595–612.

de Venecia RK, Smelser CB, and McMullen NT (1998) Parvalbumin is expressed in a reciprocal circuit linking the medial geniculate body and auditory neocortex in the rabbit. J Comp Neurol 400:349–362.

DiCarlo JJ, Lane JW, Hsiao SS, Johnson KO (1996) Marking microelectrode penetrations with fluorescent dyes. J Neurosci Methods 64:75–81.

Doron NN, Ledoux JE, Semple MN (2002) Redefining the tonotopic core of rat auditory cortex: physiological evidence for a posterior field. J Comp Neurol, 453(4): 345–360.

Edeline JM, Manunta Y, Nodal FR, Bajo VM (1999) Do auditory responses recorded from awake animals reflect the anatomical parcellation of the auditory thalamus? Hearing Res 131:135–152.

Eggermont JJ (1999) The magnitude and phase of temporal modulation transfer functions in cat auditory cortex. J Neurosci 19:2780–2788.

Eggermont JJ (2002) Temporal modulation transfer functions in cat primary auditory cortex: separating stimulus effects from neural mechanisms. J Neurophysiol 87:305–321.

Elhilali M, Ma L, Micheyl C, Oxenham AJ, Shamma SA (2009) Temporal coherence in the perceptual organization and cortical representation of auditory scenes. Neuron 61:317–329.

Ernst MD (2004) Permutation Methods: A Basis for Exact Inference. Stat Sci 19:676–685.

Fishman YI, Arezzo JC, Steinschneider M (2004) Auditory stream segregation in monkey auditory cortex: effects of frequency separation, presentation rate, and tone duration. J Acoust Soc Am 116:1656–1670.

Fishman YI, Micheyl C, Steinschneider M (2012) Neural mechanisms of rhythmic masking release in monkey primary auditory cortex: implications for models of auditory scene analysis. J Neurophysiol 107:2366–2382.

Fishman YI, Reser DH, Arezzo JC, Steinschneider M (2001) Neural correlates of auditory stream segregation in primary auditory cortex of the awake monkey. Hear Res 151:167–187.

Fitzpatrick DC, Batra R, Stanford TR, Kuwada S (1997) A neuronal population code for sound localization. Nature 388:871– 874.

Fitzpatrick DC, Kuwada S, Batra R (2000) Neural sensitivity to interaural time differences: beyond the Jeffress model. J Neurosci 20:1605–1615.

Fitzpatrick DC, Kuwada S, Batra R (2002) Transformations in processing interaural time differences between the superior olivary complex and inferior colliculus: beyond the Jeffress model. Hear Res 168:79–89.

Fortune ES, Rose GJ (2000) Short-term synaptic plasticity contributes to the temporal filtering of electrosensory information. J Neurosci 20:7122–7130.

Fujita I, Konishi M (1991) The role of GABAergic inhibition in processing of interaural time difference in the owl's auditory system. J Neurosci 11:722–739.

Gaese BH, Johnen A (2000) Coding for auditory space in the superior colliculus of the rat. Eur J Neurosci 12:1739–1752.

Gaese BH, Ostwald J (1995) Temporal coding of amplitude and frequency modulation in the rat auditory cortex. Eur J Neurosci 7:438–450.

Gai Y, Ruhland JL, Yin TCT and Tollin DJ (2013) Behavioral and Modeling Studies of Sound Localization in Cats: Effects of Stimulus Level and Duration, J Neurophysiol 110:607–620.

Games KD, Winer JA (1988) Layer V in rat auditory cortex: projections to the inferior colliculus and contralateral cortex. Hear Res 34:1–25.

Goldberg JM, Brown PB (1969) Response of binaural neurons of dog superior olivary complex to dichotic tonal stimuli: some physiological mechanisms of sound localization. J Neurophysiol 32:613–636.

Green DM, Swets JA. (1966) Signal Detection Theory and Psychophysics. New York: Wiley.

Grothe B, Pecka M, McAlpine D (2010) Mechanisms of sound localization in mammals. Physiol Rev 90:983–1012.

Hackett TA, Barkat TR, O'Brien BM, Hensch TK, Polley DB (2011) Linking topography to tonotopy in the mouse auditory thalamocortical circuit. J Neurosci 31:2983–2995.

Harrington IA, Stecker GC, Macpherson EA, Middlebrooks JC (2008) Spatial sensitivity of neurons in the anterior, posterior, and primary fields of cat auditory cortex. Hear Res 240(1-2):22–41.

Hazama M, Kimura A, Donishi T, Sakoda T, Tamai Y (2001) Topography of corticothalamic projections from the auditory cortex of the rat. Neurosci 124:655–667.

He J (2001) On and off pathways segregated at the auditory thalamus of the guinea pig. J Neurosci 21:8672–8679.

He J, Hu B (2002) Differential distribution of burst and single-spike responses in auditory thalamus. J Neurophysiol 88:2152–2156.

Heaulme M, Chambon JP, Leyris R, Molimard JC, Wermuth CG, Biziere K (1986) Biochemical characterization of the interaction of three pyridazinyl-GABA derivatives with the GABAA receptor site. Brain Res 384:224–231.

Heffner HE, Heffner RS (1985) Sound localization in wild Norway rats (Rattus norvegicus). Hear Res 19(2):151–155.

Heffner RS, Heffner HE (1988a). Sound localization acuity in the cat: effect of azimuth, signal duration, and test procedure. Hear Res 36(2-3):221–232.

Heffner RS, Heffner HE (1988b). Sound localization and use of binaural cues by the gerbil (Meriones unguiculatus). Behav Neurosci 102(3):422–428.

Heffner HE, Heffner RS (1990). Effect of bilateral auditory cortex lesions on sound localization in Japanese macaques. J Neurophysiol 64(3):915–931.

Heffner HE, Heffner RS, Contos C, Ott T (1994) Audiogram of the hooded Norway rat. Hear Res 73(2):244–247.

Heffner HE, Heffner RS (2007) Hearing ranges of laboratory animals. J Am Assoc Lab Anim Sci 46(1):20–22.

Heffner HE, Masterton B (1975) Contribution of auditory cortex to sound localization in the monkey (Macaca mulatta). J Neurophysiol 38(6):1340–1358.

Higgins NC, Storace DA, Escab MA, Read HL (2010) Specialization of binaural responses in ventral auditory cortices. J Neurosci 30(43):14522–14532.

Imig TJ, Adrian HO (1977) Binaural columns in the primary field (AI) of cat auditory cortex. Brain Res 138: 241–257.

Imig TJ, Irons WA, Samson FR (1990) Single-unit selectivity to azimuthal direction and sound pressure level of noise bursts in cat high-frequency primary auditory cortex. J Neurophysiol 63(6):1448–1466.

Irvine DRF, Park VN, Mattingley JB (1995) Responses of neurons in the inferior colliculus of the rat to interaural time and intensity differences in transient stimuli, Implications for the latency hypotheses. Hear Res 85:127–141.

Irvine DRF, Rajan R, Aitkin LM (1996) Sensitivity to interaural intensity differences of neurons in primary auditory cortex of the cat. I. types of sensitivity and effects of variations in sound pressure level. J Neurophysiol 75:75–96.

Ito M, Van Adel B, Kelly JB. (1996) Sound localization after transection of the commissure of Probst in the albino rat. J Neurophysiol 76(5):3493–3502.

Ivarsson C, baupierre Y, de Ribaupierre F (1988) Influence of auditory localization cues on neuronal activity in the auditory thalamus of the cat. J Neurophysiol 59: 586–606.

Jenkins WM, Masterton RB (1982) Sound localization: effects of unilateral lesions in central auditory system. J Neurophysiol 47(6):987–1016.

Jenkins WM, Merzenich MM (1984) Role of cat primary auditory cortex for sound-localization behavior. J Neurophysiol 52:819–847.

Jiang ZD, King AJ, Moore DR (1993) Topographic projection from the brachium of the inferior colliculus to the space mapped region of the superior colliculus in the ferret. Br J Audiol 27:344–345.

Joris PX, Schreiner CE, Rees A (2004) Neural processing of amplitude-modulated sounds. Physiol Rev 84:541–577.

Kandler K, Gillespie DC (2005) Developmental refinement of inhibitory sound-localization circuits Trends Neurosci 28:290–296.

Kavanagh GL, Kelly JB. (1986) Midline and lateral field sound localization in the albino rat (Rattus norvegicus). Behav Neurosci 100(2):200–205.

Kavanagh GL, Kelly JB. (1987) Contribution of auditory cortex to sound localization by the ferret (Mustela putorius). J Neurophysiol 57(6):1746–1766.

Kelly JB. (1980) Effects of auditory cortical lesions on sound localization by the rat. J Neurophysiol 44(6):1161–1174.

Kelly JB, Glazier SJ. (1978) Auditory cortex lesions and discrimination of spatial location by the rat. Brain Res 145(2):315–321.

Kelly JB, Glenn SL, Beaver CJ (1991) Sound frequency and binaural response properties of single neurons in rat inferior colliculus. Hear Res 56:273–280.

Kelly JB, Judge PW (1985) Effects of medial geniculate lesions on sound localization by the rat. J Neurophysiol 53:361–372.

Kelly JB, Kavanagh GL (1986) Effects of auditory cortical lesions on pure-tone sound localization by the albino rat. Behav Neurosci 100(4):569–575.

Kelly JB, Masterton B. (1977) Auditory sensitivity of the albino rat. J Comp Physiol Psychol 91(4):930–936.

Kelly JB, Sally SL. (1988) Organization of auditory cortex in the albino rat: binaural response properties. J Neurophysiol 59(6):1756–1769.

Kerr DI, Ong J, Johnston GA, Abbenante J, Prager RH (1988) 2-Hydroxy-saclofen: an improved antagonist at central and peripheral GABAB receptors. Neurosci letters 92:92–96.

Kilgard MP, Merzenich MM (1999) Distributed representation of spectral and temporal information in rat primary auditory cortex. Hear Res 134:16–28.

King AJ (2004) The superior colliculus. Curr Biol 14:R335–338.

King AJ, Hutchings ME (1987) Spatial response properties of acoustically responsive neurons in the superior colliculus of the ferret: a map of auditory space. J Neurophysiol 57:596–624.

King AJ, Jiang ZD, Moore DR (1998) Auditory brainstem projections to the ferret superior colliculus: anatomical contribution to the neural coding of sound azimuth. J Comp Neurol 390:342–365.

King AJ, Middlebrooks JC (2011) Cortical representation of auditory space. In: The auditory cortex (Winer J, Schreiner C, eds), pp 329–341. New York: Springer.

Kirby AE, Middlebrooks JC (2010) Auditory temporal acuity probed with cochlear implant stimulation and cortical recording. J Neurophysiol 103(1):531–542.

Kitzes LM, Wrege KS, Cassady JM (1980) Patterns of responses of cortical cells to binaural stimulation. J Comp Neurol 192:455–472.

Knudsen EI, Knudsen PF (1996) Disruption of auditory spatial working memory by inactivation of the forebrain archistriatum in barn owls. Nature 383:428–431.

Knudsen EI, Knudsen PF, Masino T (1993) Parallel pathways mediating both sound localization and gaze control in the forebrain and midbrain of the barn owl. J Neurosci 13:2837–2852.

Koka K, Read HL, Tollin DJ (2008) The acoustical cues to sound location in the rat: measurements of directional transfer functions. J Acoust Soc Am 123: 4297–4309.

Kondo HM, Kashino M (2009) Involvement of the thalamocortical loop in the spontaneous switching of percepts in auditory streaming. J Neurosci 29:12695–12701.

Kotak VC, Takesian AE, Sanes DH (2008) Hearing loss prevents the maturation of GABAergic transmission in the auditory cortex. Cerebral Cortex 18:2098-2108.

Kudo M, Tashiro T, Higo S, Matsuyama T, Kawamura S (1984) Ascending projections from the nucleus of the brachium of the inferior colliculus in the cat. Exp Brain Res 54:203–211.

Kuwada S, Bishop B, Alex C, Condit DW, Kim DO (2011) Spatial tuning to sound-source azimuth in the inferior colliculus of unanesthetized rabbit. J Neurophysiol 106:2698–2708.

Kyweriga M, Stewart W, Cahill C, Wehr M (2014) Synaptic mechanisms underlying interaural level difference selectivity in rat auditory cortex. J Neurophysiol 112:2561–2571.

Joris PX, Schreiner CE, Rees A (2004) Neural processing of amplitude-modulated sounds. Physiol Rev 84:541–577.

Lee CC, Middlebrooks JC (2011) Auditory cortex spatial sensitivity sharpens during task performance. Nat Neurosci 14(1):108–114.

Lee CC, Middlebrooks, JC (2013) Specialization for Sound Localization in Fields A1, DZ, and PAF of Cat Auditory Cortex. JARO 14(1):61–82.

Lesica NA, Lingner A, Grothe B (2010) Population coding of interaural time differences in gerbils and barn owls. J Neurosci 30(35):11696–11702.

Lumani A, Zhang H (2010) Responses of neurons in the rat's dorsal cortex of the inferior colliculus to monaural tone bursts. Brain Res 1351:115–129.

Macmillan, NA, Creelman, CD (2005) Detection Theory: A User's Guide, 2nd Edition, Mahwah, NJ: Erlbaum.

Maier JK, Klump GM (2006) Resolution in azimuth sound localization in the Mongolian gerbil (Meriones unguiculatus). J Acoust Soc Am 119(2):1029–1036.

Makous JC, Middlebrooks JC (1990) Two-dimensional sound localization by human listeners. J Acoust Soc Am 87(5):2188–2200.

Malhotra S, Hall AJ, and Lomber SG (2004) Cortical control of sound localization in the cat: unilateral cooling deactivation of 19 cerebral areas. J Neurophysiol 92:1625–1643.

Malhotra S, Lomber SG (2007) Sound localization during homotopic and heterotopic bilateral cooling deactivation of primary and nonprimary auditory cortical areas in the cat. J Neurophysiol 97:26–43.

Malmierca MS, Hernandez O, Rees A (2005) Intercollicular commissural projections modulate neuronal responses in the inferior colliculus. Eur J Neurosci 21: 2701–2710.

Malmierca MS, Izquierdo MA, Cristaudo S, Hernandez O, Perez-Gonzalez D, Covey E, Oliver DL (2008) A discontinuous tonotopic organization in the inferior colliculus of the rat. J Neurosci 28:4767–4776.

Malone BJ, Scott BH, Semple MN (2002) Context-dependent adaptive coding of interaural phase disparity in the auditory cortex of awake macaques. J Neurosci 22:4625–4638.

Mardia KV (1972) Statistics of directional data. London: Academic.

Martin RL, Webster WR (1987) The auditory spatial acuity of the domestic cat in the interaural horizontal and median vertical planes. Hear Res 30(2-3):239–252.

May BJ, Huang AY (1996) Sound orientation behavior in cats. I. Localization of broadband noise. J Acoust Soc Am 100(2 Pt 1):1059–1069.

McAlpine D, Grothe B (2003) Sound localization and delay lines--do mammals fit the model? Trends Neurosci 26(7):347–350.

McAlpine D, Jiang D, Shackleton TM, Palmer AR (1998) Convergent input from brainstem coincidence detectors onto delay-sensitive neurons in the inferior colliculus. J Neurosci 18:6026–6039.

McLaughlin M, Franken TP, van der Heijden M, Joris PX (2014) The interaural time difference pathway: a comparison of spectral bandwidth and correlation sensitivity at three anatomical levels J Assoc Res Otolaryngol 15(2):203–18.

Metherate R, Ashe JH (1994) Facilitation of an NMDA receptor-mediated EPSP by paired-pulse stimulation in rat neocortex via depression of GABAergic IPSPs. J Physiol 481(Pt 2):331-348.

Micheyl C, Tian B, Carlyon RP, Rauschecker JP (2005) Perceptual organization of tone sequences in the auditory cortex of awake macaques. Neuron 48:139–148.

Mickey BJ, Middlebrooks JC (2003) Representation of auditory space by cortical neurons in awake cats. J Neurosci 23(25):8649–8663.

Middlebrooks JC (2008) Auditory cortex phase locking to amplitude-modulated cochlear implant pulse trains. J Neurophysiol 100(1):76–91.

Middlebrooks JC, Bremen P (2013) Spatial stream segregation by auditory cortical neurons. J Neurosci 33:10986–11001.

Middlebrooks JC, Green DM (1991) Sound localization by human listeners. Annual review of psychology 42:135–159.

Middlebrooks JC, Knudsen EI (1984) A neural code for auditory space in the cat's superior colliculus. J Neurosci 4:2621–2634.

Middlebrooks JC, Onsan ZA (2012) Stream segregation with high spatial acuity. J Acoust Soc Am 132:3896–3911.

Middlebrooks JC, Pettigrew JD (1981) Functional classes of neurons in primary auditory cortex of the cat distinguished by sensitivity to sound location. J Neurosci 1(1):107–120.

Middlebrooks JC, Snyder RL (2007) Auditory prosthesis with a penetrating nerve array. JARO 8(2):258–279.

Middlebrooks JC, Zook JM (1983) Intrinsic organization of the cat's medial geniculate body identified by projections to binaural response-specific bands in the primary auditory cortex. J Neurosci 3:203–224.

Middlebrooks JC, Dykes RW, Merzenich MM (1980) Binaural response-specific bands in primary auditory cortex (AI) of the cat: topographical organization orthogonal to isofrequency contours. Brain Res 181:31–48.

Middlebrooks JC, Clock AE, Xu L, Green DM (1994) A panoramic code for sound location by cortical neurons. Science 264(5160):842–844.

Middlebrooks JC, Xu L, Eddins AC, Green DM (1998) Codes for sound-source location in nontonotopic auditory cortex. J Neurophysiol 80(2):863–881.

Miller LM, Recanzone GH (2009) Populations of auditory cortical neurons can accurately encode acoustic space across stimulus intensity. PNAS 106: 5931–5935.

Moore BCJ, Gockel H (2002) Factors influencing sequential stream segregation. Acta Acustica United with Acustica 88:320–332.

Moore JM, Tollin DJ, Yin TCT (2008) Can measures of sound localization acuity be related to the precision of absolute location estimates? Hear Res 238:94–109.

Mrsic-Flogel, TD, Schnupp, JWH, King, AJ (2003) Acoustic factors govern developmental sharpening of spatial tuning in the auditory cortex. Nat Neurosci 6(9):981–988.

Mrsic-Flogel TD, King AJ, Schnupp JWH (2005) Encoding of virtual acoustic space stimuli by neurons in ferret primary auditory cortex. J Neurophysiol 93(6): 3489–3503.

Nelken I, Chechik G, Mrsic-Flogel TD, King AJ, Schnupp JWH (2005) Encoding stimulus information by spike numbers and mean response time in primary auditory cortex. J Comp Neurosci 19(2):199–221.

Nodal FR, Bajo VM, Parsons CH, Schnupp JW, King AJ (2008) Sound localization behavior in ferrets: comparison of acoustic orientation and approach-to-target responses. Neurosci 154(1):397–408.

Ong J, Bexis S, Marino V, Parker DA, Kerr DI, Froestl W (2001) CGP 36216 is a selective antagonist at GABA(B) presynaptic receptors in rat brain. European journal of pharmacology 415:191–195.

Palmer AR, King AJ (1982) The representation of auditory space in the mammalian superior colliculus. Nature 299:248–249.

Park TJ, Klug A, Holinstat M, Grothe B (2004) Interaural level difference processing in the lateral superior olive and the inferior colliculus. J Neurophysiol 92:289–301.

Patterson RD (1976) Auditory filter shapes derived with noise stimuli. J Acoust Soc Am 59:640–654.

Paxinos G, Watson C (2005) The rat brain in stereotaxic coordinates (Elsevier-Academic, Burlington, VT).

Pérez ML, Peña JL (2006) Comparison of midbrain and thalamic space-specific neurons in barn owls. J Neurophysiol 95:783–90.

Pérez ML, Shanbhag SJ, Peña JL (2009) Auditory spatial tuning at the crossroads of the midbrain and forebrain. J Neurophysiol 102(3):1472–82.

Phillips DP (2008) A perceptual architecture for sound lateralization in man. Hear Res 238(1-2):124–132.

Polley DB, Read HL, Storace DA, Merzenich MM (2007) Multiparametric auditory receptive field organization across five cortical fields in the albino rat. J Neurophysiol 97(5):3621–3638.

Populin LC (2006) Monkey sound localization: head-restrained versus head-unrestrained orienting. J Neurosci 26(38):9820–9832.

Pressnitzer D, Sayles M, Micheyl C, Winter IM (2008) Perceptual organization of sound begins in the auditory periphery. Curr Biol 18:1124–1128.

Proctor L, Konishi M (1997) Representation of sound localization cues in the auditory thalamus of the barn owl. PNAS 94:10421–10425.

Rajan R, Aitkin LM, Irvine DR, McKay J (1990) Azimuthal sensitivity of neurons in primary auditory cortex of cats. I. Types of sensitivity and the effects of variations in stimulus parameters. J Neurophysiol 64:872–887.

Read HL, Miller LM, Schreiner CE, Winer JA (2008) Two thalamic pathways to primary auditory cortex. Neurosci 152:151–159.

Reale RA, Brugge JF (1990) Auditory cortical neurons are sensitive to static and continuously changing interaural phase cues. J Neurophysiol 64:1247–1260.

Redies H, Brandner S, Creutzfeldt OD (1989) Anatomy of the auditory thalamocortical system of the guinea pig. J Comp Neurol 282:489–511.

Recanzone GH, Beckerman NS (2004) Effects of intensity and location on sound location discrimination in macaque monkeys. Hear Res 198(1-2):116–124.

Recanzone GH, Makhamra SD, Guard DC (1998) Comparison of relative and absolute sound localization ability in humans. J Acoust Soc Am 103:1085–1097.

Recanzone GH, Guard DC, Phan ML, Su TK (2000) Correlation between the activity of single auditory cortical neurons and sound-localization behavior in the macaque monkey. J Neurophysiol 83(5):2723–2739.

Recanzone GH, Engle JR, Juarez-Salinas DL (2011) Spatial and temporal processing of single auditory cortical neurons and populations of neurons in the macaque monkey. Hear Res 271(1-2):115–122.

Rees A, Møller AR (1987) Stimulus properties influencing the responses of inferior colliculus neurons to amplitude-modulated sounds. Hear Res 27:129–143.

Rouiller EM, Welker E (1991) Morphology of corticothalamic terminals arising from the auditory cortex of the rat: a Phaseolus vulgaris-leucoagglutinin (PHA-L) tracing study. Hear Res 56:179–190.

Rutkowski RG, Miasnikov AA, Weinberger NM (2003) Characterisation of multiple physiological fields within the anatomical core of rat auditory cortex. Hear Res 181(1-2):116–130.

Sabin AT, Macpherson EA, Middlebrooks JC (2005): Human sound localization at near-threshold levels. Hear Res 199:124–34.

Salminen NH, May PJC, Alku P, Tiitinen H (2009) A population rate code of auditory space in the human cortex. PloS One 4(10), e7600.

Schnupp JW, King AJ (1997) Coding for auditory space in the nucleus of the brachium of the inferior colliculus in the ferret. J Neurophysiol 78:2717–2731.

Scott BH, Malone BJ, Semple MN (2007) Effect of behavioral context on representation of a patial cue in core auditory cortex of awake macaques. J Neurosci 27: 6489–6499.

Schadwinkel S, Gutschalk A (2010) Activity associated with stream segregation in human auditory cortex is similar for spatial and pitch cues. Cereb Cortex 20:2863–2873.

Schadwinkel S, Gutschalk A (2011) Transient bold activity locked to perceptual reversals of auditory streaming in human auditory cortex and inferior colliculus. J Neurophysiol 105:1977–1983.

Scholes C, Palmer AR, Sumner CJ (2011) Forward suppression in the auditory cortex is frequency-specific. Eur J Neurosci 33:1240–1251.

Schreiner CE, Urbas JV (1988) Representation of amplitude modulation in the auditory cortex of the cat. II. Comparison between cortical fields. Hear Res 32:49–63.

Semple MN, Kitzes LM (1993) Binaural processing of sound pressure level in cat primary auditory cortex: Evidence for a representation based on absolute levels rather than interaural level differences. J Neurophysiol 69:449–461.

Shackleton T, Middlebrooks J, Palmer A (2012) Spatial position related adaptation in the inferior colliculus of anesthetized guinea pigs. Abs Assoc Res Otolaryngol 35.

Shi CJ, Cassell MD (1997) Cortical, thalamic, and amygdaloid projections of rat temporal cortex. J Comp Neurol 382:153–175.

Shinn-Cunningham BG (2005) Influences of spatial cues on grouping and understanding sound. In: Proceedings of the Forum Acusticum.

Slee SJ, Young ED (2013) Linear processing of interaural level difference underlies spatial tuning in the nucleus of the brachium of the inferior colliculus. J Neurosci 33:3891–3904.

Sparks DL, Groh JM (1995) The superior colliculus: a window for viewing issues in integrative neuroscience. In The Cognitive Neurosciences, M.S. Gazzaniga, ed. (MIT Press, Cambridge, MA), pp. 565–584.

Spitzer MW, Semple MN (1995) Neurons sensitive to interaural phase disparity in gerbil superior olive: diverse monaural and temporal response properties. J Neurophysiol 73:1668–1690.

Stanford TR, Kuwada S, Batra R (1992) A comparison of the interaural time sensitivity of neurons in the inferior colliculus and thalamus of the unanesthetized rabbit. J Neurosci 12:3200–3216.

Stecker GC, Middlebrooks JC (2003) Distributed coding of sound locations in the auditory cortex. Biol Cybernetics 89(5):341–349.

Stecker GC, Mickey BJ, Macpherson EA, Middlebrooks JC (2003) Spatial sensitivity in field PAF of cat auditory cortex. J Neurophysiol 89(6):2889–2903.

Stecker GC, Harrington IA, Macpherson EA, Middlebrooks JC (2005a) Spatial sensitivity in the dorsal zone (area DZ) of cat auditory cortex. J Neurophysiol 94(2):1267–1280.

Stecker GC, Harrington IA, Middlebrooks JC (2005b). Location coding by opponent neural populations in the auditory cortex. PLoS Biol 3(3), e78.

Syka J, Popelar J, Kvasnak E, Astl J (2000) Response properties of neurons in the central nucleus and external and dorsal cortices of the inferior colliculus in guinea pig. Exp Brain Res 133:254–266.

Thompson GC, Cortez AM (1983) The inability of squirrel monkeys to localize sound after unilateral ablation of auditory cortex. Behav Brain Res 8(2):211–216.

Thompson GC, Masterton RB (1978) Brainstem auditory pathways involved in reflexive head orientation to sound. J Neurophysiol 41:1183–1202.

Tollin DJ (2008) Encoding of interaural level differences for sound localization. In: The Senses: A Comprehensive Reference. Audition, edited by Dallos P, Oertel D. San Diego, CA: Academic, Vol. 3, p. 631–654.

Tollin DJ, Yin TCT (2002) The Coding of Spatial Location by Single Units in the Lateral Superior Olive of the Cat. I. Spatial Receptive Fields in Azimuth. J Neurosci 22:1454–67.

Tollin DJ, Yin TCT (2005) Interaural phase and level difference sensitivity in low-frequency neurons in the lateral superior olive. J Neurosci 25:10648–10657.

Tollin DJ, Populin LC, Moore JM, Ruhland JL, Yin TCT (2005) Sound-localization performance in the cat: the effect of restraining the head. J Neurophysiol 93(3): 1223–1234.

van Noorden L (1975) Temporal coherence in the perception of tone sequences. PhD thesis, University of Technology, Eindhoven.

Varela JA, Sen K, Gibson J, Fost J, Abbott LF, Nelson SB (1997) A quantitative description of short-term plasticity at excitatory synapses in layer 2/3 of rat primary visual cortex. J Neurosci 17:7926–7940.

Verschooten E, Robles L, Kovacic D, Joris PX (2012) Auditory nerve frequency tuning measured with forward-masked compound action potentials. JARO 13:799–817.

Wang X, Lu T, Bendor D, Bartlett E (2008) Neural coding of temporal information in auditory thalamus and cortex. Neurosci 157:484–494.

Wehr M, Zador AM (2005) Synaptic mechanisms of forward suppression in rat auditory cortex. Neuron 47:437–445.

Werner-Reiss U, Groh JM (2008) A rate code for sound azimuth in monkey auditory cortex: implications for human neuroimaging studies. J Neurosci 28(14): 3747–3758.

Wesolek CM, Koay G, Heffner RS, Heffner HE (2010) Laboratory rats (Rattus norvegicus) do not use binaural phase differences to localize sound. Hear Res, 265(1-2):54–62.

Wightman FL, Kistler DJ (1993) Sound localization. In: Yost WA, Popper AN, Fay RR, editors. Human Psychophysics. New York: Springer-Verlag. pp. 155–192.

Winer JA, Diehl JJ, Larue DT (2001) Projections of auditory cortex to the medial geniculate body of the cat. J Comp Neurol 430:27–55.

Woods TM, Lopez SE, Long JH, Rahman JE, Recanzone GH (2006) Effects of stimulus azimuth and intensity on the single-neuron activity in the auditory cortex of the alert macaque monkey. J Neurophysiol 96(6), 3323–3337.

Yao JD, Bremen P, Middlebrooks JC (2013) Rat primary auditory cortex is tuned exclusively to the contralateral hemifield. J Neurophysiol 110:2140–2151.

Yao JD, Bremen P, Middlebrooks JC (2015) Transformation of spatial sensitivity along the ascending auditory pathway. J Neurophysiol 113:3098–3111.

Yin TCT, Chan JC (1990) Interaural time sensitivity in medial superior olive of cat. J Neurophysiol 64:465–488.

Young ED, Davis KA (2002) Circuitry and function of the cat dorsal cochlear nucleus. In: Integrative Functions in the Mammalian Auditory Pathway, D. Oertel, A.N. Popper, R.R. Fay (Eds.), Springer-Verlag, 160–206.

Zhou B, Green DM, Middlebrooks JC (1992) Characterization of external ear impulse responses using Golay codes. J Acoust Soc Am, 92(2 Pt 1):1169–1171.

Zhou Y, Wang X (2012) Level dependence of spatial processing in the primate auditory cortex. J Neurophysiol 108(3):810–826

Zwiers MP, Versnel H, Van Opstal AJ (2004) Involvement of monkey inferior colliculus in spatial hearing. J Neurosci 24:4145–4156.